Semiconductor quantum dot lasers: Genesis, prospects, and challenges

5

Frédéric Grillot[a,b], *Jianan Duan*[c], *Bozhang Dong*[d], *and Heming Huang*[a]
[a]Télécom Paris, Institut Polytechnique de Paris, Palaiseau, France, [b]Center for High Technology Material, University of New Mexico, Albuquerque, NM, United States, [c]School of Electronic and Information Engineering, Harbin Institute of Technology, Shenzhen, China, [d]Institute for Energy Efficiency, University of California Santa Barbara, Santa Barbara, CA, United States

5.1 Introduction

Over the past few decades, our daily lives have been reshaped by the emergence of new technologies. The popularization of smartphones, for example, has radically transformed our daily routine and the associated industries. Today, a wide variety of online services based on cloud computing and cluster analysis are at our fingertips. Moreover, with the ongoing construction of the Internet of Things (IoT), or the more ambitious Internet of Everything (IoE), billions of devices and sensors are connected to the network each year, hence generating real-time feedback for various monitoring purposes [1]. In addition to IoT/IoE, artificial intelligence and machine learning are booming and continuously launching more innovative applications in education, healthcare, and transportation, to name a few. As a result, global data traffic is growing every year, reaching 5 zettabytes (ZB) per month on mobile networks alone by the end of 2030, according to the recent estimates from the International Telecommunication Union [2]. At the same time, the communication infrastructure is constantly being upgraded, especially at its core, the optical layer, to accommodate the rapid growth in Internet use, which has increased at least 16-fold by 2020 compared with 2010, as reported by the International Energy Agency [3]. High-speed, low-latency optical links are among the most in-demand equipment to meet transmission capacity requirements, especially in access networks and very large-scale data centers. By 2026, the global optical transceiver market is expected to double to approximately $21 billion [4].

Currently, common optical transceivers include a semiconductor laser light source, a modulator, a (de)multiplexer, and a photodetector, all assembled around a printed circuit board (PCB). The heat generated by the electronic components can easily jeopardize stability and performance, as semiconductor lasers are generally strongly sensitive to thermal issues. In addition, the functionality of edge emitters is rather

Quantum Photonics. https://doi.org/10.1016/B978-0-323-98378-5.00008-8

limited due to their size. On the other hand, due to the complication of the hardware, additional functions are expected to be integrated into these devices. For example, to exploit the high bandwidth offered by optical fibers, wavelength-division multiplexing (WDM) solutions have been implemented in data centers for card-to-card or chip-to-chip links. In this context, photonic integration is seen as the key solution for housing all the required parts in a tiny space like an optical transceiver. At the early stages, the development of photonic integrated circuits (PICs) was quite challenging because the various optical functionalities inherently depended on a too large variety of materials, which not only limited the scalability of PICs, but also made them very expensive. Fortunately, with the maturation of integrated technologies, photonic platforms are now becoming much more publicly available [5–7].

Typical semiconductor lasers used in optical networks are mainly based on quantum well (QW) technology [7]. Despite its simple fabrication procedure, the QW laser has some intrinsic shortcomings to be considered as the ideal light source for PICs. For example, they are known to be sensitive to thermal effects, namely the wavelength and intensity can be seriously altered by temperature variation [8, 9]. This can be very problematic and costly since temperature-controlled heat sinks must often be used. In the case of on-chip WDM, serious crosstalk can occur, hence disrupting system operation. In addition, QW lasers do not naturally exhibit low phase and intensity noise, so it is difficult to utilize them in integrated communication systems. To overcome these issues, quantum dot (QD) gain materials are now considered as a much better option for PICs. Due to their atomic nature, QD lasers exhibit high optical gain [8–11], low threshold current density [11–13], large thermal stability [14, 15], narrow optical linewidth [16, 17], and low intensity noise [18, 19], thus reconciling all the most sought-after qualifications for an on-chip laser device. Furthermore, compared to QWs, QDs are individual nanostructures showing large energy sublevel separation, hence limiting the carrier escape, while the 3D carrier confinement inhibits in-plane diffusion. Therefore, when subjected to direct growth, QD lasers are less susceptible to threading dislocations (TDs) than their QW counterparts [20, 21]. Furthermore, recent results have demonstrated that integrated QD lasers on silicon can handle an excessive amount of external optical reflections and operate without optical isolators [22, 23], implying the possibility of creating low-cost optical transceivers for industrial applications. Such concept has been shown initially by Huyet et al. [24–26].

In this chapter, we highlight some of the recent progress achieved on QD lasers. It is organized as follow: in Section 5.2, we discuss in further detail the development of QD material and the fundamental aspects; Section 5.3 focuses on the phase and intensity noise properties; Section 5.4 deals with the reflection sensitivity in PICs and shows the clear advantage in using QD lasers for isolation-free applications; Sections 5.5 and 5.6 investigate high-order nonlinear properties of the QD gain media and how it can be exploited for optical frequency comb (OFC) generation; Section 5.7 introduces the modulation properties of QD lasers; finally in Section 5.8, some of the latest QD lasers-related applications are presented.

5.2 Quantum dot lasers

5.2.1 Low-dimensional semiconductor structures: An heuristic approach

Since the first demonstrations of semiconductor lasers in the early 1960s [27–30], improvement of the gain medium and light emission efficiency has become the main goal. In the late-1960s and the early 1970s, the bulk heterostructure (3D system)-based semiconductor laser was developed, hence providing an efficient carrier confinement within the active region. In particular, the invention of the double heterostructure (DH) yielded both improved photon and carrier confinement allowed for continuous waves (CWs) and room temperature lasing emission [31, 32]. For this discovery, the Nobel Prize in Physics (2000) was awarded, having a huge societal impact by moving semiconductor lasers from outside laboratories into our daily lives [33–35].

From a general viewpoint, quantum confinement in solids occurs when one or more spatial dimensions of the nanocrystal approach the de Broglie wavelength of the carrier defined by

$$\lambda_B = \frac{2\pi h}{\sqrt{2m_e^* E}} \tag{5.1}$$

In this formula, for a conduction band electron, m_e^* is the effective mass of the electron, E is the energy of the electron in excess of the gap, and h is the Planck's constant. For usual semiconductors, this distance is of the order of a few tens of nanometers. Confinement of carriers leads to a quantization of the density of states (DOS) and splits the energy band of semiconductor into discrete energy levels [36, 37]. Fig. 5.1 displays different semiconductor structures with different degrees of dimensionality, namely bulk (3D), QW (2D), quantum dash (1D), and QD (0D) [38]. The impact of the different degrees of the dimensionality, the inhomogeneous broadening, and the thermal population on the DOS is shown. The gap energy is represented by E_{gap}, whereas E_0 and E_1 show the quantized energy levels.

The quantization of the carriers in one direction of space has already been widely studied in device structures such as QW lasers [35, 38–43]. The carriers are confined along the growth axis and have a free movement in the plane of the layers. Therefore, the energy of the electrons in these structures is then of the type:

$$E_{e,n}(k) = \frac{\hbar^2 k_{//}^2}{\sqrt{2m_e}} + E_n(k_z) \tag{5.2}$$

where $\hbar$ is the reduced Planck's constant, $k_{//}$ the wave vector of the electron in the plane, E_n an energy taking discrete values due to the confinement, and k_z the wave vector component in the quantized direction, which is defined such as $\mathbf{k_z} = \sqrt{\mathbf{k^2} - \mathbf{k_{//}^2}}$.

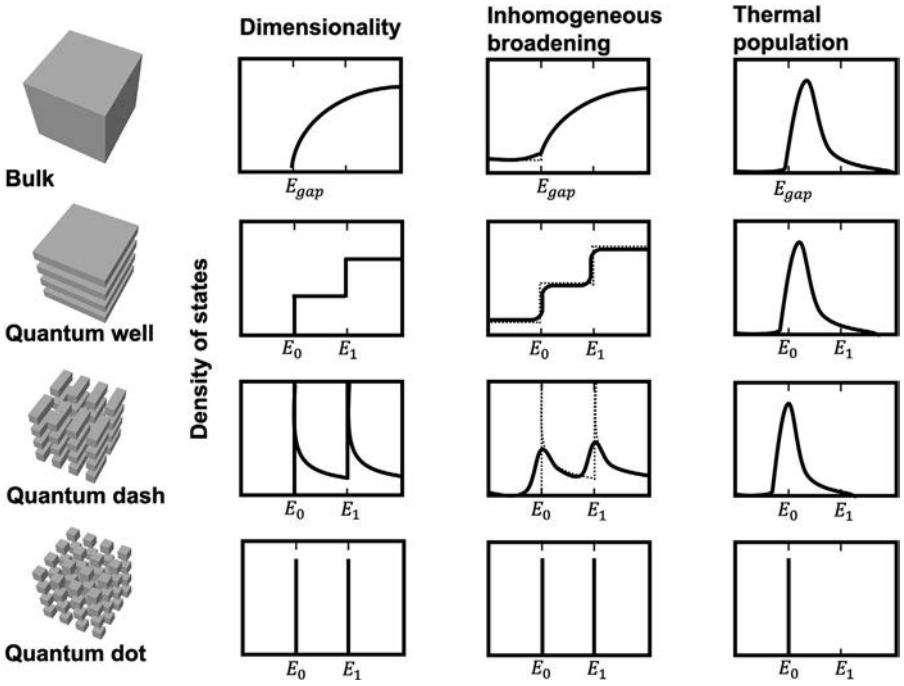

Fig. 5.1 Semiconductor structures with different degrees of dimensionality: bulk (3D), quantum well (2D), quantum dash (1D), and quantum dot (0D). The impact of the different degrees of dimensionality, inhomogeneous broadening, and thermal population on the density of states are shown. The gap energy is denoted by E_{gap}, whereas E_0 and E_1 represent quantized energy levels.

This confinement energy depends on the characteristics of the QW (width of the well and height of the barrier). As shown in Fig. 5.1, the DOS in a 2D system is then a function in step-like distribution with commutation relationships obeying $[\mathbf{H}, \mathbf{k_z}] \neq 0$ where **H** is the Hamiltonian (energy operator) of the quantum system. In particular, the introduction of QWs as the active layers of the DH lasers was theoretically deeply investigated. In particular, it was shown that the reduction of the threshold current directly results from the mutual action of the lowering of the DOS (favorable effect) and the lowering of the optical confinement (unfavorable effect). The paper also demonstrated that the poor performance of GaInAs-based QW lasers was due to the detrimental Auger effect, which is greater than in 3D lasers because of the higher carrier densities at which QW lasers operate [43].

The development of crystal growth and epitaxy techniques has allowed, since the 1970s, to combine many different semiconductor materials of different natures (confinement potentials, mismatch parameters, etc.). The growth of these materials achieved by successive stacking of layers of quantum thickness has given rise to efficient photonic devices incorporating QW, multiquantum wells (MQWs), and super lattices [44, 45]. These structures, which confine electrons in one direction in space,

have revolutionized the semiconductor laser fabrication. More efforts were then focused on the confinement of carriers in several directions of space, to further reduce the dimensionality of the structures studied. The progress in the fabrication of such structures, especially by electronic lithography, have allowed the fabrication of quantum wires/quantum dashes (1D systems) and QDs (0D systems) [40, 46]. The former allows a confinement of the carriers in two directions of space with commutation relationships such as $[\mathbf{H}, \mathbf{k_x}] \neq 0$ and $[\mathbf{H}, \mathbf{k_z}] \neq 0$. These structures always present a continuum of accessible states since the energy is not fully discretized in the direction of the dash nanostructures, hence there remains a one-dimensional continuum. As shown in Fig. 5.1, the DOS is therefore in the form of $1/\sqrt{E - E_n}$. Finally, QDs ultimately confine the carriers in the three directions of space. The energy of the carriers is perfectly discretized in the three directions, and the energy spectrum is therefore totally discrete like that of an atom [8, 38]. In QDs, all carriers are strongly localized (typical within a volume $\approx 10^3$ nm^3). It is this property of the dots which makes their main interest for practical applications because they constitute artificial atoms. Fig. 5.1 shows that the DOS of such a system is a Delta-like distribution $\delta(E - E_n)$ at the energy of each discrete quantum level E_n. The situation is thus very different from the 2D and 1D systems since, in the dots, there are no more energy continuum. In practice, QDs have lateral extensions in all three directions of space smaller than the de Broglie wavelength of the charge carriers. As a consequence of that, they have to be neither too small, otherwise no bound state is present, nor too large, meaning that the energy difference ΔE between sublevels is greater than $k_B T$ at 300 K. In addition, carriers in QDs have no well-defined wave vector namely there is no wave vector conservation and no recombination bottleneck with $[\mathbf{H}, \mathbf{k}] \neq 0$. Recombination, absorption, and gain are always excitonic (or biexcitonic) leading to a strong enhancement of the oscillator strength.

The development of QD materials results from an heuristic evolution. The first realization of QDs was nanocrystal inclusion (e.g., CdSe) in amorphous glass [47]. The dielectric environment in which these nanocrystals were elaborated proscribed for a long time their use in electrical components, and the quantum confinement was only confirmed experimentally afterwards [48]. The concept of QD lasers on the other hand was first studied by Arakawa and Sakaki in 1982 [38] and was referred back then as three-dimensional QW lasers or quantum box lasers. By assimilating real QD gain medium with QW laser under high magnetic field, experiments forecast low-threshold, high-thermal stability, and enhanced dynamic properties in QD lasers [49–52]. The fortuitous observation in 1985 of nanoclusters appearing within an InAs/GaAs superlattice, that has been later understood as Stranski-Krastanov (S-K) growth mode, opened the way to the development of these three-dimensional confined nanostructures. The S-K growth mode is one of the main underlying processes of the QD formation, which corresponds to a spinodal decomposition or submonolayer deposition [8, 9, 53]. Although in the early days, it was even difficult to grow high-quality QW heterostructures, many efforts have been devoted to overcome technological challenges [8, 54–61]. Since then, the progress made in crystal growth, as well as the numerous studies launched on this subject, have highlighted the totally discrete character of the energy spectrum of QDs. For instance, Table 5.1 depicts

Table 5.1 Threshold current density J_{th} measured in different laser structures.

Substrate	Type	J_{th} (A/cm^2)	Operating temperature (K)	Reference
GaAs	DH	10,000	300	[34]
GaAs	DH	4300	300	[33]
InP	QW	170	300	[62]
GaAs	QW	65	300	[63]
GaAs	QD	62	300	[64]
GaAs	QD	8.8	300	[13]

the threshold current density J_{th} measured in DH, QW, and QD structures [65, 66]. It is very much clear that from DH to QW, the J_{th} has been significantly reduced by three orders of magnitude, and the transition to QD lasers help to reach an unprecedented low-threshold operation at room temperature. To this end, their utilization has become very promising for replacing the currently used QWs, especially for future integrated technologies on silicon whereby many applications are foreseen even down to the quantum level implementation.

5.2.2 GaAs-based quantum dot lasers

Since the first observation of InAs QDs on GaAs substrate, initial approaches continued on the same path of developing strain-induced self-assembled QDs by molecular beam epitaxy (MBE) [54–58, 60, 61, 67–70]. Cathodoluminescence experiments revealed the delta-function-like emission characteristics of excitons in InAs/GaAs QDs [71]. The first QD laser was demonstrated by Bimberg's and Alferov's teams in 1994, the gain medium contained a singled dot layer developed by MBE [60, 72]. While strain-induced self-assembled MBE remained the mainstream growth method initially, metal-organic chemical vapor deposit (MOCVD) has also quickly been proven effective in developing InAs/GaAs QD lasers as well [15, 59, 73–82]. Some others have also attempted using patterned substrate and successfully demonstrated lasing operation; however, the threshold current density was not ideal [83]. Early studies of the QD structure for laser application was concentrated in sampling different growth conditions. Table 5.2 lists some of the important achievements in the mid-1990s to the early 2000s. InAs QDs are formed via a trade-off between the growing film strain energy and the dot surface free energy [8, 72, 92, 93]. It was shown that two sources of the strain field exist in the lattice mismatch with the substrate edge-induced strain as well as the strain-induced renormalization of surface energies, of the island facets, and of the wetting layer. Thus, the energy of a single quantum island having the shape of a pyramid with a square $L \times L$ base can be written as the following [94]:

$$\widetilde{E} = \Delta\widetilde{E}^{V}_{Elastic} + \Delta\widetilde{E}^{Renorm}_{Surface} + \widetilde{E}_{Edges} + \Delta\widetilde{E}^{Edges}_{Elastic} \tag{5.3}$$

The first term ($\sim -L^3$) is the energy of change of volume of the surface elastic energy due relaxation, the second ($\sim \pm L^2$) the change of the surface energy due to the island

Table 5.2 A nonexhaustive list of the most important works on the development of InAs-GaAs QD lasers since the first demonstration.

Year	QD composition	QD T_{growth} (°C)	Epitaxy method	QD layers	J_{th}	T_{op} (K)
1994 [60]	InAs	460–490	MBE	1	1 kA/cm^2	300
1995 [84]	$In_{0.5}Ga_{0.5}As$	510	MBE	1	0.8 kA/cm^2	85
1996 [70]	$In_{0.3}Ga_{0.7}As$	515	MBE	1	1.2 kA/cm^2	300
1996 [85]	$In_{0.4}Ga_{0.6}As$	500–550	MBE	1	650 A/cm^2	300
1996 [64]	$In_{0.5}Ga_{0.5}As$	485	MBE	3	62 A/cm^2	300
1996 [75]	InAs	485–505	MOCVD	3	220 A/cm^2	300
1998 [86]	InGaAs	512	MBE	1	270 A/cm^2	300
1998 [87]	InAs	–	MBE	2	160 A/cm^2	298
1998 [88]	InAs	–	MBE	7	82 A/cm^2	285
1999 [12]	InAs	490	MBE	1	83 A/cm^2	295
1999 [76]	InGaAs	500	MOCVD	3	210 A/cm^2	295
2000 [89]	InAs	–	MBE	1	13 A/cm^2	300
2000 [90]	InGaAs	450	MBE	3	96 A/cm^2	220
2000 [77]	InGaAs	490	MOCVD	3	110 A/cm^2	300
2001 [91]	InAs	510	MBE	6	375 A/cm^2	300
2002 [79]	$In_{0.67}Ga_{0.33}As$	485	MOCVD	3	60 A/cm^2	293

QD T_{growth}, QD growth temperature; J_{th}, lasing threshold current density; T_{op}, operating temperature.

formation, the third ($\sim +L$) the energy of the edges, and the fourth ($\sim -L \ln L$) corresponds to the energy of elastic relaxation due to the edges. The excess elastic moduli of the surface give the correction to the energy of the volume elastic relaxation, which is proportional to L^2, and corrections to all other terms are of the order of L or smaller. In practice, several parameters are involved during the growth, making the dot formations more challenging to control, hence leading to a QD size dispersion, that is, from extremely narrow emission line of single QD [71, 95, 96] to an inhomogeneously broadened gain medium [97–99].

Fabrication of QD lasers usually require growing multiple stacks of dots in the active region to increase the material gain [64, 100]. However, in doing so, careful optimization of the growth process is mandatory, because as the number of stacks increases, the strain also accumulates in each dot layer, hence necessitating using a thicker spacer in the structure, which will in turn reduce the contribution to the gain and slow down the carrier dynamics [101]. For InAs/GaAs QD lasers, the maximum number of dot layers is usually limited to 10–15 [101, 102].

Since the birth of QD lasers, the development of GaAs-based QD lasers has been extensively pursued [103]. For instance, in 1996 [64, 104], a better optimized structure was demonstrated with three dot layers and a very low room temperature threshold current density at 62 A/cm^2, a characteristic temperature of 385 K up to 300 K, and a large material gain of $\sim$105 cm^{-1}. Two years later, further breakthrough was unveiled due to the development of the "Dot-in-a-well" (DWELL) structure [12].

Such structure, in which the QDs are embedded into QWs allows a much better capture and localization of electrons into the QDs and speeds up the carrier dynamic as well as to improve the material gain due to a larger dot density up to 7.5×10^{10} cm^{-2}. In addition, with the advancement in MOCVD growth, InAs/GaAs QD lasers have been obtained with ultra-low transparency current density (<6 A/cm^2 per dot sheet) and internal losses (≈1.5 cm^{-1}) [77] with recent demonstrations exhibiting extrapolated lifetime of 5 million hours at 60°C [105]. Over time, more improvements have been further obtained in InAs/GaAs QD lasers [86, 92, 106, 107], for instance, threshold current densities down to 8.8 A/cm^2 [13], negative characteristic temperature [108, 109], high output power [77, 110], as well as prolonged device life time [79]. Furthermore, exceptional thermal stability has indeed been confirmed in GaAs-based QD, experiments demonstrated 10 Gbit/s transmission from 20°C to 70°C [14], as well as sustained CW operation at extreme temperature of 220°C, which is the highest recorded operating temperature among any kind of semiconductor lasers [21]. Recent progress has also involved tuning the GaAs-based QD lasing wavelength to other telecom bands, potentially allowing the expansion of available channels for short-reach fiber communication, hence augmenting data transmission capacity. As compared to commercial QW lasers, QD optical transmitters are much better candidates to reduce the power consumption both of the electrical pumping and the thermoelectric cooling in butterfly packaged devices [66]. In the current market, mature commercialized GaAs-based QD laser products are already provided for telecommunication applications by different companies such as Innolume GmbH and QD Laser Inc.

5.2.3 InP-based quantum dot lasers

The S-K growth has been proved to be very efficient for the realization of GaAs-based QD laser devices, with an emitting wavelength in the O-band (1260–1360 nm) that is ideal for short-reach communication links. However, since its debut, long-haul fiber communication network has always been centered in the C-band, that is, from 1530 to 1565 nm, for the simple reason that this wavelength span suffers the least loss in optical fibers (typically ∼0.2 dB/km). Therefore, it is equally necessary to manufacture QD lasers to emit around 1550 nm. While, through delicately tuned epitaxy techniques, it is possible to fabricate QDs on a GaAs substrate to emit in the 1550 nm range, the main approaches are developed around the InP substrate [78, 111, 112]. The first InAs/InP QD laser was demonstrated in 1998, initially with a lasing operation limited to 77 K [113, 114] and then at room temperature [115]. Although the InAs/InP and InAs/GaAs systems share the same material in the dots, they remain quite different from each other, mostly because the lattice mismatch in InAs/InP (3%) is smaller than that in InAs/GaAs (7%) [110]. Therefore, the challenge regarding the dot formation on InP substrates is to deal with the lattice mismatch and the complex strain distribution which tends to produce elongated dots, that is, quantum dash (QDash), a class of self-assembled nanostructures that exhibits mixed properties between quantum wire (QWire) and QD [116]. Thus, the fabrication of real InAs/InP QDs requires careful procedures to avoid the formation of QDash, for example, utilizing miscut InP(100) or InP(311)B misoriented substrates [117]. As an example, Fig. 5.2 shows

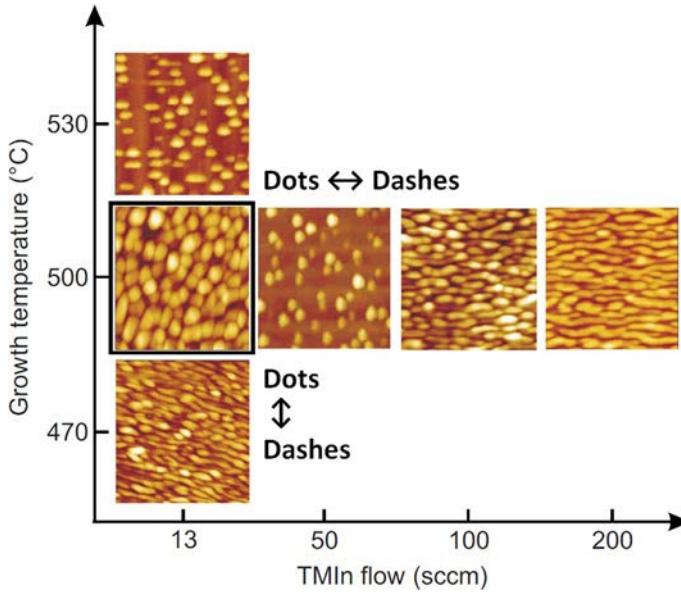

Fig. 5.2 The formation of InAs nanostructures on InP (001) as a function of trimethylindium (TMIn) flow and growth temperature.
Reprinted with permission from A. Lenz, F. Genz, H. Eisele, L. Ivanova, R. Timm, D. Franke, H. Künzel, U.W. Pohl, M. Dähne, Formation of InAs/InGaAsP quantum-dashes on InP(001), Appl. Phys. Lett. 95 (20) (2009) 203105, https://doi.org/10.1063/1.3265733, copyright 2009 AIP Publishing.

the impact of the trimethylindium (TMIn, $In(CH_3)_3$) flow and of the growth temperature on the formation of the InAs nanostructures on InP(001) substrate [118]. At 500°C, the InAs tends to form in dashes with the increase of the quantity of TMIn flow, as well as decreasing the temperature with TMIn fixed at 13 sccm.

The formation of nanostructures (dashes or dots) on InP(100) substrate strongly depends on the growth conditions and on the thickness of the InAs layer, hence a lot of efforts have been devoted to improving the growth with views of enhancing the dot density [119]. By employing chemical beam epitaxy, Allen et al. reported an InAs/InGaAsP grating coupled with external cavity QD lasers with an increased dot density of $3-6 \times 10^{10}\,cm^{-2}$ and a wavelength tuning range of 110 nm [120]. On the other hand, using GSMBE in conjunction with metal-organic vapor phase epitaxy, Lelarge et al. has obtained a very high modal gain up to $10.7\,cm^{-1}$ per layer by stacking six dot sheets in the active region [121].

Overall, although the performance of InAs/InP QD lasers are still far from those reported on GaAs-based substrate, progress has been made over the years toward demonstrating good performance for optical communications [117, 122]. For instance, in the current market, Ranovus commercializes InP-based QD comb lasers which can be used as a light source for data transmission at 100 Gbps per channel and beyond. As compared to InP(100) substrate, it has to be noted that high indexed

InP(311)B substrates can provide a higher nucleation point density, hence strongly reducing the surface migration effects and allowing the formation of more symmetrical QDs in the planar direction. Moreover, a higher dot density with a smaller dispersion in size can also be obtained. For instance, dot density of 2–7.5 $\times$ 10^{10} cm^{-2} [123, 124] with dot sizes of 3 nm in high and 30–50 nm in wide have been reported. Using an InAs/InGaAsP active region, the first InP(311)B-based QD laser was obtained including seven stack layers grown by MBE and with a dot density of 2×10^{10} cm^{-2}, displaying a lasing operation at 1400 nm at 77 K [115]. Then, using a double-capped technique, Caroff et al. achieved a significant improvement in the dot density up to 1.1×10^{11} cm^{-2} leading to a threshold current density of 23 A/cm^2 per layer [125]. One year later, by optimizing the InAs deposition process, small QDs ($\sim$20 nm) with very high density ($\sim 1.3 \times 10^{11}$ cm^{-2}) have been reported by the same group [126]. Using a strain compensation technique, Akahane et al. have demonstrated an InP(311)B-based QD laser with 20 QD stacks in the active region, and a high characteristic temperature of 148 K at room temperature [127]. Very recently, the effects of bismuth (Bi) irradiation on InAs QDs grown on an InP(311)B substrate were even investigated. It was shown that the Bi irradiation reduces the temperature dependence of the emission wavelength in the highly stacked InAs QD laser [128]. Another very recent paper also reported temperature-insensitive characteristics with an infinite characteristic temperature up to 50°C and 120°C CW operation [129]. Unfortunately, applications of InAs/InP(311)B QD lasers remain extremely limited since the fabrication requires a complex technological process not very much compatible with the industrial standards.

5.2.4 Quantum dot lasers toward integration

The initial concept of PICs was proposed by Stewart Miller in 1969 [130], at a time when the integrated electronic industry was dawning. Following the significant progress in the development of semiconductor alloy and hence the improvement of diode lasers, interest in integrated optical communication system was rapidly growing. For instance, hybrid approaches have been quickly suggested in the 1980s based on the incorporation of guided lightwave system on silicon [131–134]. However, these early designs were heavily focused on the use of complementary metal-oxide-semiconductor (CMOS) wafers [107], while building a complete on-chip optical communication system requires much more photonic building blocks like modulators, waveguides, photodetectors, amplifiers, attenuators, (de)multiplexers, etc., and it was only until the early 1990s that most of these basic optical components became available for integration [7]. Nevertheless, the first primitive PIC came out in 1986 [135], where MQW lasers and modulators were integrated together on the same InP substrate, hence forming electro-absorption modulated laser (EML) modules. These EMLs were then commercialized and deployed in WDM systems by the end of 1990s [7, 136]. In 2004, commercial dense wavelength-division multiplexing (DWDM) PIC transmitter and receiver chips were introduced, with data traffic volume of 100 Gbit/s [137]; while a decade later, these PIC devices could handle 2.25 Tbit/s transmission capacity over 40 channels [138].

Despite these rapid advances, the utilization of the common III–V alloy platforms like InP and GaAs remain limited by several aspects: (1) the relatively low refractive index contrast on these wafers does not grant a good optical mode confinement, hence waveguides generally exhibit considerable insertion loss, bending loss, and bending radii, leading to rather limited performance and bulky footprint [139, 140]; (2) commercially, wafer sizes are restricted (GaAs $\leq$6 inches, InP $\leq$4 inches), compared to that of silicon wafers (over 12 inches, or 300 mm), III–V wafer yield is lagging behind [141]; (3) limited compatibility with silicon-based CMOS technology renders the derived devices modular in nature [142, 143]. In contrast, the silicon platform offers unparalleled advantages such as high-volume industrial manufacturing, low-cost production, outstanding material compatibility (supporting integration of Ge, SiO_2, Si_3N_4, etc.), and most importantly, the possibility of leveraging highly optimized CMOS manufacturing processes and materials to achieve high integration densities [143–146]. The main challenge of silicon photonics, however, is to engineer active building blocks like laser diodes and optical amplifiers. Silicon itself is an indirect bandgap material, therefore, III–V materials need to be imported to provide optical gain in near-infrared and short-wavelength infrared range [21, 143, 147].

On the hybrid integration front, one of the initial approaches was demonstrated by Bowers et al. in 2006, where MQW laser diode was packaged on a silicon wafer via a wafer bonding technique [148]. Multiple groups have pursued this track and worked out remarkably high-performance devices [149–157]. Nevertheless, this hybrid integration approach using QW devices has its own limitation. As previously discussed, QW lasers do not exhibit intrinsic low threshold nor thermal steadiness, and these properties have indeed manifested in the reported PICs [148, 150, 152, 156]. Since the ultimate goal of silicon photonics is to integrate PICs close to heat-radiating CMOS-based digital circuits, device cooling can become exceedingly challenging [21]. To this end, due to the ultimate carrier localization, QD laser displays more reliable characteristics, thus it can be considered as a much better suited candidate in contrast to its QW counterparts [23]. Lately, industrial institutions like Hewlett-Packard Enterprise and Cisco have started to embrace hybrid III–V QD/Si solutions [158, 159].

On the other hand, hybrid integration often requires extraordinarily complicate and precise alignment in the copackaging process [21] that can potentially compromise the scalability of the III–V/Si chip [40, 46, 143]. Thereupon, the monolithic approach—heterogeneous integration of III–V compound on silicon was proposed [160]. On this stage, QW device is no longer a decent option, as monolithic-grown QW lasers, due to their structural nature, can be awfully sensitive to the crystal defects like the common TDs. As aforementioned, QD lasers, however, are rather immune to this specific issue, thanks to the fact that QD gain media consisting of individual dots [40, 46, 147]. The 3D confinement provided by QDs prevents carriers from migrating to dislocations. In other words, the efficient carrier capture by QDs, combined with the localized nature of excitons hinders the carrier diffusion toward dislocations making QDs powerful candidates for achieving efficient light-emitting devices on silicon. Since the demonstration of the first epitaxially grown QD array on Si wafer by Gérard et al. in 1996 [161], as well as the first room-temperature QD laser monolithically grown on Si wafer by Mi et al. in 2005 [162], this approach has drawn massive attention from

academics and industries. In 2008, the first QD laser directly developed on silicon operating at 1.3 μm was introduced by Arakawa's group [163]. Following this significant development, resources are pooled into improving the epitaxy growth [157, 164, 165]. Before long, TD interference has been largely reduced [20], pushing the QD device performance at the height and even beyond that of the native substrate level mostly with MBE [143], and more recently by demonstrating a fully CMOS-compatible silicon approach by MOCVD direct heteroepitaxy, the latter being inferred more desirable for high-volume production [166]. Very recently, novel QD and QDash material systems have also been demonstrated for silicon integration [167–170], bringing more optical functionalities on to Si platform, and unleashing even more potential of silicon photonics into industrial applications [171]. In this context, Tower Semiconductor and Quintessent also announced a partnership to create a foundry silicon photonics platform with integrated QD Lasers [172].

Moreover, the insensitivity of QD lasers against external reflection offers a workaround to the optical feedback issue in photonic integration. Usually, there are many interfaces on a PIC chip, for example, between different materials, between building blocks, as well as from the passive and active interfaces/transition; all can potentially generate unwanted parasitic reflections that would destabilize the laser and render the optical signal transmission inoperable. Up to date, there are still no low-cost and efficient solutions to incorporate an optical isolator to overcome such obstacle. QD lasers, however, inheriting excellent feedback resistance can resist high amount of optical reflections [173] and operate without an optical isolator [23].

5.3 Noise properties of quantum dot lasers

Low noise semiconductor lasers are required in many areas such as high-performance coherent communications [174], radio-frequency (RF) photonics [175], optical atomic clock [176], frequency synthesis [177], spectroscopy [178], and distributed sensing systems [179]. In semiconductor lasers, quantum fluctuations alter both intensity and phase of the optical field, hence leading to frequency and intensity noises [180]. The frequency noise (FN) determines the spectral linewidth of the laser. Apart from the FN, the optical sources with low relative intensity noise (RIN) are highly desired not only for optical communication systems, but also for radar-related applications. This section highlights the narrow linewidth and low RIN operation of QD lasers.

5.3.1 Spectral linewidth

The FN in semiconductor lasers results from low-frequency flicker noise, spontaneous emission noise, as well as carrier generation and recombination noise. The flicker noise arises from current source, thermal fluctuations, and internal electrical noise. The remaining noise sources are white noise and govern the intrinsic spectral linewidth of the laser, which is fundamentally driven by a phase diffusion process contributed from both spontaneous emission and phase-amplitude coupling effect. Fig. 5.3 schematically illustrates the phase-amplitude coupling effect on the phase

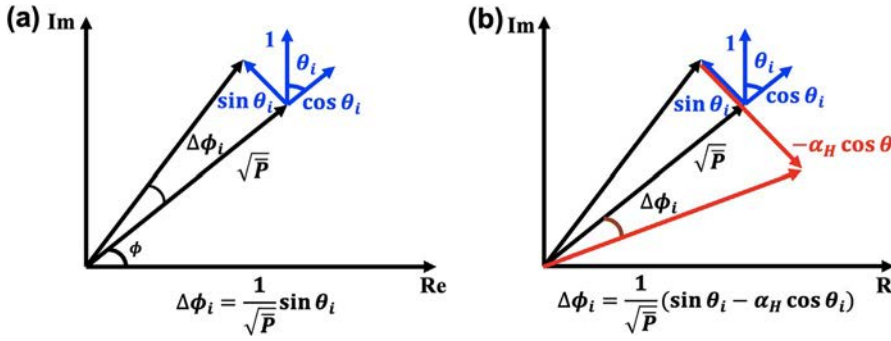

Fig. 5.3 Schematic comparison of the phase diffusion ($\Delta\phi_i$) of the lasing field between direct action of the spontaneous emission events only (A) and joint action of both spontaneous emission events and phase-amplitude coupling (B). The corresponding phase change for each case is indicated by the relationship, where the amplitude and the phase of the lasing field are denoted by $\sqrt{\bar{P}}$ and ϕ, respectively.

diffusion of the lasing field. The linewidth enhancement factor (α_H-factor) is associated with the interaction between the intensity and phase of the lasing field and is used to quantitatively describe the phase-amplitude coupling effect. The spectral linewidth of semiconductor lasers is expressed by the modified Schawlow-Townes expression [181]:

$$\Delta\nu = \frac{\Gamma g_{th} v_g^2 \alpha_m h\nu}{4\pi P_0} n_{sp}(1+\alpha_H^2) \tag{5.4}$$

where Γg_{th} is the threshold modal gain, α_m is the transmission loss, $h\nu$ is the photon energy, P_0 is the optical output power, n_{sp} is the population inversion factor, and ν_g is the group velocity. For a Fabry-Pérot resonator, the α_m can be expressed as

$$\alpha_m = \frac{1}{2L}\ln\left(\frac{1}{R_1 R_2}\right) \tag{5.5}$$

where L is the cavity length, and R_1 and R_2 are the power facet reflectivity. From Eq. (5.4), the spectral linewidth can be reduced not only by decreasing the α_m or the α_H-factor, but also by increasing the output power P_0. The decrease of the α_m can be achieved by means of increasing the cavity length or the facet reflectivity. An example is a fully integrated extended distributed Bragg reflector (DBR) laser with ~1 kHz linewidth and a ring-assisted DBR laser with less than 500 Hz linewidth [182, 183].

Furthermore, the definition of the spectral linewidth can be equivalently reexpressed in terms of quality factor by [184]

$$\Delta\nu = \frac{\pi h\nu^3}{QQ_{ext}\eta_d(I-I_{th})} n_{sp}(1+\alpha_H^2) \tag{5.6}$$

where the total quality factor (Q-factor), internal quality factor (Q_i-factor), and external quality factor (Q_{ext}-factor) can be defined as [184]

$$Q = 2\pi\nu\tau_p = \frac{2\pi\nu}{\nu_g(\alpha_i + \alpha_m)} \tag{5.7}$$

$$Q_i = \frac{2\pi\nu}{\nu_g\alpha_i} \tag{5.8}$$

$$Q_{ext} = \frac{2\pi\nu}{\nu_g\alpha_m} \tag{5.9}$$

with τ_p is the cavity photon lifetime, ν is the laser frequency, and α_i is the material loss. The three quality factors are linked by

$$\frac{1}{Q} = \frac{1}{Q_i} + \frac{1}{Q_{ext}} \tag{5.10}$$

Therefore, in Eq. (5.4), the modal gain $\Gamma g_{th} = \alpha_i + \alpha_m$ is replaced with its expression versus total quality factor with $\frac{2\pi\nu}{\nu_g Q}$, mirror losses α_m by $\frac{2\pi\nu}{\nu_g Q_{ext}}$ as well as the optical output power P_0 by $\eta_d(I - I_{th})$, with η_d the external differential efficiency and I_{th} the threshold current. From Eq. (5.6), the spectral linewidth can be always reduced by increasing the Q-factor through the increase of the cavity photon lifetime and the decrease of the losses (see Eq. 5.7). For example, one solution based on considering a distributed feedback (DFB) laser was proposed wherein light is generated from the III–V material and stored into the low-loss silicon material. An initial design made with QW technology and having a high Q unveiled spectral linewidths five times smaller than any other semiconductor lasers [151, 185]. Linewidth reduction can also be achieved by using a gain medium made with self-assembled QDs from which the shape of the DOS as well as the carrier confinement can substantially improve the laser performance. Therefore, spectral linewidths below 100 kHz have been typically reported for both InAs/GaAs and InAs/InP QD lasers [16, 103, 186–190].

In addition to that, reducing the spectral linewidth can be achieved due to the α_H-factor of QD lasers that can be minimized and stabilized over a wide temperature range [191] including at very high temperature (200°C) [192]. To develop a high-performance single-mode source for high-temperature operation, a design relying on a large optical wavelength detuning (OWD) can be utilized [193]. The OWD refers to the optical frequency mismatch between the DFB wavelength and the optical gain peak. The OWD varies with temperature due to the different temperature-dependent variation of Bragg wavelength and optical gain peak [194]. In particular, the OWD technique allows for a high output power as well as a high side-mode suppression ratio (SMSR) near the lasing wavelength over a wide temperature range. Fig. 5.4 depicts the α_H-factor of an InAs/GaAs QD DFB laser with OWD as a function of temperature, at twice the laser's threshold. By increasing the temperature from 15°C to 75°C, the OWD reduces from 30 to 0 nm. Here, the InAs/GaAs QD DFB laser exhibits excellent

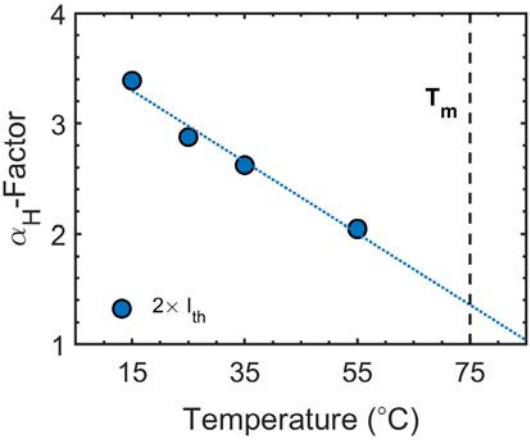

Fig. 5.4 Linewidth enhancement factor (α_H-factor) as a function of temperature at twice threshold for the QD DFB laser. The optimum temperature condition at 75°C is marked by the *dashed black line*.

temperature stability with threshold current as low as 6 mA at 55°C. In addition, the OWD reduction is associated with an increase of differential gain, hence leading to a decrease of α_H-factor from 3.4 to 2 when the device temperature is increased from 15°C to 55°C. If the temperature is raised close to the optimum condition T_m (represented by the vertical dashed line in Fig. 5.4), the α_H-factor can even be further reduced closed to its optimum value, which is expected to be around 1.4 at 75°C.

Fig. 5.5A gives the optical spectrum when the temperature is increased from 15°C to 55°C. The DFB laser exhibits strong and robust single mode emission with an SMSR well beyond 40 dB. Therefore, minimizing the α_H has a direct impact on the spectral linewidth at high temperatures. The latter is measured through a self-heterodyne interferometric method. Fig. 5.5B presents the temperature-dependent linewidth as a function of the bias current ranging from $2 \times I_{th}$ to $4.5 \times I_{th}$. All linewidths are extracted from a Voigt fitting. In any condition, the spectral lines are outstanding below 600 kHz with a minimum of 179 kHz. At 55°C, the linewidths

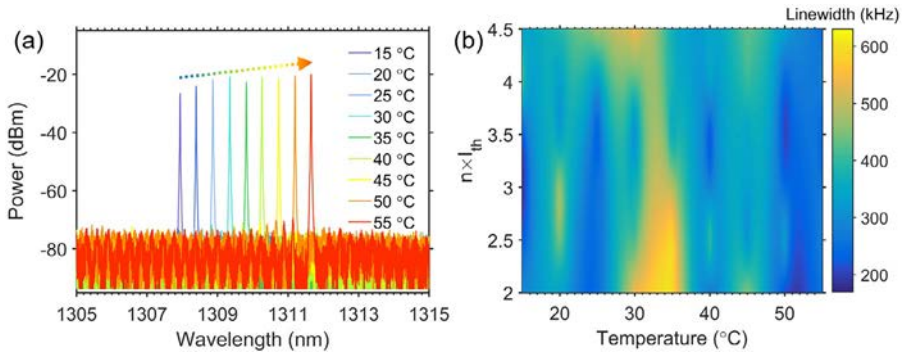

Fig. 5.5 (A) Optical spectra of QD DFB laser under different temperature. (B) The mapping for the Voigt fitted linewidth at different bias current and temperature.

are all below 300 kHz and flatten out as the current increases. Therefore, the smaller α_H-factor contributes to further narrowing and stabilizing the FN at high temperatures. Let us stress that epitaxial QD DFB lasers on silicon also show some extraordinary narrow linewidth characteristics. For instance, Fig. 5.6A displays the structure of a QD DFB laser on silicon, whereas Fig. 5.6B illustrates the corresponding FN spectrum from which a spectral line of 26 kHz is extracted [190]. Very recently a record-narrow intrinsic linewidth of 1.62 kHz was reported on an InAs/GaAs QD laser at 55°C with a minimum averaged RIN of only −166 dB/Hz between 0.1 and 20 GHz at 25°C [195].

To further squeeze the optical linewidth down to its physical limit, on-chip self-injection locking (SIL) is an emerging technology. By taking advantage of the ultra-high-quality factor of silicon nitride (SiN) microresonator [196], self-injection-locked semiconductor lasers can achieve Hertz-level optical linewidth [197].

An example is given in Fig. 5.7A where the linewidth of a QD DFB laser optically coupled to a high-Q SiN resonator is predicted to be at the Hz-level [198]. The calculation of the spontaneous emission limited linewidth combines the gain clamping and frequency locking of composite-cavity modes, describing details of emission spectra from below to above lasing threshold [198]. Fig. 5.7B shows the simulation of the ASE spectrum during the transition to narrow linewidth operation. Above the lasing threshold, the lineshape deviates from the Lorentzian function below threshold to a better fit of a Gaussian function. Fig. 5.7C reveals the minimum lasing linewidth as a function of effective coupling between III–V and SiN sections. The curves are for nonresonant (black solid), resonant wide (red dotted), and resonant narrow (blue dashed) configurations. Indeed, the simulations suggest the possibility of laser linewidth reduction by six orders of magnitude from that of the high-Q passive cavity and the FWHM of 0.6 Hz with SiN cavity $Q = 6 \times 10^7$ is achieved. The theoretical

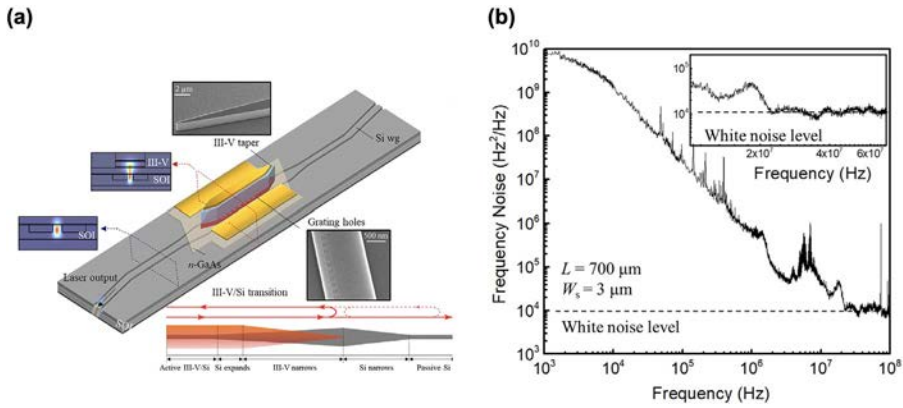

Fig. 5.6 (A) Schematic representation of a QD DFB laser on silicon; (B) corresponding frequency noise spectrum.
Reprinted with permission from Y. Wan, C. Xiang, J. Guo, R. Koscica, M.J. Kennedy, J. Selvidge, Z. Zhang, L. Chang, W. Xie, D. Huang, A.C. Gossard, J.E. Bowers, High speed evanescent quantum-dot lasers on Si, Laser Photonics Rev. 15 (2021), https://doi.org/10.1002/lpor.202100057, copyright 2021 Wiley-VCH GmbH.

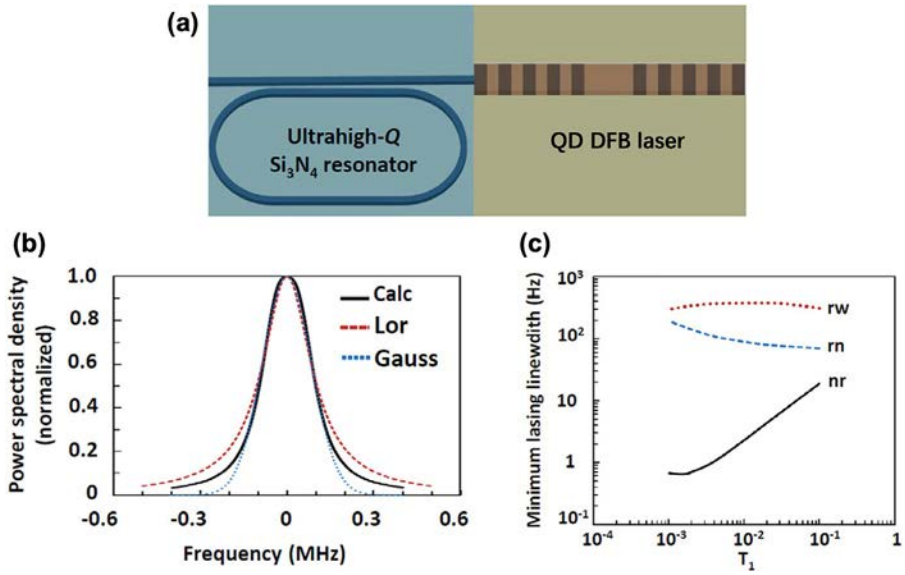

Fig. 5.7 (A) Schematic representation of a QD DFB laser optically coupled to a high-Q SiN resonator. (B) Amplified spontaneous emission spectrum from III–V/SiN laser above lasing threshold ($1.1 \times I_{th}$). (C) Minimum lasing linewidth as a function of effective coupling between III–V and SiN sections. The *curves* are for nonresonant (nr, *black solid*) and resonant wide (rw, *red dotted*), and resonant narrow (rn, *blue dashed*) configurations.
Reprinted with permission from W.W. Chow, Y. Wan, J.E. Bowers, F. Grillot, Analysis of the spontaneous emission limited linewidth of an integrated III-V/SiN laser, Laser Photonics Rev. (2022) 2100620, https://doi.org/10.1002/lpor.202100620, copyright 2022 Wiley-VCH GmbH.

approach used to describe the linewidth of the III–V/SiN laser relies on using composite-cavity eigenmodes to analyze the combination of the III–V section combined with the passive SiN resonator. It includes a multimode laser interaction to treat mode competition and wave mixing, a quantum-optical contributions from spontaneous emission, and composite laser/free-space eigenmodes to describe outcoupling and coupling among components within an extended cavity. This approach is similar to that incorporating the Langevin noise providing that it added the complication of having a complex resonator geometry and a more consistent treatment of outcoupling. Given the above elements, the starting point of the linewidth analysis consists of deriving the equation of motion for the photon annihilation operator in a composite-cavity mode such as

$$\frac{dA}{dt} = (g - \gamma_{cav}/2)A - \beta AA^{\dagger}A + G \tag{5.11}$$

where g and β are the linear and nonlinear amplitude gain coefficients, and G is the Langevin force operator from spontaneous emission. Neglecting the photon number fluctuations, the quantum optical contribution to the frequency-determining equation can therefore be expressed such as

$$\frac{d\phi}{dt} = \frac{i}{2\sqrt{n_p}}[G(t)e^{i\phi(t)} - G^{\dagger}(t)e^{-i\phi(t)}] \tag{5.12}$$

For the correlations involving the Langevin force operators, it becomes for the second-order correlation:

$$\langle G^{\dagger}(t)G(t')\rangle + \langle G(t')G^{\dagger}(t)\rangle = 2\gamma_{cav}\delta(t-t') \tag{5.13}$$

The delta function describes the discontinuous changes in intensity and phase during spontaneous emission events. As for the correlation associated with the phase, it reads as follows:

$$\langle \phi(t)\phi(t)\rangle = \gamma_{cav}t/2n_p \tag{5.14}$$

with n_p the number of photons. Finally, to account for phase diffusion due to spontaneous emission, a damping term is furthermore incorporated to the semiclassical frequency determining equation. Overall, it is pointed out that the linewidth reduction first occurs after reaching the threshold due to gain clamping, as for single-cavity lasers according to the Schawlow-Townes description. Then, there is an intermediate dynamical region, where locking to the high-Q SiN passive resonator begins to take place. Finally, at sufficiently high injection current, total locking of III–V laser and SiN resonator is achieved, resulting in significant linewidth reduction, up to as much as seven orders of magnitude reduction compared to that of the high-Q SiN passive resonator. Depending on whether one consider QW or QD active regions, the extension and laser performance differ throughout the stages due to different linewidth enhancement factors. Nevertheless, both can produce linewidth narrowing down to Hz-level. Also it is known that solitary QW lasers suffer from high α_H that is even larger at injection current and that QD size dispersion gives rise to strong homogeneous and inhomogeneous broadening effects. Fig. 5.8A and B demonstrates that the utilization of the SiN microring resonator enables QW or QD integrated III–V/SiN devices when locked—to properly bypass these aforementioned drawbacks, as both devices are able to achieve similar spectral linewidth performance, even at higher current injections. On the top of that, Fig. 5.8C confirms that QD devices do so more efficiently, while the QW emits higher optical powers [199].

5.3.2 Relative intensity noise

The RIN of semiconductor lasers describes the fluctuations of laser optical power, which mainly results from the intrinsic frequency fluctuations caused by spontaneous emission and carrier noise [19]. The RIN of the laser is defined as [41]

$$RIN = \frac{\overline{i^2}}{\overline{I_{laser}}^2} = \frac{\sigma_{laser}^2}{\overline{I_{laser}}^2} \tag{5.15}$$

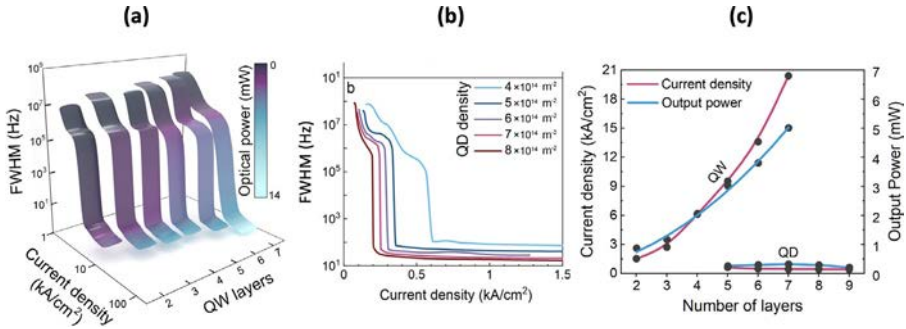

Fig. 5.8 (A) Linewidth and lasing characteristics of the integrated III–V/SiN QW laser as a function of the injected current density and number of QW layers; (B) linewidth FWHM of the III–V/SiN QD laser as a function of the injection current density for different QD densities; (C) comparison of the lock conditions, where the steep reduction in the intrinsic linewidth occurs, in terms of the required injection current density and corresponding output power as functions of the number of layers for the integrated III–V/SiN QW and QD lasers. Reprinted with permission from E. Alkhazraji, W.W. Chow, F. Grillot, J.E. Bowers, W. Yating, Linewidth narrowing in self-injection-locked on-chip lasers, Light Sci. Appl. 12 (161) (2023) 1–10, https://doi.org/10.1038/s41377-023-01172-9, copyright 2023 Springer Nature.

where $\overline{I_{laser}}$ is the average laser intensity, i is the temporal fluctuations of the laser intensity, and σ^2_{laser} is the variance of the laser noise. In the experiment, the RIN can be calculated as follows [200]

$$RIN(dB/Hz) = 10 \times \log_{10}\left[\frac{(S_{Total} - S_{Thermal})/(RBW \times G) - S_{Shot}}{P_{DC}}\right] \tag{5.16}$$

where S_{Total} is the total noise measured by the electrical spectrum analyzer (ESA), $S_{Thermal} = 4k_BT/R_L$ is the thermal noise with k_B the Boltzmann constant, T the temperature, and R_L the load resistance of the ESA. The thermal noise is determined when the laser is turned off and is independent on the optical power. The shot noise is defined such as $S_{Shot} = 2qI_{DC}R_L$ with q the elementary charge and I_{DC} the DC current. Finally, P_{DC} is the electrical DC power, RBW the resolution bandwidth of the ESA, and G the total gain of the experimental setup.

The RIN degrades the signal-to-noise ratio of laser source and increases the bit-error rate (BER), hence affecting the performance of high-speed communication system [41]. In LIDAR-related applications, the intensity noise of the laser source is required to be close to the shot noise [201]. In continuous-variable quantum key distribution (CV-QKD) using coherent states, any noise beyond the obligatory quantum shot noise can crucially affect the security of the resulting key. Therefore, the utilization of quiet opto-electronics sources and detectors operating at the shot noise level is mandatory [202, 203]. Typical InAs/GaAs and InAs/InP QD lasers exhibit RIN levels as low as −160 dB/Hz [204, 205]. Furthermore, the RIN of the sole ES emission is more compressed than that of the sole GS emission [206]. InAs/GaAs QD comb lasers

also showed remarkable low RIN operation of −160 dB/Hz, which meets the requirements for high-speed PAM-4 modulation and WDM networks standards [207]. More recently, a RIN below −165 dB/Hz was reported on an InAs/GaAs QD DFB laser with laterally coupled dielectric gratings [208]. Last but not least, it was shown that epitaxial QD lasers exhibit a higher RIN level typically from −140 to −150 dB/Hz for silicon-based lasers while that of germanium based is much higher of −120 dB/Hz [209–211]. Such a degradation is due to the high density of crystalline defects including primarily TDs and antiphase domains.

Fig. 5.9A–C compares the bias current dependence of the RIN characteristics between an epitaxial QD lasers on silicon (with and without p-doping) and a QW laser. The RIN level is relatively high at near-zero frequency due to the mixing between the thermal noise, the current source noise, and the mode partition effect [211]. For each bias current, the RIN spectrum exhibits a resonance peak at several GHz corresponding to the relaxation oscillation frequency (ROF). With the increase of the bias current, the amplitude of the resonance peak and the whole RIN level are suppressed and saturated at −150 dB/Hz for both undoped and p-doped cases. By contrast, the QW laser displays a higher RIN of −135 dB/Hz due to a weaker damping between electron photon energy-state populations. Fig. 5.9D depicts the comparison of the averaged RIN values (between 1 and 4 GHz) of the QD lasers for a temperature range from 15°C to 35°C. Without p-doping, the RIN increases from −140 dB/Hz at 15°C to −134 dB/Hz at 35°C while the other stays rather constant thanks to the p-doping induced stable threshold current with temperature. Further

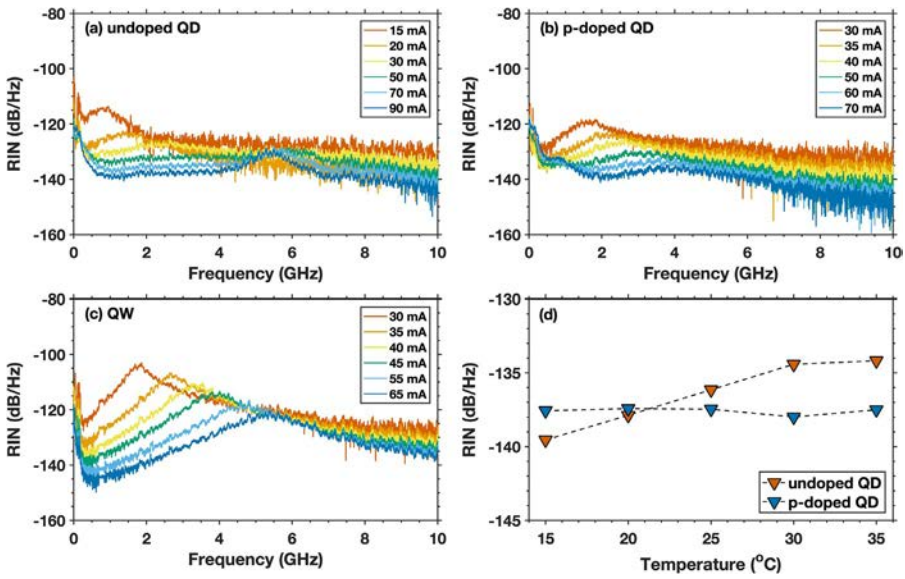

Fig. 5.9 RIN spectra up to 10 GHz versus various bias current for (A) undoped QD laser, (B) p-doped QD laser, and (C) QW laser. (D) Comparison of averaged RIN values from 1 to 4 GHz with temperature between undoped QD and p-doped QD lasers.

enhanced temperature performances can be achieved in QD lasers by spatially separated dual-doping which includes p-type modulation doping in barrier layers and n-type direct doping in QDs simultaneously [212].

5.3.3 Dynamic properties

The intensity noise is driven by the ROF (f_{RO}) and the damping factor γ which can be both extracted from the RIN spectrum through the expression [41]:

$$RIN(\omega) = \frac{a + b\omega^2}{\left(\omega^2 - \omega_{RO}^2\right)^2 + \gamma^2\omega^2} \tag{5.17}$$

where ω_{RO} is the angular ROF, and a and b are coefficients used for the curve-fitting. Fig. 5.10A shows the linear evolution of damping factor with the squared ROF following the relationship $\gamma = Kf_{RO}^2 + \gamma_0$ with K a constant parameter and γ_0 the damping factor offset inversely proportional to the differential carrier lifetime. The damping factor of the undoped QD laser exhibits a large value up to 33 GHz with a K-factor of 4.7 ns and a γ_0 of 1.5 GHz. When the hole doping is introduced, the damping and the K are both reduced to 27 GHz and 1.7 ns, respectively, leading to a shorter carrier lifetime. On the contrary, the damping factor of the QW laser rises steadily to 10 GHz with a smaller K-factor of 0.2 ns and larger γ_0 of 4.0 GHz. Thanks to a higher occupation of the QD hole levers producing a stronger reduction of the hole scattering rates [213], the hole doping is proved to be efficient for achieving better modulation capability [214, 215]. In this circumstance, the improvement remains on the margin. For instance, the 3-dB modulation bandwidth $f_{3dB,max} = 2\pi/K$ of the QD laser only increases from 1.9 to 5.9 GHz thanks to the p-doing, whereas the QW laser naturally displays a 38.6 GHz optical bandwidth. Although the dynamic properties can be further improved by better optimizing the laser structure and the doping level in the active region [216, 217], the large damping of QD lasers is

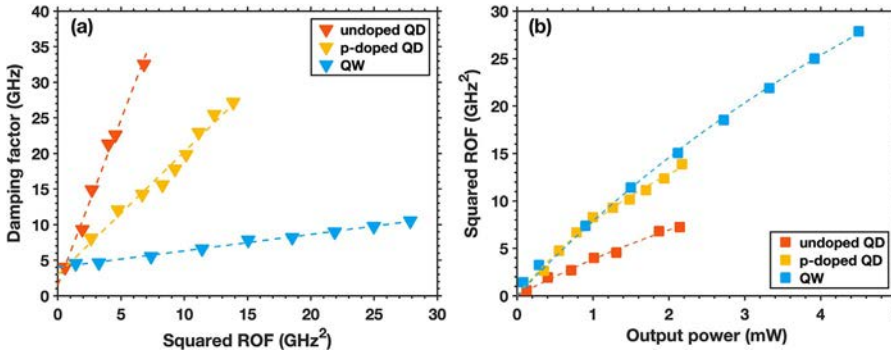

Fig. 5.10 (A) Damping factor versus the squared relaxation oscillation frequency and (B) squared relaxation oscillation frequency versus the output power for undoped QD laser, p-doped QD laser, and QW laser, respectively.

detrimental for direct modulation applications but remains highly beneficial for reflection insensitivity as discussed hereinafter.

In semiconductor lasers, the ROF is also related to the gain compression, which describes the decrease of the gain with optical intensity. This nonlinear effect is caused by several physical processes such as carrier heating (CH), and spatial and spectral hole burning (SHB) [218, 219]. In the case of sole GS emission QD laser, the gain compression can be extracted by curve-fitting the squared ROF as a function of the output power following the expression $f_{RO}^2 = \frac{AP}{1 + \epsilon_P P}$ [186, 219] where ϵ_P is the gain compression factor related to the output power P and A is the modulation efficiency. Then, the gain compression factor related to photon density (S) can be directly retrieved from $\epsilon_S = \epsilon_P P/S$. Applying the curve-fitting on Fig. 5.10B, a gain compression factor of 5.7×10^{-16} cm^3 is found for the undoped QD laser and 1.0×10^{-15} cm^3 for the p-doped one due to the increased internal loss. The gain compression is found larger in QD lasers in comparison with that of the QW laser for which a value of 3.1×10^{-17} cm^3 is extracted. Those values are in agreement with prior works already published in the literature [41, 186, 219]. Together, these results confirm that the structure of the QDs sets the limit of the modulation capability due to the high damping and large gain nonlinearities [215, 220]. High-speed properties of directly modulated QD lasers are discussed later on in this review chapter. Nevertheless, using an optimized p-doping engineering is a clear gain lever effect for reaching high-quality QD materials that are required in silicon photonics applications.

5.4 Reflection insensitivity of quantum dot lasers

The integration of optical functions on a microelectronic chip brings many innovative perspectives, along with the possibility to enhance the performance of PICs [143]. However, each additional integrated component can produce external optical feedback to any on-chip laser. Therefore, the laser can become unstable outputting complex nonlinear dynamics like periodic or chaotic oscillations. The III–V/Si hybrid lasers using flip-chip or wafer-bonding technology have already shown good performance but remain quite sensitive to optical feedback [151, 221, 222]. With this technology, the different parasitic reflections result from the vertical grating couplers and the multiple passive and active interfaces/transitions between the III–V material and the silicon [223–225]. Furthermore, the amplified spontaneous emission (ASE) noises generated by active building blocks such as semiconductor optical amplifiers (SOAs) or active waveguides integrated in the PICs can also be responsible for additional incoherent feedback [226]. Altogether these various sources of reflection can be very problematic regarding the laser stability.

To protect the on-chip laser from parasitic optical feedback, integrated optical isolators are required to maintain the laser functionality and stability. On-chip optical isolators are usually based on spatiotemporal modulation, nonlinear, or magneto-optic effects [227]. Although high-performance on-chip optical isolators are already reported, the nonnegligible insertion loss associated with a complicated fabrication process currently limit their applicability in silicon technologies [228, 229].

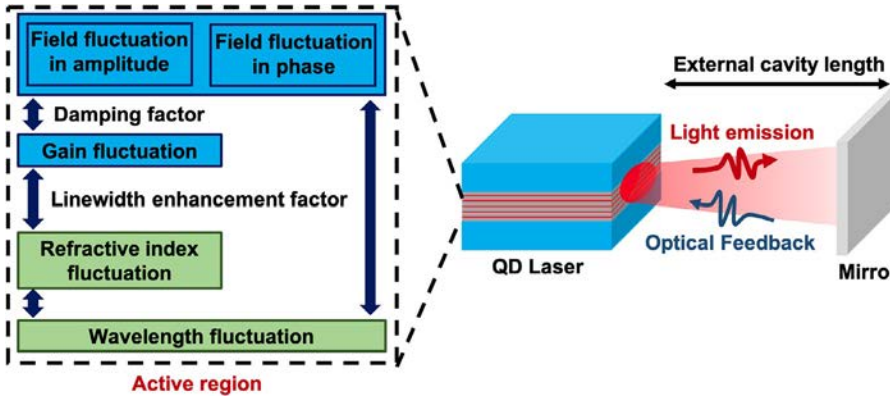

Fig. 5.11 Fundamental processes involved in a quantum dot laser subject to external optical feedback.

Therefore, the development of feedback insensitive on-chip laser sources remains nowadays a major objective for silicon photonics-related applications. In this context, we show hereinafter that semiconductor QD lasers monolithically grown on silicon can offer a strong feedback immunity while preserving low-cost, high-yield, energy-efficient, and a much better scalability [230].

Fig. 5.11 schematically describes the fundamental processes involved when a semiconductor QD laser operates under optical feedback. The phase-amplitude coupling in the active region is represented by field fluctuations both in amplitude and phase. The feedback coupled into the laser cavity by the output facet leads to a perturbation of the photon density. The field fluctuation in amplitude is modulated by the damping effect and then connected to the carrier density and optical gain. The gain fluctuation affects the refractive index through the α_H-factor, which results in a shift of the lasing wavelength. Furthermore, the field fluctuation in phase caused by the returned field is also related to wavelength fluctuations. In some cases, the interaction of the intensity and phase loop can produce laser severe instabilities such as chaotic oscillations (coherence collapse) [231–233].

In optical communications, the feedback sensitivity is usually analyzed through the critical feedback level (r_{crit}), which corresponds to the birth of the laser destabilization associated with the first Hopf bifurcation [234]. The feedback strength r_{ext} is defined as the ratio between the returned power in the laser cavity (P_{return}) to the free-space emitted laser power (P_{out}) at the coupling facet, such as $r_{ext} = P_{return}/P_{out}$. For a certain feedback level, the onset of destabilization takes place at $r_{ext} = r_{crit}$, where r_{crit} is given by [235]

$$r_{crit} = \frac{\tau_{in}^2 \gamma^2}{16 C_l^2} \left(\frac{1 + \alpha_H^2}{\alpha_H^4} \right) \tag{5.18}$$

with γ is the damping factor, $\tau_{in} = 2n_{int}L_c/c$ is the internal cavity photon round-trip time with n_{int} and L_c being the refractive index and the cavity length of the laser,

α_H is the linewidth enhancement factor, and C_l is the coupling coefficient of the laser's front facet toward the external cavity [236]. Eq. (5.18) gives insights on how to increase the feedback immunity of a semiconductor laser. Several optimization paths can be therefore considered as follows:

(1) Reducing the coupling of the laser with the external world by considering a higher front facet reflectivity [237]. For instance, using a high-power reflectivity on the rear-facet and a front-facet left as-cleaved offers a good balance between a high feedback resistance and sufficient optical output power [238]. Furthermore, the increase of the cavity photon round-trip time with longer cavities also increases the feedback resistance as discussed hereinafter.

(2) A large damping factor is beneficial for achieving a large feedback immunity. When the laser is over-damped, the gain fluctuations introduced by the photon-density variation are suppressed. Fig. 5.10 already proves that QD lasers exhibit stronger damping factor than QW lasers, which is clearly in favor of optical-isolation-free applications.

(3) Minimizing the α_H is a way of increasing the reflection insensitivity. A higher critical feedback level is also paired with a smaller α_H-factor. Semiconductor lasers with bulk and QW active region usually have α_H of about 2–5 [41]. By comparison, QD lasers can output much lower α_H values, which contributes to a higher feedback resistance [191]. However, the magnitude of the α_H mainly depends on the QD size dispersion. Therefore, it is of paramount importance to tightly control the inhomogeneous width of the gain to concentrate the oscillator strength at the resonance transition.

(4) In QD lasers, the onset of r_{crit} strongly depends on the excited-to-ground-state threshold current ratio. A robust ground state (GS) emission without switching to higher energy states usually confers a higher degree of stability [173].

(5) Engineering a laser cavity with a high Q-factor, namely a longer cavity photon lifetime [226]. Considering the quality factor (Q), the coupling coefficient C can be written as follows:

$$C = \frac{\omega\tau_{ext}}{Q}\sqrt{1+\alpha_H^2}\sqrt{r_{ext}} \tag{5.19}$$

with ω the angular frequency. This equation shows that when the Q is large enough, the C can be kept to a minimal value thus providing a relative feedback insensitivity regardless of the feedback strength [184].

Together, these knobs can be activated to enhance the laser stability against unwanted reflections [22, 213, 239], which is exactly what happens in QD lasers [24, 240, 241]. The optical feedback is known to increase the RIN of semiconductor lasers, especially under the coherence collapse operation that begins with the undamping of the relaxation oscillations, namely when the feedback strength exceeds the r_{crit}. Fig. 5.12A shows the typical RIN spectra for an InAs/GaAs QD FP laser with optical feedback both above and below the r_{crit} [24]. The measured r_{crit} is at -8 dB, which is much higher than that of QW lasers. In addition, Fig. 5.12B demonstrates that InAs/GaAs QD DFB lasers exhibit a low RIN level below -140 dB/Hz even under -8 dB external optical feedback both at 25°C and 70°C [242]. On the other hand, the RIN in QW DFB laser started to increase at feedback strength of -16 dB and became higher than -120 dB/Hz at -14 dB. These experimental results clearly pointed out that the strong feedback resistance observed in QD lasers fundamentally result from their overdamped nature.

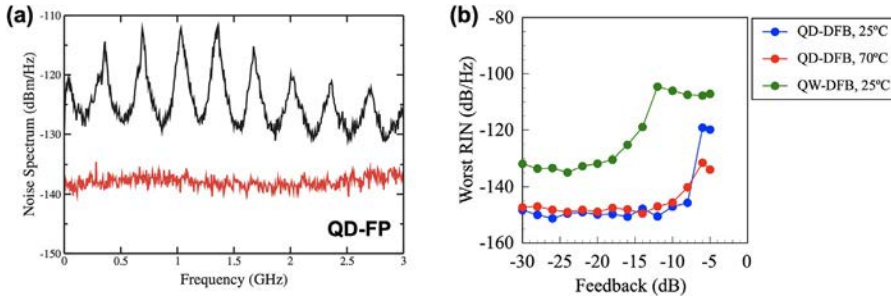

Fig. 5.12 (A) RIN spectra of InAs/GaAs QD FP laser above (*black curve*) and below (*red curve*) the critical feedback level. (B) Worst RIN value of InAs/GaAs QD and QW DFB lasers as functions of feedback strength.
(A) Reprinted with permission from D. O'Brien, S.P. Hegarty, G. Huyet, J.G. McInerney, T. Kettler, M. Laemmlin, D. Bimberg, V.M. Ustinov, A.E. Zhukov, S.S. Mikhrin, A.R. Kovsh, Feedback sensitivity of 1.3 μm InAs/GaAs quantum dot lasers, Electron. Lett. 39 (25) (2003) 1, https://doi.org/10.1049/el:20031153, copyright 2003 IET. (B) Reprinted with permission from M. Matsuda, N. Yasuoka, K. Nishi, K. Takemasa, T. Yamamoto, M. Sugawara, Y. Arakawa, Low-noise characteristics on 1.3-μm-wavelength quantum-dot DFB lasers under external optical feedback, in: 2018 IEEE International Semiconductor Laser Conference (ISLC), 2018, pp. 1–2, https://doi.org/10.1109/ISLC.2018.8516191, copyright 2018 IEEE.

Regarding silicon integration, an initial work on reflection insensitivity was achieved with a hybrid InAs/GaAs QD transmitter on silicon for core I/O applications. In this work, the QD transmitter made with a 5 × 5-mm Si photonics platform, a CMOS driver, and QD laser showed a 25 Gbit/s error-free transmission without optical isolator [243]. Thereafter, a complete feedback insensitivity was also demonstrated in the case of epitaxial QD lasers directly grown on silicon. Fig. 5.13 depicts the optical and RF spectra of the epitaxial QD laser on silicon and QW lasers with respect to the feedback strength r_{ext}. The external cavity length is 7 m (long-delay regime), which corresponds to an external cavity frequency of 14 MHz. Even though a PIC does not experience such long delay optical reflections, this configuration is studied here because it corresponds to the most stringent feedback conditions for the laser. As shown, the QD laser demonstrates a remarkable stability against optical feedback even at the maximum feedback strength of −7.4 dB, meaning that the coherence collapse start taking place beyond the r_{crit} does not even show up in the range of feedback level considered in the experiment. Only a slight red-shift of the modal wavelength is observed while the RF response does not show any sign of nonlinear oscillations. It is noted that when the external cavity is reduced below 50 cm (short-delay regime), the laser remains chaos-free up to −1.55 dB feedback strength [244]. By contrast, the QW laser is not disturbed until −25 dB, which corresponds to the r_{crit} associated with the onset of the undamping of the relaxation oscillations. At higher feedback levels, the QW laser starts experiencing the classical route to chaos leading to the coherence collapse state with strong broadening of the FP modes and intense chaotic oscillations observed in the RF domain. Let us note that the high thermal stability of the QD laser is also beneficial for maintaining this remarkable feedback insensitivity at high temperature [245].

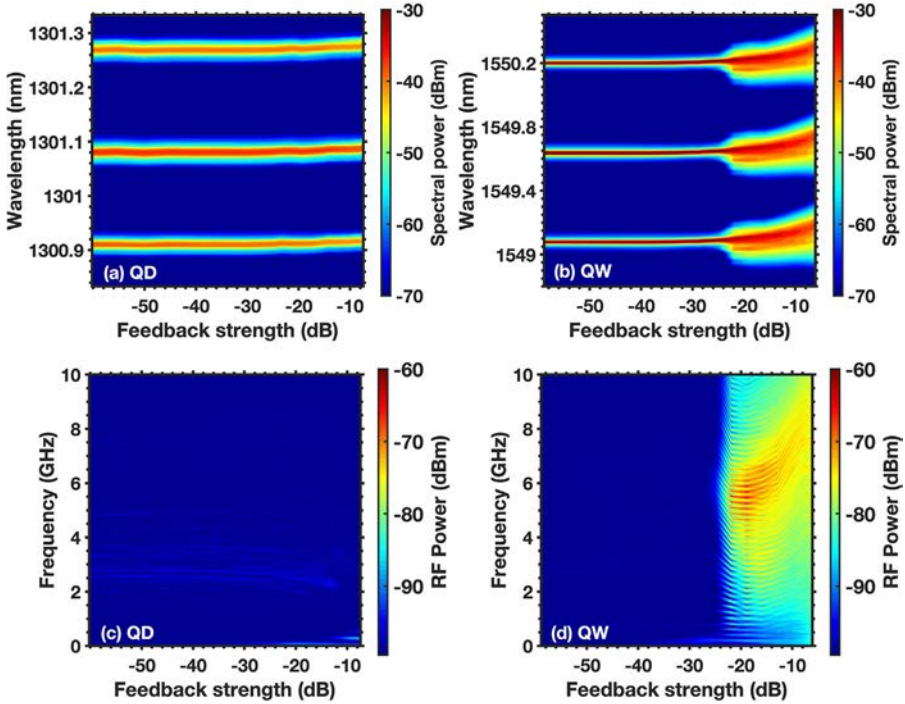

Fig. 5.13 Optical spectral mappings versus feedback strength for (A) QD lasers on silicon and (B) QW laser. Radio-frequency spectral mappings versus feedback strength for (C) QD lasers on silicon and (D) QW laser.

Test bed experiments with external modulation are also performed both for the epitaxial QD laser on silicon and the QW laser operating with and without optical feedback. Both lasers are introduced into a fiberized transmission line that includes a Mach-Zehnder external modulator and a 2 km long single mode fiber coil. The modulation format is on-off keying at 10 Gbit/s. Fig. 5.14A depicts the BER plots in term of received power for the QD laser without feedback (solitary) and under −7.4 dB maximal feedback strength for the back-to-back (B2B) configuration and after transmission of 2 km. Whatever the configuration, BER plots between the solitary case and the highest feedback level case overlap each other, hence indicating an excellent stability for high-speed transmission. The power penalty after transmission is about 2 dB at 10^{-9}, which is due to the fiber chromatic dispersion and to the residual ASE noise after propagation in the SOA. Fig. 5.14C also shows that the eye diagram keeps open after transmission with maximal optical feedback of −7.4 dB. Fig. 5.14B displays the BER plot for the QW laser only for the B2B configuration. When the QW laser is operated at −44 dB feedback strength, namely below the r_{crit}, the BER is found already affected with a 2 dB power penalty at 10^{-9}. Biasing the laser at −24 dB above r_{crit} results in a strong degradation of the transmission performance. In such a case, the laser operates in the coherence collapse regime in which the data transmission is no

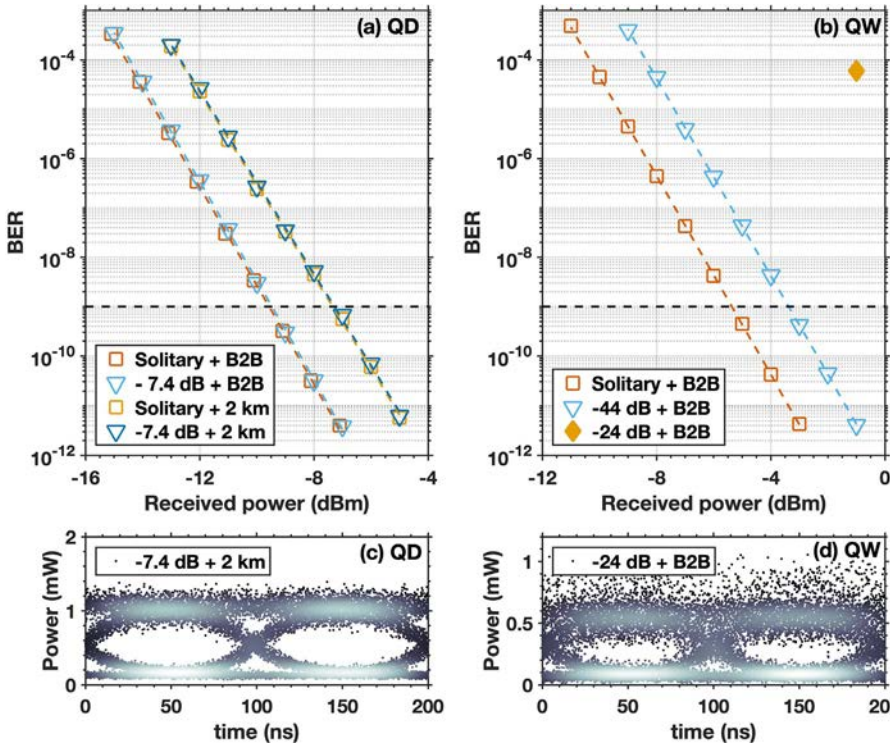

Fig. 5.14 (A) QD laser: bit error rate (BER) at 10 Gbit/s (external modulation) for back-to-back (B2B) and after transmission of 2 km with and without feedback. (B) QW laser: BER at 10 Gbit/s (external modulation) for B2B with and without feedback. (C) Eye diagram of the QD laser after transmission of 2 km with −7.4 dB feedback. (D) Eye diagram of the QW laser for B2B with −24 dB feedback.

longer possible as also confirmed by the noisy eye diagram shown in Fig. 5.14D. The corresponding BER value is measured at 6×10^{-5} for a received power of −1 dBm, which is the power limit of the photodiode in the experiment under study. Nevertheless, because this BER value is extremely large, a noise floor is definitely expected at higher received powers.

The reflection sensitivity of epitaxial QD lasers on silicon can also be evaluated under direct modulation. Direct modulation is a modulation technique, where the amplitude of the optical wave is modified by varying the strength of the laser excitation. Therefore, this feedback investigation is particularly relevant because direct modulation contributes to expand the phase-space dynamic hence resulting in adding another degree of freedom to the laser [246]. Fig. 5.15A depicts the BER of the QD laser with a direct modulation rate at 6 Gbit/s. The solitary laser without external feedback keeps an error-free operation in both B2B and transmission configurations with a BER level below 10^{-10}. Under feedback strength of −9 dB, the BER is increased up to 10^{-9} in the B2B case, then to 10^{-7} after 2 km transmission. Despite the degradation of

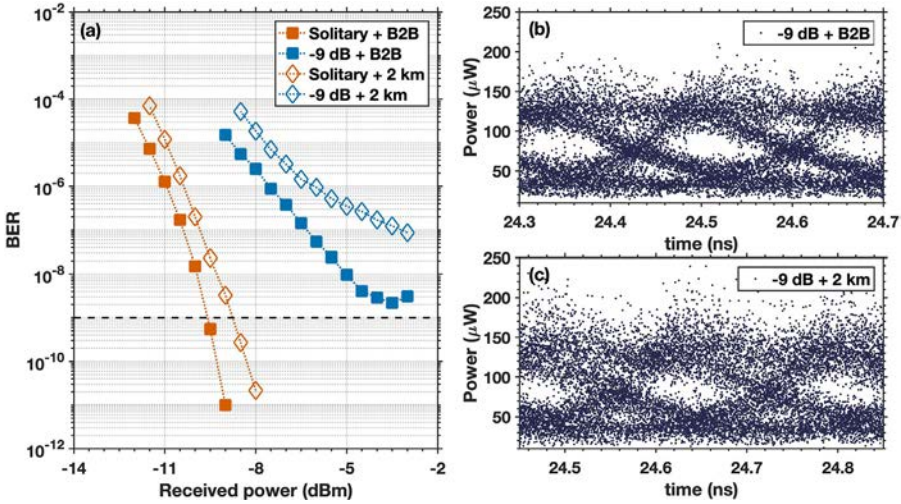

Fig. 5.15 (A) Bit error rate (BER) curve at 6 Gbit/s (direct modulation) for back-to-back (B2B) and after transmission of 2 km with and without feedback for the epitaxial QD laser. (B) Eye diagram of QD laser for B2B with −9 dB optical feedback. (C) Eye diagram after transmission of 2 km with −9 dB feedback.

the BER performance, the QD laser still shows a reasonable transmission under −9 dB optical feedback with open eyes for B2B and transmission. The IEEE 802.3ah standard indicates that the feedback tolerance of an optical interconnect should be higher than −26 dB [246]. Obviously, no short-distance data transmission is touted to experience a feedback strength as large as −9 dB, hence the actual BER can even perform better in a real application. A fortiori, a directly modulated QD laser on native substrate, also shows a high degree of resistance to back-reflections with a low BER at 10 Gbit/s under feedback strength of −9 dB [247]. To sum, these results confirm the great stability of the QD laser on silicon as compared to the QW ones, which is a peculiar feature for reflection insensitive transmissions on PICs. This remarkable feature results from various contributions. First, the low α_H-factor due to the high QD uniformity combined to a robust ground-state emission. To a lesser extent, the carrier lifetime which is reduced because of the threading dislocation density (TDD) and epitaxial defects can possibly contribute to further increase the damping factor.

5.5 Four-wave mixing in quantum dot lasers

Four-wave mixing (FWM) in microresonator has been studied extensively during the past decades, which is an important approach for on-chip OFC generation. The FWM in a single-section QD laser is also regarded as an efficient approach for self-mode locking, which leads to a phase locking of each cavity mode and a high optical bandwidth [248–250]. In particular, a single mode-locked frequency comb laser can

potentially replace the large number of lasers presently necessary for the task, thus reducing the footprint of PICs. Therefore, FWM technique exhibits a strong potential to be applied to all-optical signal processing, WDM application, and coherent communication technologies [251, 252]. Nevertheless, there is always debate on whether the mode-locking behavior is attributed to SML or unaccounted saturable absorption inside the laser cavity. The yield of SML devices remains uncontrollable, which prevents them from being applied industrially. In this context, it is of significant importance to have a deeper understanding than we have presently for the intricate interplay of physics associated with mode competition and FWM in QD laser.

Both theoretical and experimental studies of FWM in SOA have been investigated extensively. However, those theories are not capable for explaining the FWM process in a semiconductor laser. Examples, such as the group velocity dispersion (GVD), the gain saturation, the mode competition, and the multiwave mixing, are usually missed. Nevertheless, those nonlinear properties can largely affect the frequency comb generation from a laser. Recently, an improved FWM theory for semiconductor laser that includes the aforementioned nonlinear process has been proposed [253], which contributes to an understanding and a controlling of FWM for SML generation from QD laser. To analyze the FWM mechanism of epitaxial QD lasers on silicon, a probe-drive injection configuration is investigated.

Fig. 5.16 schematically displays a simplified nondegenerate FWM process in the QD gain medium. Two traveling waves marked drive and probe oscillate and generate a new pair of waves, drive conversion and signal, respectively. The drive photon is first applied to injection lock the QD laser, and the interaction between the probe photon and the drive photon will generate new photons through the third-order nonlinear susceptibility ($\chi^{(3)}$) of the QD semiconductor material. Despite only four waves are shown here, all lasing modes of a multimode laser can serve as the drive and the probe photons for the FWM process. To study the FWM conversion efficiency (CE), the converted signal of the probe conversion is analyzed.

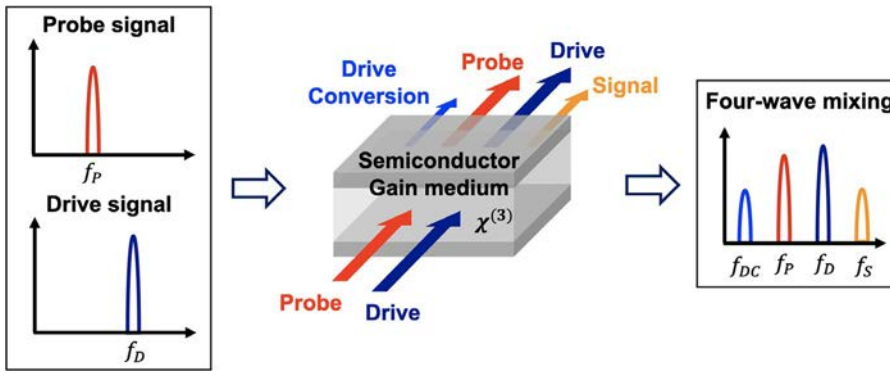

Fig. 5.16 Schematic representation of the four-wave mixing process in the active region of the laser as well as the corresponding spectra.

5.5.1 Nonlinear conversion

Different from the FWM process in SOA, the FWM in semiconductor laser is much more complex. Because of the wavelength selection by the FP cavity, the FWM efficiency is dependent on the phase, the polarization, and the wavelength of the optical field. To maximize the power of the generated signal photon, the probe laser must be applied to one longitudinal mode, which results in a discrete FWM bandwidth that is a multiple of the free spectral range (FSR) of the laser cavity. The FWM bandwidth refers to the frequency detuning between the probe and the drive laser, that is, $\Delta = \nu_p - \nu_d$, where ν_p and ν_d denote the optical frequency of these two lasers. Depending on whether Δ is negative or positive, the FWM process can be further classified into Stokes condition and anti-Stokes conditions. To extract the FWM coefficient, two external low-noise tunable lasers are utilized as the drive and the probe laser. The phases of these two lasers must be well adjusted by polarization controllers before they are sent for injection locking the QD laser.

Fig. 5.17A depicts the FWM spectra of a p-doped QD laser in the Stokes condition. The FSR of the QD laser studied is 30 GHz. By applying the probe laser at a longitudinal mode apart from the drive laser, the power of the generated signal photon exhibits a dependence of the power of the probe photon, as shown by the different colored curves in Fig. 5.17A. To analyze the FWM efficiency that is dependent on the $\chi^{(3)}$, a commonly used approach is the CE, which is expressed as $\eta_{CE} = \frac{P_{Signal}}{P_{Probe}}$ with P_{Signal} the optical power of the converted signal and P_{Probe} the probe signal power injected into the laser [254]. The power of these two photons are measured from the optical spectrum after considering the laser-fiber coupling loss and the fiber loss. The η_{CE} is then expressed in logarithmic scale (in dB). To evaluate the FWM efficiency of QD laser, the measured η_{CE} of an undoped QD, a p-doped QD, and a QW laser as a function of the probe-drive frequency detuning are shown in Fig. 5.17B. Without ambiguity, the p-doped QD laser exhibits the highest FWM efficiency in presence of a η_{CE} as large as -4 dB, which is 9 and 24 dB greater than

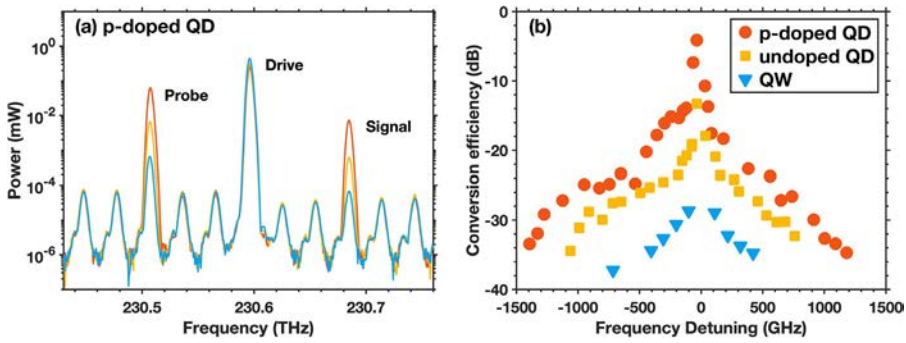

Fig. 5.17 (A) Optical spectrum of four-wave mixing for p-doped QD laser in Stokes condition with frequency detuning of -89 GHz. The *different colored lines* indicate signal power increases with increasing probe power. (B) Conversion efficiency of four-wave mixing for p-doped QD, undoped QD, and QW lasers as a function of probe-drive frequency detuning.

the maximum η_{CE} of the undoped QD laser and the QW laser, respectively. On the other hand, the FWM bandwidth of the p-doped QD laser is also much larger than that of its counterparts. In both Stokes and anti-Stokes conditions, the FWM bandwidth of the p-doped device exceeds terahertz. The remarkable improvement of FWM efficiency and bandwidth observed from the p-doped device is attributed to its fast carrier dynamics offered by the high-performance QD. The FWM process relies on multiple nonlinear process including carrier density pulsation (CDP), CH, and SHB [255, 256]. In the low-frequency detuning region, the frequency conversion is determined by the CDP, which is induced by the probe-drive beating. Despite the fact that the CDP becomes weaker with the increase of frequency detuning, the CH and the SHB that is on the scale of subpicosecond is able to keep a frequency conversion [257–261]. As a result, the nonlinear effects of the p-doped QD laser are amplified due to the improved material gain that results from the high QD uniformity, reduced TDD, and the p-modulation doping [191, 217]. It is worth stressing that the $\chi^{(3)}$ can be expressed as a sum of the contributions of the aforementioned individual processes, which is discussed hereinafter. In addition, the near-zero α_H-factor offered by QD is also beneficial for improving the symmetry of gain profile thus the FWM bandwidth.

Fig. 5.18A represents the optical spectrum and spectral-dependent α_M-factor with different modulation frequency at twice threshold current. The α_M is extracted by the optical phase modulation method, describing the above-threshold α_H-factor [262]. The α_H-factor and corner frequency (f_c) were obtained by fitting α_M at different modulation frequency (f_m) according to the following equation:

$$\alpha_M(f_m) = \alpha_H \sqrt{1 + \left(\frac{f_c}{f_m}\right)^2} \tag{5.20}$$

Since the fitting gives $f_c \ll f_m$, it is possible to take $\alpha_M \approx \alpha_H$ at 13 GHz. Over a wide bandwidth, the α_H shows a linear increase with increasing lasing wavelength. A semiconductor comb laser with an FWM process exhibits a significant dependence

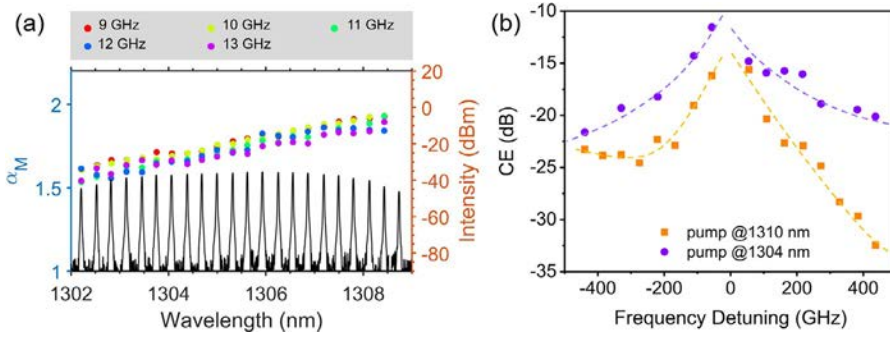

Fig. 5.18 (A) Spectral dependence of the α_M-factor with different modulation frequency at twice threshold current. (B) The four-wave mixing conversion efficiency as a function of the frequency detuning at two injection-locking wavelengths of 1304 and 1310 nm, respectively.

on the α_H-factor as shown in Fig. 5.18B. Therefore, when the injection locked at 1304 nm ($\alpha_H = 1.6$), the CE is high and symmetrical at positive and negative frequency detuning. The CE is significantly lower when the injection locked at 1310 nm ($\alpha_H = 2.0$). Consequently, a small α_H-factor facilitates the generation of higher conversion efficiencies and better symmetry of the Stokes and anti-Stokes conversions. This is important for understanding the dynamics of the mode-locking and frequency combs.

5.5.2 Third-order nonlinear susceptibility and group velocity dispersion

To analyze the FWM process in semiconductor lasers, a microscopic level model that contains a full treatment of the quantum mechanical electron-hole polarization is investigated [253]. Different from the CE described earlier, the FWM efficiency is described by the signal-drive ratio η_{sd} and the probe-drive ratio η_{pd}, which is based on a first-principle multimode laser theory [256]. The η_{sd} is defined as the ratio of signal power to drive power, whereas η_{pd} denotes the ratio of probe power to drive power. After taking into account all the nonlinear processes that contribute to the gain saturation, the mode competition, and the multiwave mixing, the FWM coefficient is expressed as follows:

$$\xi = \frac{c}{2\nu_d n_B}\left(\frac{\wp}{2\hbar\gamma}\right)^2 \Gamma(k_d, k_p, k_s)\frac{|\Lambda^{(3)}(\nu_d, \nu_p, \nu_s)|}{Re(\Lambda^{(1)}(\nu_d))} \tag{5.21}$$

where $\xi \equiv \chi^{(3)}/g_s$ with g_s is the material gain. c, n_B, $\wp$, and γ denote the speed of light in vacuum, the background refractive index, the GaAs bulk dipole matrix element, and the dephasing rate, respectively. The contributions of CDP, CH, and SHB to the $\chi^{(3)}$ are summed into $\Gamma(k_d, k_p, k_s)$ and $\Lambda^{(3)}(\nu_d, \nu_p, \nu_s)$, in which k_n and ν_n account for the wave vector and the field frequencies, respectively ($n = d, p, s$ for drive, probe, and signal fields, respectively). The spectral component of the linear susceptibility is described by $\Lambda^{(1)}$. In the case of QD or QW, $\Lambda^{(1)}$ and $\Lambda^{(3)}$ include a sum over the inhomogeneous QD distribution or a sum over conduction and valence band states, respectively.

The detailed expression for the contribution to ξ and its input parameters are described in an earlier paper [253]. Compared to the definition of η_{CE}, Eq. (5.21) allows for extracting an FWM coefficient that is independent of laser configuration, which is much more straightforward to study the FWM efficiency that is determined by the optical nonlinearity. In simulation, the input parameters for the model are determined by anchoring the computed laser behavior to the measured one. Experimental results including the light-current curves and lasing spectra in free-running operation and in injection-locking operation are well analyzed to have accurate input parameters for simulation.

Fig. 5.19 depicts the η_{sd} as a function of η_{pd} in theory (dashed line) and in experiment (solid markers) for the p-doped QD laser (red), the undoped QD laser (yellow),

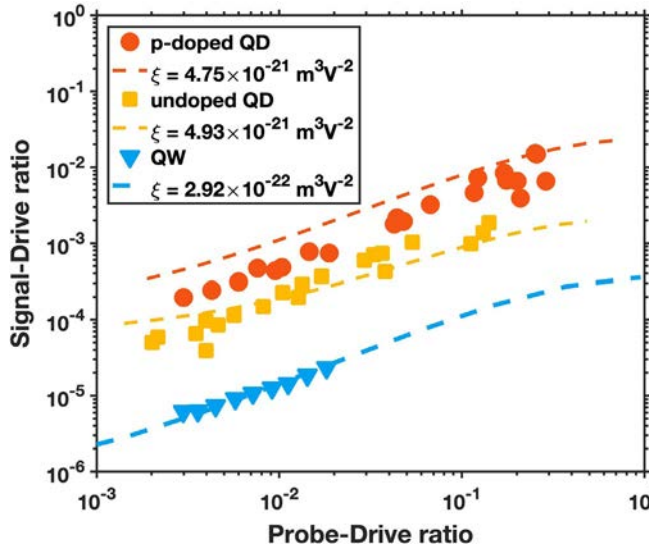

Fig. 5.19 Signal-drive ratio as a function of probe-drive ratio for p-doped QD, undoped QD, and QW lasers. The *dashed curves* are calculated from multimode laser theory indicating the corresponding FWM coefficient.

and the QW laser (blue). The frequency detuning for all devices is fixed between 110 and 120 GHz for a fair comparison. The good agreement between the simulation and the experiment demonstrates that the improved FWM efficiency observed from the QD lasers is attributed to their large optical nonlinearity. The calculated FWM coefficient of the p-doped and the undoped QD device is 4.75×10^{-21} and $4.93 \times 10^{-21}\mathrm{m}^3\mathrm{V}^{-2}$, respectively. On the contrary, the calculated FWM coefficient is much lower at $2.92 \times 10^{-22}\mathrm{m}^3\mathrm{V}^{-2}$ for the QW laser. As a result of the large $\chi^{(3)}$, the FWM efficiency of QD laser is more than one order of magnitude stronger than that of the QW laser. Therefore, the SML that is observed from the QD laser can be attributed to the FWM rather than the unaccounted intracavity absorption. Despite the fact that the CE of the p-doped QD laser is higher than that of the undoped laser in experiment, the calculated FWM coefficient of the former is a little lower. The underestimated FWM coefficient for the p-doped device could be attributed to the extraabsorption in the active region brought by the p-modulation doping. It is worth stressing that the internal loss can be further reduced by applying an optimal doping density [263].

On the other hand, the occurrence of SML in QD laser not only depends on the FWM, but also relies on a balance between the optical nonlinearity and the intracavity GVD. According to the definition of GVD in Ref. [264], the GVD of a semiconductor laser can be calculated by the derivative of group refractive index to the wavelength. The wavelength-dependent group refractive index is derived from the FSR of the laser cavity. Fig. 5.20 depicts the optical frequency-dependent GVD that includes both the contributions of the QD/QW active region and the GaAs waveguide for the p-doped QD laser (red) and the QW laser (blue). The GVD at gain peak for the QD laser and the

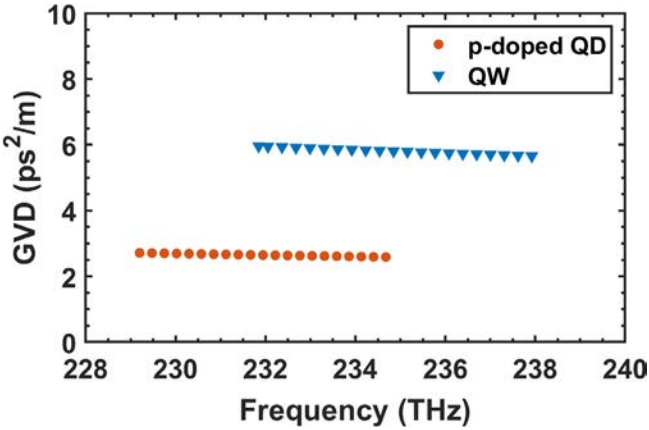

Fig. 5.20 Group velocity dispersion (GVD) as a function of optical frequency for the p-doped QD (*red*) and QW (*blue*) laser.

QW laser are 2.66 and 5.82 ps^2/m, respectively. It is worth pointing out that the GVD observed from the single-section QD laser is comparable with passively mode-locked lasers (MLLs) [265]. As a consequence, the low GVD offered by the QD active region along with the rich optical nonlinearity pave the way for the realization of SML in QD laser. Despite the fact that the GVD is not included in Eq. (5.21), its contribution to the SML has been discussed in the literature [253, 266]. Last but not least, the FWM theory described in this section reveals that the CE of the QD laser has not attained its theoretical limit, which can be further improved.

5.6 Quantum dot optical frequency comb

Since the demonstration of laser diode, it was once a big challenge to count, measure, and phase-coherently control the optical frequencies by utilizing the RFs due to the difference in frequency of a factor of 10^5. As a result of this gap, it was not possible to realize a timing keeping at hundreds of terahertz, nor would the tests of fundamental physics such as the optical spectroscopy of energy eigenstates in atoms and molecules be reliable. Nevertheless, the introduction to the laser frequency comb in the late 1990s revolutionized the precise measurements of frequency and time, due to its potential for playing as a "light gear" which is reliable and accurate to count optical cycles on the femtosecond (10^{-15} s) time scale.

The generation of OFC relies on a combination of laser physics, including the ultrafast optical pulse generation, nonlinear optics, and electrooptics. For different potential applications of frequency combs, it is necessary to control the comb spacing, the stability of pulse energy, and the timing jitter. Recently, Kerr nonlinear microcomb and electrooptic frequency comb are regarded as promising solutions for on-chip frequency comb generation, due to their compatibility with CMOS industry. With the pumping of a CW single-frequency laser, both these approaches allow for generating

octave-spanning frequency comb along with high repetition rate. Despite the remarkable performance of these OFC technologies, the inconveniences such as the requirement of high pumping power over hundreds of milliwatts, the low CE, and the complexity of photonic integration that gives rise to a lower reliability and a higher cost must be addressed before they are commercially available. In this context, the mature passively mode-locked frequency comb technology offers an energy-efficient and low-cost solution. Previously, high-performance passively MLLs that take advantage of semiconductor QDs have been demonstrated, which exhibit strong potential to be applied to DWDM system for high-speed optical communications [267]. In particular, the high tolerance for the defects that arise during the epitaxial growth of III–Vs on Si that offered by quantized QDs, which has been discussed earlier in this chapter, paves the way for developing compact OFC generators for silicon-based PIC.

5.6.1 Passive mode-locking and device structure

Passive mode-locking relies on a nonlinear optical element, that is, saturable absorber (SA), whose loss depends on the laser pulse intensity. As a result, the loss decreases with the increase of pulse intensity in the presence of the loss modulation being synchronized automatically with the laser pulses. In contrast to the actively mode-locked device, the pulse-shortening effect in the passively MLL is more efficient if the response time of the SA is sufficiently fast. When the laser operates at the steady state, the circulating short pulse maintains its shape indefinitely through a balance between nonlinearity and dispersion. As a consequence, the generated pulse train with identical envelop results in a perfectly regular comb behavior in the optical frequency domain.

Fig. 5.21 depicts the dynamics of the saturable gain and loss functions, and the pulse generation process that are calculated for a two-section QD laser. At the slow stage where the intracavity loss (dashed yellow plot in Fig. 5.21, Q) is higher than gain (solid red plot in Fig. 5.21, G), the absorber remains opaque which prevents the generation of any pulse. The negative net gain is described by the dotted black plot in Fig. 5.21A. With the increase of intracavity photon density, the pulse that arrives in the low-intensity light (leading edge of the pulse) is absorbed, and it saturates the SA, which then transmits high-intensity light. As a consequence, a positive net gain window is opened and the optical pulse is generated (solid blue plot in Fig. 5.21B). At this fast stage, the SA usually recovers faster than the gain, which results in the leading edge of pulse faster than the trailing edge [268]. The next pulse will be generated after the photons circulate within one round-trip time in the laser cavity, hence the pulse repetition rate is inversely proportional to the cavity length. It is worth stressing that the SA recovery time can be further reduced by applying a reverse bias on it, which is a commonly used approach for generating faster optical pulses [269].

Benefiting from the fast carrier dynamics, the QD laser is an ideal solution for the generation of ultra-short pulse and high optical bandwidth [269]. Two-section MLL in which the SA section is placed at the edge of laser cavity have been extensively studied during the past decades [267, 270–276]. A sketch of a 20 GHz two-section

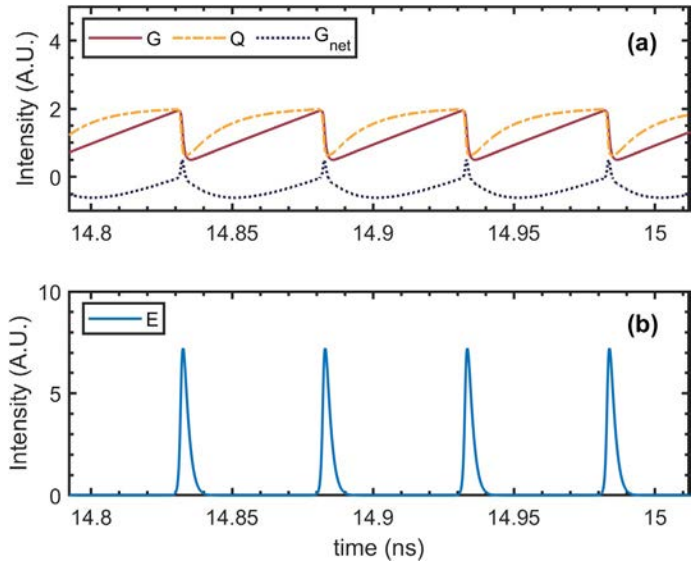

Fig. 5.21 (A) Calculated saturable gain (*red solid line*), loss (*yellow dashed line*), and net gain (*black dotted line*). (B) Calculated pulse train.

mode-locked QD laser is shown in Fig. 5.22A. The growth techniques for the active region of the QD-MLL are similar with those for the aforementioned FP devices, except for five-layer chirped QD in the active region. The height of each QD laser ranging from 3 to 7 mm is designed for broadening the bandwidth of the gain spectrum [276]. The active region of laser is then p-modulation doped to improve the thermal stability for high-temperature operation [277]. A trapezoidal gain section whose width ranges from 3 to 6 μm gain section is a strategy to improve the mode-locking performance in terms of pulse width and output power [278].

As discussed earlier, passive mode-locking does not require electrical sinusoidal signal. The optical pulse train of a monolithic passively MLL is converted afterwards

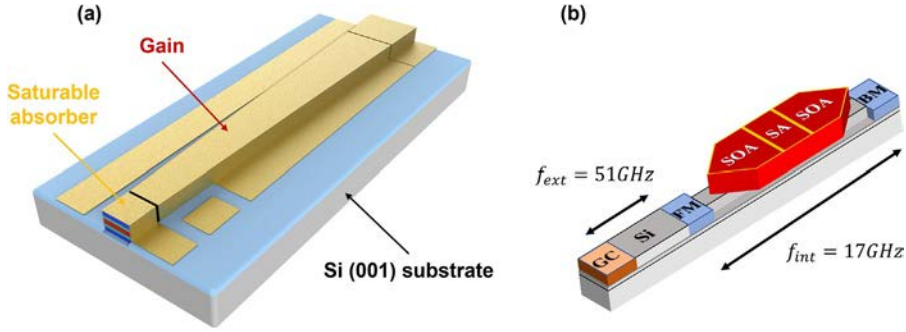

Fig. 5.22 Schematic diagram of (A) 20 GHz two-section quantum-dot mode-locked laser epitaxially grown on silicon, and (B) 102 GHz colliding-pulse mode-locked (CPML) quantum-dot laser heterogeneously grown on silicon.

to an electrical signal at the same frequency by using a high-speed photodetector. A more convenient method is based on the direct extraction of the electrical signal from the SA [279]. When an optical pulse enters the reverse-biased absorber section, free carriers are created. Due to the built-in electric field, the free carriers are swept out of the absorber yielding a pulsed photocurrent. For instance, Fig. 5.23A shows a comparison of the two RF spectra for an InAs/GaAs QD MLL, which reveals a peak frequency of 38.61701 and 38.61706 GHz for the directly extracted electrical signal and for the one generated from the optical pulse train, respectively. The 50 kHz deviation lies well within the carrier 3-dB linewidth of 187.3 kHz. As no photodiode is required, the direct extraction yields a 6.3 dB lower noise level whereas the peak power of the extracted signal amounts to 32.8 dBm, thus being diminished by 9.8 dB as compared to the optical pulse train. Fig. 5.23B depicts the single-sideband (SSB) phase noise power density traces of both electrical and optical signals. A very similar progression is revealed, hence demonstrating that the properties of the directly extracted electrical signal from the absorber section are essentially conformed to those obtained for the optical pulse train. It is worth stressing that the higher high-offset frequency phase noise observed from the extracted electrical signal is attributed to the lower RF power; an RF amplifier contributes to an improvement of integrated timing jitter from 359 to 90 fs. Therefore, the absorber can be used as an intrawaveguide photodetector enabling electrical signals to be generated with high conversion efficiencies and simultaneously along with the optical pulse train [279]. The ultra-fast recovery time of QD SA achieves this goal, meaning that both electrical and optical pulses are generated simultaneously without additional power consumption.

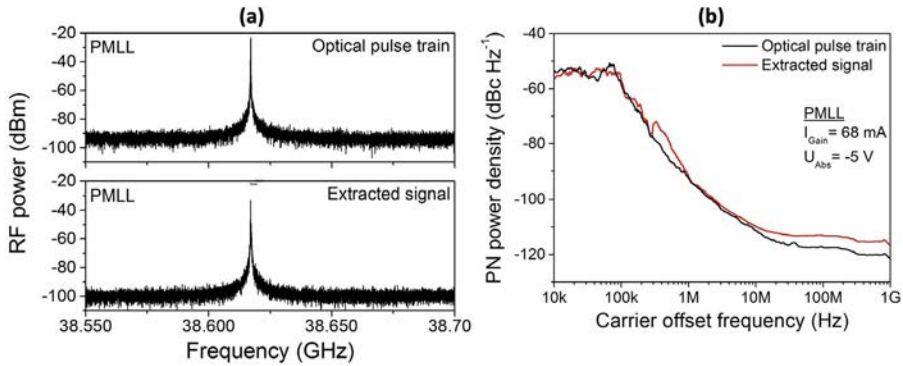

Fig. 5.23 (A) RF spectra of the directly extracted electrical signal from the SA and the one generated from the optical pulse train, respectively. (B) Phase-noise traces of the directly extracted electrical signal from the SA and the one generated from the optical pulse train using a photodiode, respectively.

Reprinted with permission from F. Grillot, D. Arsenijevic, H. Huang, D. Bimberg, Ultrafast and nonlinear dynamics of InAs/GaAs semiconductor quantum dot lasers, in: D.L. Huffaker, H. Eisele (Eds.), Quantum Dots and Nanostructures: Growth, Characterization, and Modeling XV, vol. 10543, International Society for Optics and Photonics, SPIE, 2018, https://doi.org/10.1117/12.2299678, copyright 2018, SPIE.

Despite the high performance demonstrated in two-section QD laser, it is a challenge to realize a high repetition rate at the order of 100 GHz which is required for DWDM system. Since the repetition rate is determined by the laser cavity length L_{cav} through the relationship $f_{rep} = v_g/L_{cav}$ with v_g the group velocity in the cavity, the laser cavity length should be reduced below 400 μm to have a repetition rate exceeding 100 GHz. Nevertheless, the consequent decrease of optical gain and increase of mirror loss definitely result in an inefficient laser emission. To address this issue, a colliding-pulse mode-locking (CPML) structure can be applied to QD laser to have an efficient output and a high repetition rate simultaneously [280–282]. Fig. 5.22B depicts a sketch of the 1.3-μm hybrid-silicon QD frequency comb laser with repetition rate at 102 GHz. Its 2.3-mm-long internal cavity gives a fundamental 17 GHz FSR in the optical frequency domain. A 120-μm-long SA is placed at the center for pulse colliding, hence the FSR is doubled to 34 GHz. The active region is made of a commercial GaAs-based QD-containing epi stack that is heterogeneously grown on a silicon-on-insulator (SOI) wafer. The front and rear facets of the internal cavity are connected to a front mirror (FM) and a back mirror (BM) whose power reflectivities are ∽50% and ∽100%, respectively. To further increase the FSR, a 0.75-mm-long (51 GHz) external cavity is placed outside the FM to take advantage of the sixth harmonic of the fundamental repetition rate through the vernier effect.

Table 5.3 summarizes recent progress in QD frequency comb laser that is based on passive mode-locking technique.

Table 5.3 Mode-locking performance of QD lasers.

Substrate	Type	Repetition rate (GHz)	Pulse duration (ps)	TBP[a]	3-dB optical bandwidth (THz)	Year
InP	QDash	92	0.312	0.457	1.472	2008 [283]
InP	QDash	101	–	–	1.2	2009 [284]
InP	QDash	48–346	0.8	0.46	–	2011 [285]
InP	QD	50	0.43	–	1.65	2020 [286]
InP	QDash	34.2	–	–	1.6	2021 [287]
GaAs	QD	21	0.39	1	–	2005 [288]
GaAs	QD	7.2–51	6.4	1.7	–	2007 [280]
GaAs	QD	39–237	0.36	0.5	–	2009 [281]
GaAs	QD	40	0.7	0.5	–	2010 [274]
GaAs	QD	60	–	–	2.46	2022 [289]
GaAs	QD	100	0.466	0.472	0.78	2022 [290]
GaAs	QD	100	0.81	0.45	1.9	2022 [207]
GaAs	QD	60	0.495	–	2.2	2023 [291]
Si	QD	102	–	–	1.4	2018 [158]
Si	QD	20	5	–	1.14	2019 [276]
Si	QD	15.5	–	–	2.1	2022 [292]

[a] Time-bandwidth product.

5.6.2 Mode-locking and frequency comb generation

Low-noise and high-bandwidth frequency comb lasers are of significant importance for developing high-speed optical transceivers. On one hand, optical time-division multiplexing and optical sampling are based on pulsed source with low timing jitter. On the other hand, a large number of comb lines offered by a high optical bandwidth allows for improving the transmission capacity while keeping a small footprint. In this section, the mode-locking dynamics of the two-section QD laser are first analyzed.

As aforementioned, passive mode-locking by taking advantage of the QD with fast saturable absorption allows for generating optical pulses with hundreds of femtosecond pulse width. As a consequence, QD MLL is a promising solution for ultra-broadband OFC generation, as shown in Fig. 5.24A. On the other hand, a short pulse generation also relies on a low GVD. In Section 5.5, the authors have demonstrated that the GVD in QD laser is much lower than that in conventional QW laser, which is another driving force for forming an ultra-short optical pulse. It is worth stressing that the reverse bias on the SA is beneficial for further decreasing the GVD thus reducing the pulse width, as depicted in Fig. 5.24C. In addition to the pulse width, the timing jitter of a pulse train is also an important factor for ultra-precise timekeeper. To analyze the timing jitter, the RF beatnote of laser repetition rate is a widely used approach [294]. By taking advantage of the high four-wave-mixing efficiency in QD laser, as introduced in Section 5.5, the consequent self-mode-locking effect is capable of generating an ultra-stable pulse train with subkilohertz RF beatnote, as shown in Fig. 5.24B [295]. To further stabilize a pulse train, approaches such as external optical feedback have been regarded as an efficient solution. While a prior study demonstrated that the RF beatnote can be squeezed by a factor of 13.6 dB, as shown in Fig. 5.24D, some recent work has pushed this squeezing factor to 20 dB [296–298].

Finally, another paradigm for high-power, ultra-fast pulse production from compact semiconductor lasers with multisections including quantum confined active media is the phenomenon of superradiance [299]. First proposed in 1954 for atomic ensembles in a gaseous medium, superradiance is thought to arise from the mutual phasing of oscillators in an ensemble, leading to phase-coherent collective radiative emission. The key conditions that need to be simultaneously fulfilled for achieving superradiance emission are the creation of a very large electron-hole density, a resonant electromagnetic field that can facilitate the coupling of electrons in the valence band and holes in the conduction band, hence leading to a collection of resonantly coupled excitons. Multisection laser devices with QW active medium and made with an in-built SA section have been shown to provide a conductive environment for these conditions to be satisfied, and for superradiant pulse emission to take place [300]. In this context, QD material system has received tremendous attention over the past couple of decades, on account of its superior properties, such as high gain amplification over a very wide bandwidth and ultra-fast carrier dynamics. Therefore, QDs have been investigated with the aim of evaluating their potential for cooperative emission, and results suggest interaction ranges on the order of at least several tens of nanometers [301]. A demonstration of this phenomenon in a QD multisection semiconductor laser was reported with pulse formation at a wavelength of 1270 nm and a repetition rate of 5 MHz, with pulse widths as narrow as 320 fs [302].

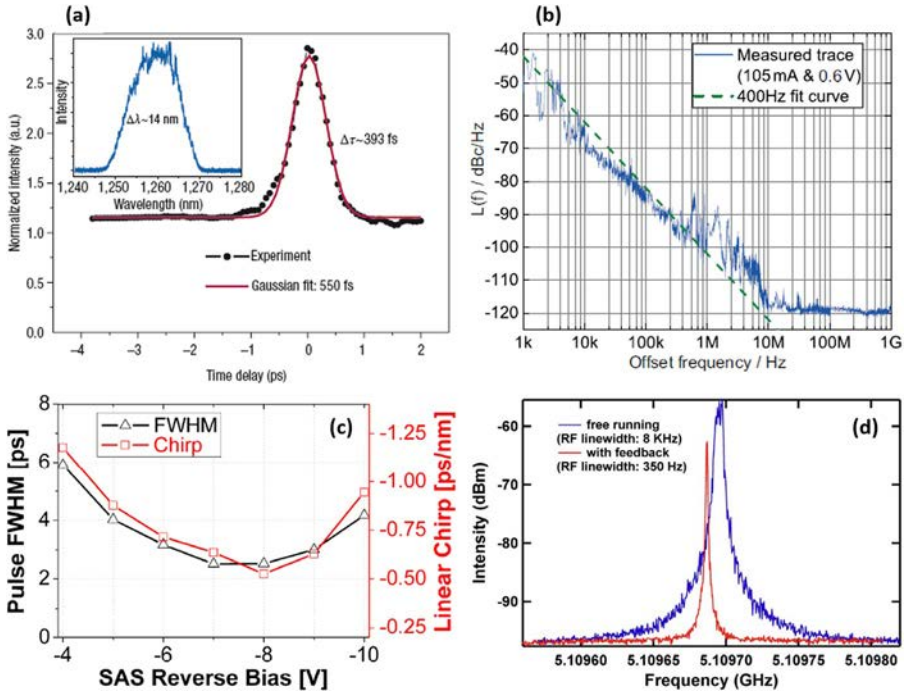

Fig. 5.24 Characterizations of QD passively mode-locked laser. (A) Short pulse width at 393 fs along with 14 nm gain bandwidth. (B) Low timing jitter with RF linewidth of the beatnote at 400 Hz. (C) SA reverse bias-dependent pulse width and dispersion. (D) RF linewidth of the beatnote with (*red*) and without (*blue*) self-injection locking.
(A) Reprinted with permission from E.U. Rafailov, M.A. Cataluna, W. Sibbett, Mode-locked quantum-dot lasers, Nat. Photonics 1 (7) (2007) 395–401, https://doi.org/10.1038/nphoton.2007.120, copyright 2007, Springer Nature. (B) Reprinted with permission from D. Auth, S. Liu, J. Norman, J.E. Bowers, S. Breuer, Passively mode-locked semiconductor quantum dot on silicon laser with 400 Hz RF line width, Opt. Express 27 (19) (2019) 27256–27266, https://doi.org/10.1364/OE.27.027256, copyright 2019, Optica Publishing Group. (C) Reprinted with permission from H. Schmeckebier, G. Fiol, C. Meuer, D. Arsenijević, D. Bimberg, Complete pulse characterization of quantum-dot mode-locked lasers suitable for optical communication up to 160 Gbit/s, Opt. Express 18 (4) (2010) 3415–3425, https://doi.org/10.1364/OE.18.003415, copyright 2010, Optica Publishing Group. (D) Reprinted with permission from C.-Y. Lin, F. Grillot, N.A. Naderi, Y. Li, L.F. Lester, RF linewidth reduction in a quantum dot passively mode-locked laser subject to external optical feedback, Appl. Phys. Lett. 96 (5) (2010) 051118, https://doi.org/10.1063/1.3299714, copyright 2010, AIP Publishing.

In addition to the amplitude-modulated (AM) frequency comb that delivers ultra-fast optical pulses, the formation of a frequency comb can be also driven by the frequency modulation [303]. More recently, the broadband and flat-topped frequency-modulated (FM) comb induced by FWM and Kerr nonlinearity has experienced a renaissance, and the generation of FM comb relies on a fast gain medium such as QD [291, 304]. In contrast to the conventional AM comb, the emission of FM comb is quasi-CW, which is promising for DWDM applications since it

minimizes the severe thermal nonlinearities caused by strong optical pulses. The FM comb dynamics in QD laser was first demonstrated in single-section devices; however, it is recently revealed that an additional SA section inside the laser cavity contributes to a greater Kerr nonlinearity to improve the comb bandwidth [291]. Fig. 5.25C depicts the emission of an InAs/InP two-section QD comb source whose 3-dB optical bandwidth is as large as 1.65 THz [286]. Such a flat-topped FM comb source is thus promising for DWDM PICs in which a large number of equally spaced comb lines are required. It is worth emphasizing that the Kerr nonlinearity in multi-section QD lasers can be practically engineered by the SA reverse bias, which results

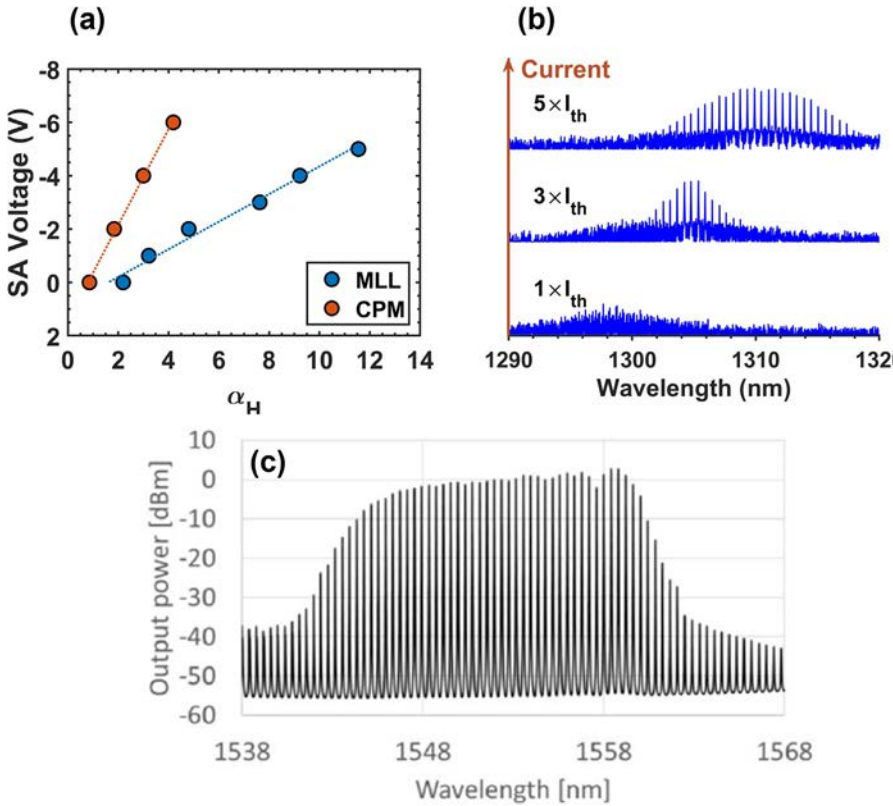

Fig. 5.25 (A) Linewidth enhancement factor at threshold of a 20 GHz two-section QD mode-locked laser (MLL, *blue*) epitaxially grown on silicon, and a 102 GHz colliding-pulse mode-locked (CPM, *red*) QD laser heterogeneously grown on silicon. (B) Evolution of the optical spectrum of the 102 GHz QD comb laser with gain current. The number of lines is enhanced through the increase of homogeneous broadening in QD. (C) Optical spectrum of an InAs/InP QD mode-locked laser whose 3-dB comb bandwidth is 1.65 THz.
(C) Reprinted with permission from M. Zander, W. Rehbein, M. Moehrle, S. Breuer, D. Franke, M. Schell, K. Kolpatzeck, J.C. Balzer, High performance BH InAs/InP QD and InGaAsP/InP QW mode-locked lasers as comb and pulse sources, in: Optical Fiber Communication Conference, Optica Publishing Group, 2020, courtesy of Prof. Martin Schell and Dr. Martin Möhrle.

from the increase of α_H-factor [249, 294]. In a fast gain medium such as QD, the modal gains are tightly coupled to the intracavity field intensity, thus the modal phases can be shifted by the intracavity field intensity through the finite α_H-factors and a giant Kerr nonlinearity takes place [291]. Fig. 5.25A depicts the effective α_H-factor at threshold for a two-section QD MLL (blue) and a multisection QD frequency comb laser (CPM, red). With the increase of SA reverse bias, the increase of α_H-factor is beneficial to improving the FM comb bandwidth. A record 3-dB optical bandwidth as large as 2.2 THz has been recently reported [291]. In FM operation, the optical bandwidth of QD laser is dependent on the effective α_H-factor by following the relationship $\alpha_e = \sqrt{\frac{1}{\Delta\nu} \times \int_{comb} \alpha_H^2(\nu')d\nu'}$. Despite the fact that a large α_H is beneficial for improving the comb bandwidth, a strongly biased SA destabilizes the FM operation; a too large phase-amplitude coupling also increases the mode competition, which decreases the possibility to have wide comb regimes. On the other hand, the generation of FM comb is also determined by spatial hole burning (SpaHB) that allows for improving the optical bandwidth. The spatial hole burning is particularly important in FP cavities (as opposed to ring cavities, for instance) wherein two counter propagating waves with the same wavelength interfere thus forming a standing-wave pattern. Recently, a numerical modelling based on Maxwell-Bloch equations has shown that an increase of the homogeneous width can produce a larger number of modes in the optical spectrum [305]. Fig. 5.25B depicts the comb spectra of a multisection QD laser in different gain bias conditions, the increased homogeneous broadening of QD active region gives rise to a large improvement of optical bandwidth. Last but not least, the carrier lifetime also plays an important role in the formation of frequency comb dynamics [305]. Therefore, by reducing the carrier lifetime by controlling the operation temperature, a relevant increase of the number of modes can be generated.

5.6.3 Self-injection locking

In recent years, DWDM application demands for ultra-broadband frequency comb laser for high-speed optical communication. Despite the huge progress in QD frequency comb laser, the performance of each comb line was used to be a great issue. Compared to the DFB laser array, the optical linewidth of a single comb line in QD frequency comb laser is in general on the order of megahertz [276, 287], which prevents this type of comb source for advanced format modulation, that is, 16-QAM. Nevertheless, an optimization of cavity design allows for improving the bandwidth and noise properties of a QD frequency comb laser. Fig. 5.26A demonstrates that the QD laser is able to generate a flat-top frequency comb with 3-dB bandwidth at 11.5 nm, along with low-noise comb line with optical linewidth at 440 kHz. The improved optical linewidth allows for 40 Gbaud PAM-4 modulation from a single comb line [207]. By taking advantage of the large number of comb lines offered by the QD laser, QD-based frequency comb generator is able to support 12 Tbit/s optical transmission [287, 306].

In Section 5.4, our discussions demonstrate how a semiconductor laser can suffer from strong instabilities due to the external back-reflections. Despite the

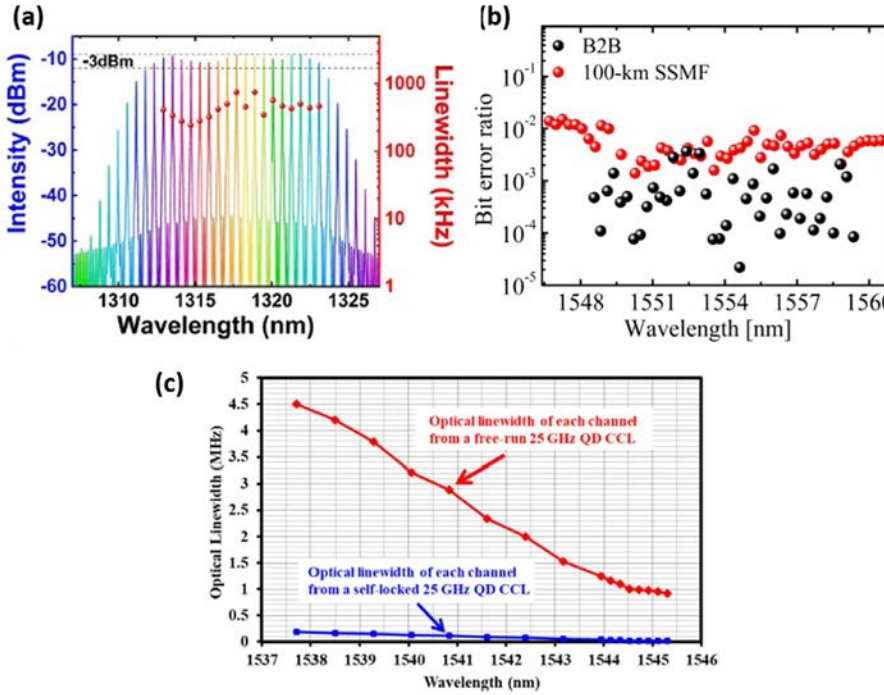

Fig. 5.26 Noise and transmission performance of QD frequency comb laser. (A) Optical spectrum of a QD comb laser on GaAs substrate with 3-dB optical bandwidth at 11.5 nm and optical linewidth of each line at 440 kHz. (B) Bit-error rate of a QD comb laser on InP substrate with 16-QAM modulation for 10.8 Tbit/s transmission. (C) Optical linewidth of 39 comb lines with (*blue*) and without (*red*) self-injection locking.
(A) Reprinted with permission from J.-Z. Huang, Z.-T. Ji, J.-J. Chen, W.-Q. Wei, J.-L. Qin, Z.-H. Wang, Z.-Y. Li, T. Wang, X. Xiao, J.-J. Zhang, Ultra-broadband flat-top quantum dot comb lasers, Photonics Res. 10 (5) (2022) 1308–1316, https://doi.org/10.1364/PRJ.446349, copyright 2022, Chinese Laser Press. (B, C) Reprinted with permission from Z. Lu, J. Liu, P.J. Poole, Y. Mao, J. Weber, G. Liu, P. Barrios, InAs/InP quantum dash semiconductor coherent comb lasers and their applications in optical networks, J. Lightwave Technol. 39 (12) (2021) 3751–3760, https://doi.org/10.1109/JLT.2020.3043284, copyright 2021, IEEE.

inconvenience brought by the coherence collapse, which is typical laser dynamics in feedback regime IV, a weak optical feedback in regime II can be an efficient approach to stabilize the phase noise of a laser. The so-called SIL has been proved an efficient solution for ultra-quiet oscillator generation [197]. It is worth noting that the SIL in regime II depends on the phase of the external cavity, which must be optimized for an efficient stabilization, otherwise the phase noise can be degraded [293, 294]. Fig. 5.26C depicts the optical linewidth for each comb line of a QD comb laser with (blue) and without (red) SIL. The SIL technique allows the phase noise of each line to be squeezed from megahertz to 12 kHz by a factor of 19 dB, which meets the requirement of advanced format modulation, that is, 16-QAM and 32-QAM, for tens Tbit/s and beyond coherent optical networking systems [306]. To achieve a fully integrated

SIL approach for on-chip QD frequency comb laser, high-Q microresonator and waveguide could be potential solutions [196, 307].

5.6.4 External-injection locking

External optical injection locking (OIL) is a well-known technique that is able to influence the laser dynamics [308]. In particular, the OIL technique exhibits a strong potential to be applied to the direct-detection fiber links to improve their performances. Examples as the reduction of chirp-induced dispersion and nonlinear distortion, the decrease of intensity and FN, and the large increase of the ROF thus the modulation bandwidth have been reported [309–311]. In addition to the aforementioned SIL approach, OIL allows for a squeezing of phase noise for each comb line to the phase noise of the injected master lasers, as shown in Fig. 5.27A [312]. By taking advantage

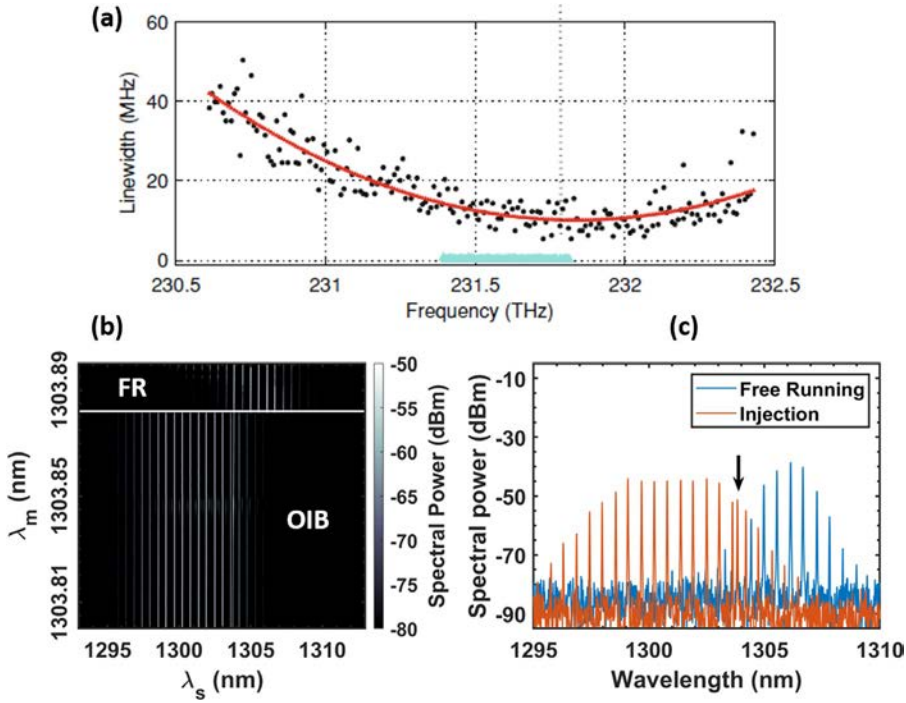

Fig. 5.27 Optical injection-locking operation: (A) Optical linewidth of each comb line is squeezed to the phase noise of the master laser by dual-tone optical injection. (B) Spectral power of a 102 GHz QD comb laser on Si as a function of its wavelength and the master laser wavelength. (C) Optical spectra of the QD-OFC in free-running (*blue*) and in optical injection (*red*) operation. *FR*, free-running regime; *OIB*, optical injection broadening regime.
(A) Reprinted with permission from T. Habruseva, N. Rebrova, S.P. Hegarty, G. Huyet, Mode-locked semiconductor lasers with optical injection, in: Quantum Dot Devices, Springer, 2012, pp. 65–91, https://doi.org/10.1007/978-1-4614-3570-9_4, copyright 2012, Springer Nature.

of the commercial external cavity lasers with hertz-level linewidth, the performance of QD laser can be greatly improved.

In addition to the phase noise squeezing, the OIL can be also utilized to improve the optical bandwidth of QD-based frequency comb laser through FWM, which is promising for WDM applications. Fig. 5.27B depicts the spectral power mapping of the 102 GHz comb laser as a function of its wavelength and injection wavelength of the master laser. The optical spectra of the comb laser in free-running operation (blue) and in optical injection operation (red) are shown in Fig. 5.27C, where the longitudinal mode that is injected is marked by the black arrow. Despite the frequency comb region suffers from an overall blue-shift, the laser optical bandwidth is largely improved in presence of the 3-dB bandwidth increasing from 1 to 3.5 nm (i.e., from 204 to 714 GHz) along with the full bandwidth above the noise floor increasing from 5 to 9.5 nm (i.e., from 1 to 1.94 THz). In particular, the laser exhibits a stable locking state in presence of an optical injection broadening (OIB) regime more than 82 pm for the master laser wavelength. It is worth stressing that the injection wavelength also plays a crucial role in the OIB dynamics, which has been discussed in the literature [249].

5.7 High-speed modulation

Direct modulation of light with QD lasers has attracted great interest for both short and long distance high-speed optical communication systems. Direct modulation is simply achieved by using a direct RF modulation of the laser's injection current. It alleviates the requirement of bulky and lossy external modulators in the transmitter, thus providing a cost and energy-efficient solution. Table 5.4 summarizes the main performance of directly modulated QD and QDash lasers operating at 1.3 and 1.5 μm. The best dynamic performance ever achieved at 1.5 μm reported a modulation bandwidth as large as 17.5 GHz on an InAs/InP(100) QD laser [216]. Fig. 5.28A shows the bias current-dependent modulation response of this laser with 6 QD layers. The wide 3-dB modulation bandwidth is attributed to the narrow gain profile and a high differential gain resulting from the reduction of the size distribution. Fig. 5.28B demonstrates that the QD laser can also be modulated with a multilevel modulation format (PAM4) at room temperature. The eye diagram is still opened even at 25 GBaud/s (50 Gbit/s), which is a record value for 1.5 μm QD lasers. Other performance have been reported for (100)InP-based QD lasers operating at 1.5 μm, such as a 3-dB modulation bandwidth of 5 GHz in [18]. Interestingly, in this work, the laser showed a much higher large signal modulation capability of 15 Gbit/s with a 4 dB extinction ratio. This discrepancy between the small and large signal performances was attributed to the large nonlinear gain compression effect. Through the optimization of the barrier width and the number of stack layers, the modulation bandwidth was increased to 9 GHz along with a large signal modulation up to 22 Gbit/s for an extinction ratio of 3 dB [314]. The tunnel injection and p-doping techniques can also be considered to further enhance the modulation bandwidth up to 14.4 GHz [316].

Table 5.4 Threshold current (I_{th}) and 3-dB modulation bandwidth ($f_{3dB,\ max}$) of QD and QDash lasers operating at 1.3 and 1.5 μm.

Substrate	Wavelength (μm)	Type	I_{th} (mA)	$f_{3dB,max}$ (GHz)	Reference
InP	1.5	QD FP	41	4.8	[313]
InP	1.5	QD FP	38	5	[18]
InP	1.5	QD FP	20	9.1	[314]
InP	1.5	QD FP	11.2	12.1	[315]
InP	1.5	QD FP	13.4	14.4	[316]
InP	1.5	QD FP	25	17.5	[216]
InP	1.5	QDash FP	47	7.4	[317]
InP	1.5	QDash FP	34	8	[318]
InP	1.5	QDash FP	25	10	[319]
InP	1.5	QDash FP	55	12	[320]
InP	1.5	QDash DFB	65	7.6	[321]
InP	1.5	QDash DFB	4.8	9.6	[204]
InP	1.5	QDash DFB	50	10	[322]
InP	1.5	QDash DFB	30	10	[323]
InP	1.5	QDash DFB	35	10	[324]
GaAs	1.3	QD FP	15	3.8	[325]
GaAS	1.3	QD FP	17	7.8	[326]
GaAs	1.3	QD FP	7.3	8	[14]
GaAs	1.3	QD FP	9.2	9.2	[315]
GaAs	1.3	QD FP	2.2	9.3	[327]
GaAs	1.3	QD FP	11	11	[328]
GaAs	1.3	QD FP	10	11.9	[329]
GaAs	1.3	QD FP	10.9	13.1	[330]
GaAs	1.3	QD DFB	5	4.9	[186]
GaAs	1.3	QD DFB	6.8	11.4	[331]
Si	1.3	QD FP	19	1.6	[332]
Si	1.3	QD FP	14	6.5	[241]
Si	1.3	QD DFB	20	2.8	[333]
SOI	1.3	QD DFB	4	13	[190]
GaAs	1.3	QD VCSEL	4	2.5	[334]
GaAs	1.3	QD VCSEL	6	3	[335]

Although QD lasers grown on (311)B InP substrate show limited application range, let us note that a modulation bandwidth of 4.8 GHz has been reported [313]. As for QDash lasers on (100)InP substrate, most works employed the p-doping technique to improve the modulation bandwidth and to reduce the chirp [319, 320, 324]. For example, the modulation bandwidth was increased from 6 GHz for the undoped laser to 8 GHz with p-doping [320]. On the other hand, the tunnel injection technique can further increase the modulation bandwidth beyond 10 GHz, while reducing the chirp toward zero [316, 320].

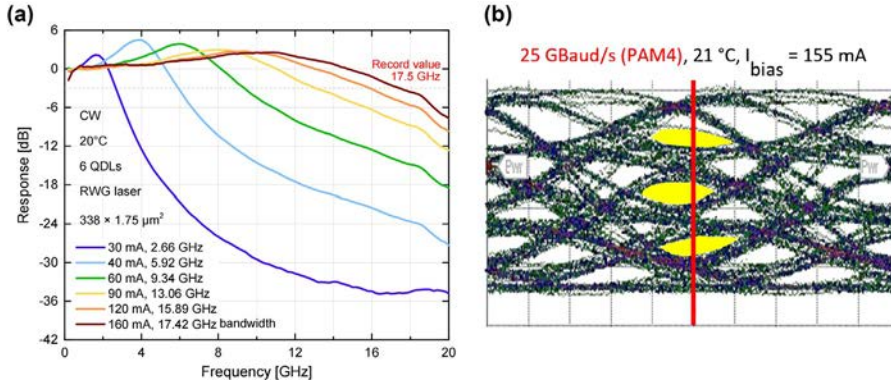

Fig. 5.28 (A) Small-signal modulation response of InAs/InP QD FP laser. (B) Large signal PAM4 modulation of InAs/InP QD FP laser showing the high data rate of 25 GBaud/s (50 Gbit/s).
Reprinted with permission from A. Abdollahinia, S. Banyoudeh, A. Rippien, F. Schnabel, O. Eyal, I. Cestier, I. Kalifa, E. Mentovich, G. Eisenstein, J.P. Reithmaier, Temperature stability of static and dynamic properties of 1.55 μm quantum dot lasers, Opt. Express 26 (5) (2018) 6056–6066, https://doi.org/10.1364/OE.26.006056, copyright 2018, Optica Publishing Group.

For 1.3 μm InAs/GaAs QD lasers grown on GaAs substrate with GS lasing, a record bandwidth of 13.1 GHz was reported [330] by reducing the GaAs barrier thickness. Furthermore, a standard p-doped QD laser emitting on the sole GS with maximum bandwidth of 7.2 GHz was demonstrated [315]. In contrast, the graded p-doping technique can improve the carrier transport hence leading to a better modulation bandwidth of 9.2 GHz as shown in Fig. 5.29A. The increase in small-signal bandwidth reinforces the ability of direct modulation at higher bit rates in the large-signal regime. Fig. 5.29C depicts the maximum error-free bit rate of 22.5 Gbit/s. Compared to the sole GS laser, the sole ES laser shows a slightly higher bandwidth of 11.7 GHz (Fig. 5.29B) which is attributed to the lower gain compression factor and larger differential gain [315]. The maximum BER is 27.5 Gbit/s as shown in Fig. 5.29D. On the opposite, the QD laser directly grown on silicon has slightly inferior modulation bandwidth and modulation efficiency [241]. Last but not least, a record evanescent QD DFB laser on silicon with a 3-dB modulation bandwidth of 13 GHz, a threshold current of 4 mA, an SMSR of 60 dB is realized [190].

Compared to edge emitting lasers, vertical cavity surface emitting lasers (VCSELs) offer multiple advantages such as small footprint, low threshold current, efficient signal-to-fiber coupling, and more temperature-stable wavelength, which are important for high data rate communications [336–338]. The first QD VCSEL operated at room-temperature was realized in 1996 with a CW operating current of 32 mA [339, 340]. The major breakthrough of QD VCSEL came out in 1997 with a very low threshold current below 200 μA [341]. Regarding the modulation performance, 850 nm QD VCSELs have shown 3-dB modulation bandwidth of 18 GHz and record data transmission of 56 Gbit/s at 85°C [342]. Additionally, for 980 nm QD VCSELs, maximum bandwidth of 18 GHz and bit rate of 35 Gbit/s at 85°C operation are achieved in [343].

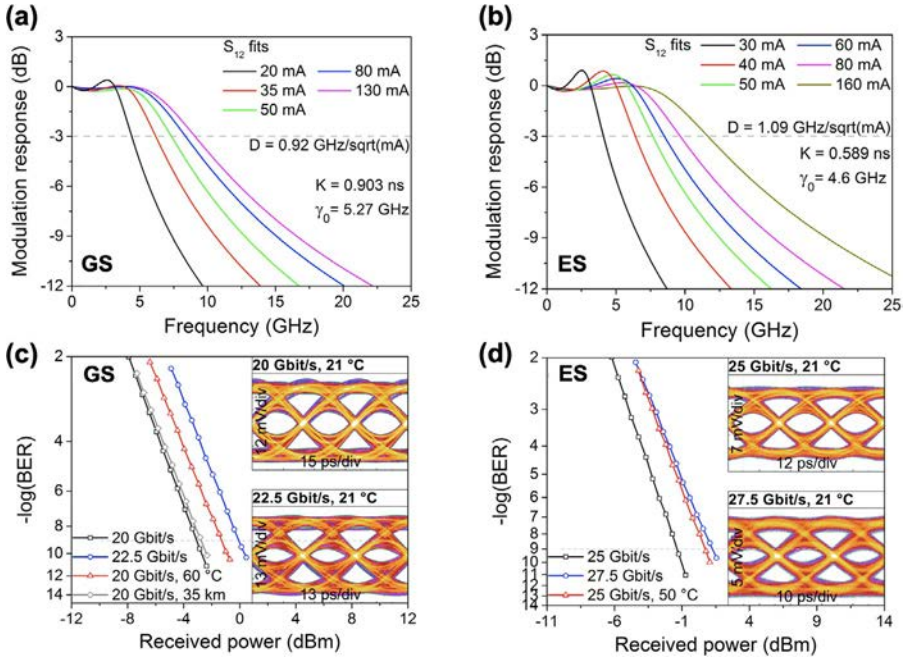

Fig. 5.29 Current-dependent modulation transfer function of the GS (A) and ES (B) InAs/GaAs QD lasers. Bit-error rates of the GS (C) and ES (D) InAs/GaAs QD lasers with eye diagrams in *insets*.

Reprinted with permission from D. Arsenijević, D. Bimberg, Quantum-dot lasers for 35 Gbit/s pulse-amplitude modulation and 160 Gbit/s differential quadrature phase-shift keying, in: Semiconductor Lasers and Laser Dynamics VII, vol. 9892, International Society for Optics and Photonics, SPIE, 2016, https://doi.org/10.1117/12.2230758, copyright 2016, SPIE.

The first GaAs-based 1.3 μm QD VCSEL operating in pulsed mode at room temperature and with a threshold current below 2 mA was reported [344]. In 2009, the efficient CW lasing operation at room temperature of the 1.3 μm QD VCSELs was obtained [345]. However, it turned out that large thermal effects limit the modulation bandwidth between 2 and 3 GHz of 1.3 μm QD VCSELs [334, 335]. Let us stress that very recently, the first demonstration of a 1.5 μm VCSEL based on InAs QDs on InP was reported with CW, low threshold, and room temperature operation along with a stable output polarization state [346]. This novel achievement can potentially open the door to further development of 1.5 μm high-speed QD VCSELs.

As of today, modulation capabilities of QD lasers remain still below expectation by comparison with their QW counterparts, but we believe that there is still room for progress. Therefore, further improvement in the modal gain of QD lasers is of great significance for high-speed modulation. The increase of modal gain can be realized by increasing the dot density, reducing the epitaxial defects as well as by introducing the p-doping in the active region.

5.8 Quantum dot microlasers

For decades, huge progress in the miniaturization and the large-scale electronic integrated circuits (IC) that was guided by Moore's law had led to drastic improvement of performance and simultaneous decrease in cost. Nevertheless, it is a big challenge to reproduce this event in PIC. One of the most important obstacles in the development of small-footprint and large-scale PIC comes from the large size of photonic devices. For both electronic and photonic components, their sizes are limited to the wavelengths [347]. Therefore, the photonic devices are made much larger than the electronic devices, due to the much longer wavelength of photons compared to electrons. In the past two decades, some pioneering studies aimed at pushing the size of photonic devices to their limitations thus to accommodate both electronic and photonic devices on a single chip. In particular, the lasers that benefit from the material recombination and methods of fabrication have demonstrated record miniaturization. Examples, such as microdisk laser [348], photonic wire laser [349], photonic crystal laser [350], and random lasers [351], have been reported.

Not only the wavelength, but also the modal gain and the internal loss of laser cavity limit the miniaturization of laser. Benefiting from the quantized DOS that improves the modal gain, the QD active region is a promising solution for microlaser [82, 277, 352, 353]. A prior study demonstrated that the size of QD-based microring lasers that were directly grown on silicon substrate could be reduced to the micrometer scale, as shown in Fig. 5.30A–C. By reducing the radius of microring to 5 μm, the electrically pumped QD laser exhibited submilliamp threshold current at room temperature (Fig. 5.30E). By taking advantage of the high thermal stability of QD, these devices could operate in CW mode up to 100°C (Fig. 5.30D). Despite the limited output power on the order of microwatt, the microlaser that contains a few number of QD exhibits a strong potential for single-photon generation [337, 354–357]. Recently, QD laser made of photonic crystal cavity is regarded as a potential solution for silicon PIC, due to the high Q-factor, ultra-small mode volume, and large Purcell factor offered by the cavity design [358]. By taking advantage of high-performance QD material, electrically pumped photonic crystal laser allows for high power output over 10 mW, and high-temperature operation at 70°C [359]. In this context, small-footprint and high-performance QD laser will play an important role in next-generation silicon PIC and future quantum PIC.

On the other hand, laser devices in such form factor received attention for their potential candidacy in other advanced applications such as neuromorphic computing. Recent work from Hewlett-Packard Labs [360, 361] has proven the possibility of optical memory, by using a QD microring laser with finely tuned structure on Si platform. These devices shows not only CW operation up to 70°C with considerable output power, but also impressive energy efficiency in transmitting signals (1.2 pJ/bit) [360]. Most importantly, with the right input, these lasers can behave as a memristor [361], therefore offering a novel approach to emulate neurons optically, based on what innovative neuromorphic computing PIC chips can be built, and can benefit as well the intrinsic advantages from QD lasers, for example, less energy needed

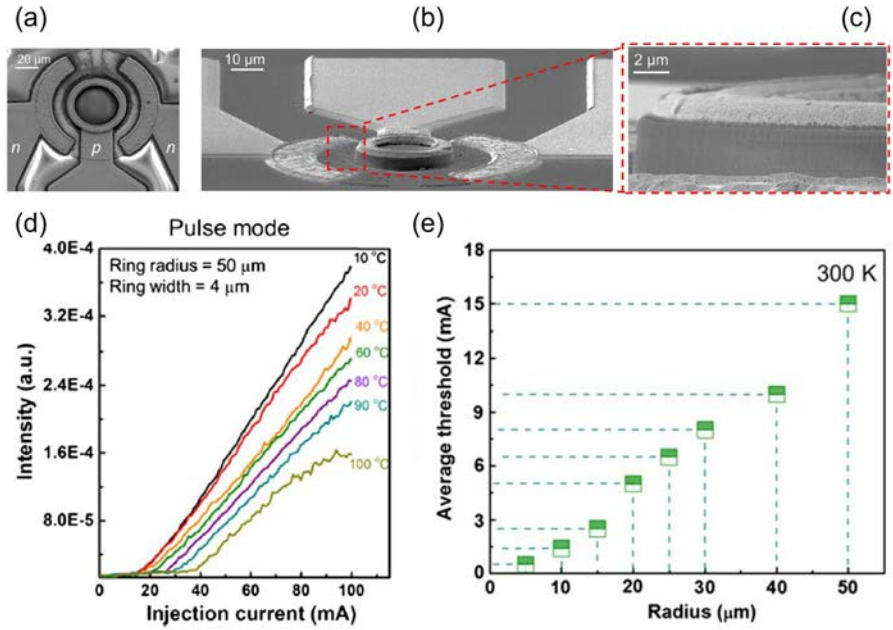

Fig. 5.30 SEM of the QD microlaser from (A) top view and (B) cross-sectional view. (C) Zoomed-in SEM image of the mesa. (D) Measured L-I curve from the microring laser with a radius of 50 μm as a function of temperature under pulsed pump condition. (E) Average threshold current as a function of radius at room temperature.
Reprinted with permission from Y. Wan, J. Norman, Q. Li, M.J. Kennedy, D. Liang, C. Zhang, D. Huang, Z. Zhang, A.Y. Liu, A. Torres, D. Jung, A.C. Gossard, E.L. Hu, K.M. Lau, J.E. Bowers, 1.3 μm submilliamp threshold quantum dot micro-lasers on Si, Optica 4 (8) (2017) 940–944, https://doi.org/10.1364/OPTICA.4.000940, copyright 2017, Optica Publishing Group.

for both cooling and power supply. Furthermore, an optical neuron requires fewer electric wiring, meaning reduced noises and heating problem, leading to more efficient on-chip communication.

5.9 Conclusions

This chapter reviewed the genesis, the most recent findings, and the prospects of QD lasers. Thanks to their compactness, great thermal stability, and large reflection immunity, QD lasers are excellent candidates for low energy consumption and optical-isolation-free PICs. When directly grown on silicon, they can even offer much superior FWM efficiency than their QW devices counterparts, which is vital for achieving efficient frequency comb operation. Given that their remarkable intensity and phase noise properties, QD lasers can be meaningful for coherent technologies, on-chip atomic clock, optical radars (i.e., LIDARs), and spectroscopy. Future perspective also involve

using QDs embedded in microcavities for single-photon generators, squeezed-photon beams, entangled systems for quantum cryptography, and computing [362]. Self-assembled QDs can also be very promising for reaching midinfrared and THz optical wavelengths using quantum cascade heterostructures [363, 364]. The development of visible light sources grown on silicon has also become of growing interest for a variety of applications near the infrared. A recent work has shown room temperature lasing of electrically pumped InP/GaAsP QD lasers directly grown on silicon emitting at 750 nm [365, 366]. QD lasers heterogeneously integrated on silicon carbide (SiC) can also be a promising approach for achieving high-temperature stability [239]. Finally, QD lasers emitting at 1050 nm can also be considered as an alternative to bulky and expensive solid-state lasers or superluminescent diodes for state-of-the-art ophthalmic optical coherence tomography applications [275]. As a conclusion, about 40 years later after their discovery, we strongly believe that QD solutions can be implemented into industrial products to sustain the growing needs of the communication and information society. Overall, in this review chapter, we have tried to highlight the most promising areas for these technologies, hence putting in practical use QD lasers. In particular, we would like to remind that the direct growth of QD InAs is a key enabling technology for obtaining efficient light-emitting devices. Overall, QD photonic devices are the most effective solution for photo-electronization servers, addressing optical connectivity in artificial intelligence, machine learning, high-performance computing, and data center markets. Finally, we would also like to emphasize that their deployment onto the market is a direct consequence of the strong development of nanotechnology over the last 20 years and therefore provides a solid foundation for the delivery of efficient photonic solutions.

Acknowledgments

Authors acknowledge Professor L.F. Lester from the Virginia Tech, Blacksburg, United States; Professor J.E. Bowers from the University of California Santa Barbara, United States; Professor D. Bimberg from the TU Berlin, Germany, and the Changchun Institute of Optics, Fine Mechanics and Physics, Chinese Academy of Sciences, China; Dr. P. Poole from the NRC Canada, Ottawa, Canada; Dr. D. Liang from the HP Labs, Milpitas, United States; Dr. W.W. Chow from the Sandia National Laboratories, Albuquerque, United States; Professor C. Wang from the ShanghaiTech University, Shanghai, China, as well as S. Ding, T. Renaud, and S. Zhao from the Télécom Paris, Institut Polytechnique de Paris, France. Authors acknowledge the financial support of the Institut Mines Telecom, the Air Force Office of Scientific Research (AFSOR), and the Center for Integrated Nanotechnologies (CINT) through user proposals.

References

[1] Transforma Insights, Current IoT Forecast Highlights, Transforma Insights, 2022. Technical Report.

[2] F. Tariq, M.R.A. Khandaker, K.-K. Wong, M.A. Imran, M. Bennis, M. Debbah, A speculative study on 6G, IEEE Wirel. Commun. 27 (4) (2020) 118–125, https://doi.org/10.1109/MWC.001.1900488.

[3] G. Kamiya, Data Centres and Data Transmission Networks, International Energy Agency, 2021. Technical Report.
[4] M. Vallo, E. Mounier, Optical Transceivers For Datacom & Telecom Market 2021, Yole Development Market & Technology Report, 2021. Technical Report.
[5] Y. Arakawa, T. Nakamura, Y. Urino, T. Fujita, Silicon photonics for next generation system integration platform, IEEE Commun. Mag. 51 (3) (2013) 72–77, https://doi.org/10.1109/MCOM.2013.6476868.
[6] K. Ławniczuk, L.M. Augustin, N. Grote, M.J. Wale, M.K. Smit, K.A. Williams, Open access to technology platforms for InP-based photonic integrated circuits, Adv. Opt. Technol. 4 (2) (2015) 157–165, https://doi.org/10.1515/aot-2015-0012.
[7] F. Kish, V. Lal, P. Evans, S.W. Corzine, M. Ziari, T. Butrie, M. Reffle, H.-S. Tsai, A. Dentai, J. Pleumeekers, M. Missey, M. Fisher, S. Murthy, R. Salvatore, P. Samra, S. Demars, N. Kim, A. James, A. Hosseini, P. Studenkov, M. Lauermann, R. Going, M. Lu, J. Zhang, J. Tang, J. Bostak, T. Vallaitis, M. Kuntz, D. Pavinski, A. Karanicolas, B. Behnia, D. Engel, O. Khayam, N. Modi, M.R. Chitgarha, P. Mertz, W. Ko, R. Maher, J. Osenbach, J.T. Rahn, H. Sun, K.-T. Wu, M. Mitchell, D. Welch, System-on-chip photonic integrated circuits, IEEE J. Sel. Top. Quantum Electron. 24 (1) (2018) 1–20, https://doi.org/10.1109/JSTQE.2017.2717863.
[8] D. Bimberg, M. Grundmanm, N.N. Ledentsov, Quantum Dots Heterostructures, Wiley, 1999.
[9] M. Sugawara (Ed.), Self-Assembled InGaAs/GaAs Quantum Dots, Academic Press, 1999.
[10] N. Kirstaedter, O.G. Schmidt, N.N. Ledentsov, D. Bimberg, V.M. Ustinov, A.Yu. Egorov, A.E. Zhukov, M.V. Maximov, P.S. Kop'ev, Zh.I. Alferov, Gain and differential gain of single layer InAs/GaAs quantum dot injection lasers, Appl. Phys. Lett. 69 (9) (1996) 1226–1228, https://doi.org/10.1063/1.117419.
[11] D. Bimberg, N. Kirstaedter, N.N. Ledentsov, Zh.I. Alferov, P.S. Kopév, V.M. Ustinov, InGaAs-GaAs quantum-dot lasers, IEEE J. Sel. Top. Quantum Electron. 3 (2) (1997) 196–205, https://doi.org/10.1109/2944.605656.
[12] L.F. Lester, A. Stintz, H. Li, T.C. Newell, E.A. Pease, B.A. Fuchs, K.J. Malloy, Optical characteristics of 1.24-μm InAs quantum-dot laser diodes, IEEE Photon. Technol. Lett. 11 (8) (1999) 931–933, https://doi.org/10.1109/68.775303.
[13] D.G. Deppe, K. Shavritranuruk, G. Ozgur, H. Chen, S. Freisem, Quantum dot laser diode with low threshold and low internal loss, Electron. Lett. 45 (2009) 54–56, https://doi.org/10.1049/el:20092873.
[14] K. Otsubo, N. Hatori, M. Ishida, S. Okumura, T. Akiyama, Y. Nakata, H. Ebe, M. Sugawara, Y. Arakawa, Temperature-insensitive eye-opening under 10-Gb/s modulation of 1.3-μm p-doped quantum-dot lasers without current adjustments, Jpn J. Appl. Phys. 43 (8B) (2004) L1124–L1126, https://doi.org/10.1143/JJAP.43.L1124.
[15] M.V. Maximov, I.V. Kochnev, Y.M. Shernyakov, S.V. Zaitsev, N.Y. Gordeev, A.F. Tsatsulńikov, A.V. Sakharov, I.L. Krestnikov, P.S. Kopév, Z.I. Alferov, N.N. Ledentsov, D. Bimberg, A.O. Kosogov, P. Werner, U. Gösele, InGaAs/GaAs quantum dot lasers with ultrahigh characteristic temperature ($T_0 = 385$K) grown by metal organic chemical vapour deposition, Jpn J. Appl. Phys. 36 (1997) 4221–4223, https://doi.org/10.1143/jjap.36.4221.
[16] J. Duan, H. Huang, Z.G. Lu, P.J. Poole, C. Wang, F. Grillot, Narrow spectral linewidth in InAs/InP quantum dot distributed feedback lasers, Appl. Phys. Lett. 112 (12) (2018) 121102, https://doi.org/10.1063/1.5022480.

[17] T. Septon, A. Becker, S. Gosh, G. Shtendel, V. Sichkovskyi, F. Schnabel, A. Sengül, M. Bjelica, B. Witzigmann, J.P. Reithmaier, G. Eisenstein, Large linewidth reduction in semiconductor lasers based on atom-like gain material, Optica 6 (8) (2019) 1071–1077, https://doi.org/10.1364/OPTICA.6.001071.
[18] D. Gready, G. Eisenstein, C. Gilfert, V. Ivanov, J.P. Reithmaier, High-speed low-noise InAs/InAlGaAs/InP 1.55-μm quantum-dot lasers, IEEE Photon. Technol. Lett. 24 (10) (2012) 809–811, https://doi.org/10.1109/LPT.2012.2188506.
[19] J. Duan, X.-G. Wang, Y.-G. Zhou, C. Wang, F. Grillot, Carrier-noise-enhanced relative intensity noise of quantum dot lasers, IEEE J. Quantum Electron. 54 (6) (2018) 1–7, https://doi.org/10.1109/JQE.2018.2880452.
[20] D. Jung, P.G. Callahan, B. Shin, K. Mukherjee, A.C. Gossard, J.E. Bowers, Low threading dislocation density GaAs growth on on-axis GaP/Si (001), J. Appl. Phys. 122 (22) (2017) 225703, https://doi.org/10.1063/1.5001360.
[21] Y. Arakawa, T. Nakamura, J. Kwoen, Chapter Three - Quantum dot lasers for silicon photonics, in: S. Lourdudoss, J.E. Bowers, C. Jagadish (Eds.), Future Directions in Silicon Photonics, Semiconductors and Semimetals, vol. 101, Chapter 5, Elsevier, 2019, pp. 91–138, https://doi.org/10.1016/bs.semsem.2019.07.007.
[22] J. Duan, H. Huang, B. Dong, D. Jung, J.C. Norman, J.E. Bowers, F. Grillot, 1.3-μm Reflection insensitive InAs/GaAs quantum dot lasers directly grown on silicon, IEEE Photon. Technol. Lett. 31 (5) (2019) 345–348, https://doi.org/10.1109/LPT.2019.2895049.
[23] Y. Arakawa, T. Nakamura, K. Kurata, Highlights of 10-years of research in a Japanese Si photonics project, in: 2022 Optical Fiber Communications Conference and Exhibition (OFC), 2022, pp. 1–4.
[24] D. O'Brien, S.P. Hegarty, G. Huyet, J.G. McInerney, T. Kettler, M. Laemmlin, D. Bimberg, V.M. Ustinov, A.E. Zhukov, S.S. Mikhrin, A.R. Kovsh, Feedback sensitivity of 1.3 μm InAs/GaAs quantum dot lasers, Electron. Lett. 39 (25) (2003) 1, https://doi.org/10.1049/el:20031153.
[25] G. Huyet, D. O'Brien, S.P. Hegarty, J.G. McInerney, A.V. Uskov, D. Bimberg, C. Ribbat, V.M. Ustinov, A.E. Zhukov, S.S. Mikhrin, A.R. Kovsh, J.K. White, K. Hinzer, A.J. SpringThorpe, Quantum dot semiconductor lasers with optical feedback, Phys. Status Solidi A 201 (2) (2004) 345–352, https://doi.org/10.1002/pssa.200303971.
[26] D. O'Brien, S.P. Hegarty, G. Huyet, A.V. Uskov, Sensitivity of quantum-dot semiconductor lasers to optical feedback, Opt. Lett. 29 (10) (2004) 1072–1074, https://doi.org/10.1364/OL.29.001072.
[27] Z.I. Alferov, R.F. Kazarinov. Semiconductor laser with electric pumping, Inventor's Certificate No. 181737 (in Russian), Application No. 950840, priority as of March 30, 1963.
[28] R.N. Hall, G.E. Fenner, J.D. Kingsley, T.J. Soltys, R.O. Carlson, Coherent light emission from GaAs junctions, Phys. Rev. Lett. 9 (1962) 366–368, https://doi.org/10.1103/PhysRevLett.9.366.
[29] N. Holonyak Jr, S.F. Bevacqua, Coherent (visible) light emission from $Ga(As_{1-x}P_x)$ junctions, Appl. Phys. Lett. 1 (4) (1962) 82–83, https://doi.org/10.1063/1.1753706.
[30] M.I. Nathan, W.P. Dumke, G. Burns, F.H. Dill, G. Lasher, Stimulated emission of radiation from GaAs *p-n* junctions, Appl. Phys. Lett. 1 (3) (1962) 62–64, https://doi.org/10.1063/1.1777371.
[31] H. Kroemer, A proposed class of hetero-junction injection lasers, Proc. IEEE 51 (12) (1963) 1782–1783, https://doi.org/10.1109/PROC.1963.2706.
[32] Zh.I. Alferov, V.M. Andreev, E.L. Portnoi, M.K. Trukan, AlAs-GaAs heterojunction injection lasers with a low room-temperature threshold, Fiz. Tekh. Poluprovodn. 3 (1969) 1328.

[33] I. Hayashi, M.B. Panish, F.K. Reinhart, GaAs-$Al_xGa_{1-x}As$ double heterostructure injection lasers, J. Appl. Phys. 42 (5) (1971) 1929–1941, https://doi.org/10.1063/1.1660469.
[34] R.D. Burnham, N. Holonyak Jr., H.W. Korb, H.M. Macksey, D.R. Scifres, J.B. Woodhouse, Zh.I. Alferov, Double heterojunction AlGaAsP quaternary lasers, Appl. Phys. Lett. 19 (2) (1971) 25–28, https://doi.org/10.1063/1.1653807.
[35] R. Dingle, C.H. Henry. Quantum effects in heterostructure lasers. U.S. Patent 3982207, 1976.
[36] M. Grundmann, O. Stier, D. Bimberg, InAs/GaAs pyramidal quantum dots: strain distribution, optical phonons, and electronic structure, Phys. Rev. B 52 (1995) 11969–11981, https://doi.org/10.1103/PhysRevB.52.11969.
[37] O. Stier, M. Grundmann, D. Bimberg, Electronic and optical properties of strained quantum dots modeled by 8-band k ·p theory, Phys. Rev. B 59 (1999) 5688–5701, https://doi.org/10.1103/PhysRevB.59.5688.
[38] Y. Arakawa, H. Sakaki, Multidimensional quantum well laser and temperature dependence of its threshold current, Appl. Phys. Lett. 40 (11) (1982) 939–941, https://doi.org/10.1063/1.92959.
[39] K. Petermann, Laser Diode Modulation and Noise, Advances in Opto-Electronics, Springer, Dordrecht, 1988.
[40] C. Weisbuch, J. Nagle, On the impact of low-dimensionality in quantum-well, wire, dot-semiconductor lasers, in: S.P. Beaumont, C.M. Sotomayor-Torrès (Eds.), Science and Engineering of One- and Zero-Dimensional Semiconductors, NATO ASI Series, vol. 214, Springer US, 1990, pp. 309–316, https://doi.org/10.1007/978-1-4684-5733-9_29.
[41] L.A. Coldren, S.W. Corzine, M.L. Mashanovitch, Diode Lasers and Photonic Integrated Circuits, John Wiley & Sons, 2012, https://doi.org/10.1002/9781118148167.
[42] P. Blood, Quantum Confined Laser Devices: Optical Gain and Recombination in Semiconductors, Oxford University Press, 2015, https://doi.org/10.1093/acprof:oso/9780199644513.001.0001.
[43] J. Nagle, C. Weisbuch, The physics of low-dimensional effects in quantum well lasers, in: F. Capasso, G.H. Doehler, J.N. Schulman (Eds.), Quantum Well and Superlattice Physics II, vol. 0943, International Society for Optics and Photonics, SPIE, 1988, pp. 76–83, https://doi.org/10.1117/12.947293.
[44] L. Esaki, R. Tsu, Superlattice and negative differential conductivity in semiconductors, IBM J. Res. Dev. 14 (1) (1970) 61–65, https://doi.org/10.1147/rd.141.0061.
[45] E.A. Rezek, N. Holonyak, B.A. Vojak, G.E. Stillman, J.A. Rossi, D.L. Keune, J.D. Fairing, LPE $In_{1-x}Ga_xP_{1-z}As_z$ $x \sim 0.12$, $z \sim 0.26$ DH laser with multiple thin-layer (<500 Å) active region, Appl. Phys. Lett. 31 (4) (1977) 288–290, https://doi.org/10.1063/1.89665.
[46] C. Weisbuch, B. Vinter, CHAPTER VI - Towards 1D and 0D physics and devices, in: C. Weisbuch, B. Vinter (Eds.), Quantum Semiconductor Structures, Academic Press, San Diego, 1991, pp. 189–215, https://doi.org/10.1016/B978-0-08-051557-1.50010-X.
[47] H.P. Rockspy, The colour of selenium ruby glasses, J. Soc. Glass Technol. 16 (1932) 171.
[48] A.I. Ekimov, A.A. Onushenko, Size quantization of the electron energy spectrum in a microscopic semiconductor crystal, J. Exp. Theor. Phys. Lett. 40 (1984) 337.
[49] Y. Arakawa, H. Sakaki, M. Nishioka, H. Okamoto, N. Miura, Spontaneous emission characteristics of quantum well lasers in strong magnetic fields - an approach to quantum-well-box light source, Jpn J. Appl. Phys. 22 (1983) L804–L806, https://doi.org/10.1143/JJAP.22.L804.
[50] Y. Arakawa, K. Vahala, A. Yariv, Quantum noise and dynamics in quantum well and quantum wire lasers, Appl. Phys. Lett. 45 (9) (1984) 950–952, https://doi.org/10.1063/1.95453.

[51] Y. Arakawa, A. Yariv, Quantum well lasers-Gain, spectra, dynamics, IEEE J. Quantum Electron. 22 (9) (1986) 1887–1899, https://doi.org/10.1109/JQE.1986.1073185.
[52] Y. Arakawa, K. Vahala, A. Yariv, Dynamic and spectral properties of semiconductor lasers with quantum-well and quantum-wire effects, Surf. Sci. 174 (1) (1986) 155–162, https://doi.org/10.1016/0039-6028(86)90401-2.
[53] L. Goldstein, F. Glas, J.-Y. Marzin, M.N. Charasse, G. Le Roux, Growth by molecular beam epitaxy and characterization of InAs/GaAs strained-layer superlattices, Appl. Phys. Lett. 47 (10) (1985) 1099–1101, https://doi.org/10.1063/1.96342.
[54] F. Glas, C. Guille, P. Henoc, F. Houzay, TEM study of the molecular beam epitaxy island growth of InAs on GaAs, in: Microscopy of Semiconducting Materials, CRC Press, 1987, p. 6, https://doi.org/10.1201/9781003069621-11.
[55] S. Guha, A. Madhukar, K.C. Rajkumar, Onset of incoherency and defect introduction in the initial stages of molecular beam epitaxical growth of highly strained $In_xGa_{1-x}As$ on GaAs(100), Appl. Phys. Lett. 57 (20) (1990) 2110–2112, https://doi.org/10.1063/1.103914.
[56] C.W. Snyder, B.G. Orr, D. Kessler, L.M. Sander, Effect of strain on surface morphology in highly strained InGaAs films, Phys. Rev. Lett. 66 (1991) 3032–3035, https://doi.org/10.1103/PhysRevLett.66.3032.
[57] M. Tabuchi, S. Noda, A. Sasaki, Mesoscopic structure in lattice-mismatched hetero-epitaxial interface layers, in: Science and Technology of Mesoscopic Structures, Springer, Tokyo, 1992, pp. 379–384, https://doi.org/10.1007/978-4-431-66922-7_39.
[58] D. Leonard, M. Krishnamurthy, C.M. Reaves, S.P. Denbaars, P.M. Petroff, Direct formation of quantum-sized dots from uniform coherent islands of InGaAs on GaAs surfaces, Appl. Phys. Lett. 63 (23) (1993) 3203–3205, https://doi.org/10.1063/1.110199.
[59] J. Oshinowo, M. Nishioka, S. Ishida, Y. Arakawa, Highly uniform InGaAs/GaAs quantum dots (∼15 nm) by metalorganic chemical vapor deposition, Appl. Phys. Lett. 65 (11) (1994) 1421–1423, https://doi.org/10.1063/1.112070.
[60] N. Kirstaedter, N.N. Ledentsov, M. Grundmann, D. Bimberg, V.M. Ustinov, S.S. Ruvimov, M.V. Maximov, P.S. Kopév, Zh.I. Alferov, U. Richter, P. Werner, U. Gösele, J. Heydenreich, Low threshold, large T_0 injection laser emission from (InGa)As quantum dots, Electron. Lett. 30 (17) (1994) 1416–1417, https://doi.org/10.1049/el_19940939.
[61] J.M. Gérard, Prospects of high-efficiency quantum boxes obtained by direct epitaxial growth, in: E. Burstein, C. Weisbuch (Eds.), Confined Electrons and Photons: New Physics and Applications, NATO Science Series B: Physics, vol. 430, Springer US, 1995, pp. 357–381, https://doi.org/10.1007/978-1-4615-1963-8_13.
[62] W.T. Tsang, F.S. Choa, M.C. Wu, Y.K. Chen, A.M. Sergent, P.F. Sciortino, Very low threshold single quantum well graded-index separate confinement heterostructure InGaAs/InGaAsP lasers grown by chemical beam epitaxy, Appl. Phys. Lett. 58 (23) (1991) 2610–2612, https://doi.org/10.1063/1.104838.
[63] H.K. Choi, C.A. Wang, InGaAs/AlGaAs strained single quantum well diode lasers with extremely low threshold current density and high efficiency, Appl. Phys. Lett. 57 (4) (1990) 321–323, https://doi.org/10.1063/1.103678.
[64] N.N. Ledentsov, V.A. Shchukin, M. Grundmann, N. Kirstaedter, J. Böhrer, O. Schmidt, D. Bimberg, V.M. Ustinov, A.Yu. Egorov, A.E. Zhukov, P.S. Kopév, S.V. Zaitsev, N.Yu. Gordeev, Zh.I. Alferov, A.I. Borovkov, A.O. Kosogov, S.S. Ruvimov, P. Werner, U. Gösele, J. Heydenreich, Direct formation of vertically coupled quantum dots in Stranski-Krastanow growth, Phys. Rev. B 54 (12) (1996) 8743–8750, https://doi.org/10.1103/PhysRevB.54.8743.

[65] D. Bimberg, Quantum dots for lasers, amplifiers and computing, J. Phys. D Appl. Phys. 38 (13) (2005) 2055–2058, https://doi.org/10.1088/0022-3727/38/13/001.
[66] P. Poole, Chapter 11 - InP-based quantum dot lasers, in: J.J. Coleman, A.C. Bryce, C. Jagadish (Eds.), Advances in Semiconductor Lasers, Semiconductors and Semimetals, vol. 86, Elsevier, 2012, pp. 419–453, https://doi.org/10.1016/B978-0-12-391066-0.00011-3.
[67] J.Y. Marzin, J.M. Gérard, A. Izraël, D. Barrier, G. Bastard, Photoluminescence of single InAs quantum dots obtained by self-organized growth on GaAs, Phys. Rev. Lett. 73 (1994) 716–719, https://doi.org/10.1103/PhysRevLett.73.716.
[68] J.M. Moison, F. Houzay, F. Barthe, L. Leprince, E. André, O. Vatel, Self-organized growth of regular nanometer-scale InAs dots on GaAs, Appl. Phys. Lett. 64 (2) (1994) 196–198, https://doi.org/10.1063/1.111502.
[69] A. Moritz, R. Wirth, A. Hangleiter, A. Kurtenbach, K. Eberl, Optical gain and lasing in self-assembled InP/GaInP quantum dots, Appl. Phys. Lett. 69 (2) (1996) 212–214, https://doi.org/10.1063/1.117375.
[70] R. Mirin, A. Gossard, J.E. Bowers, Room temperature lasing from InGaAs quantum dots, Electron. Lett. 32 (18) (1996) 1732–1734, https://doi.org/10.1049/el_19961147.
[71] M. Grundmann, J. Christen, N.N. Ledentsov, J. Böhrer, D. Bimberg, S.S. Ruvimov, P. Werner, U. Richter, U. Gösele, J. Heydenreich, V.M. Ustinov, A.Yu. Egorov, A.E. Zhukov, P.S. Kopév, Zh.I. Alferov, Ultranarrow luminescence lines from single quantum dots, Phys. Rev. Lett. 74 (20) (1995) 4043–4046, https://doi.org/10.1103/PhysRevLett.74.4043.
[72] V.A. Shchukin, N.N. Ledentsov, D. Bimberg, Epitaxy of Nanostructures, NanoScience and Technology, Springer, Berlin, Heidelberg, 2004, https://doi.org/10.1007/978-3-662-07066-6.
[73] Y. Nagamune, M. Nishioka, S. Tsukamoto, Y. Arakawa, GaAs quantum dots with lateral dimension of 25 nm fabricated by selective metalorganic chemical vapor deposition growth, Appl. Phys. Lett. 64 (19) (1994) 2495–2497, https://doi.org/10.1063/1.111577.
[74] M. Kitamura, M. Nishioka, J. Oshinowo, Y. Arakawa, *In situ* fabrication of self-aligned InGaAs quantum dots on GaAs multiatomic steps by metalorganic chemical vapor deposition, Appl. Phys. Lett. 66 (26) (1995) 3663–3665, https://doi.org/10.1063/1.114133.
[75] F. Heinrichsdorff, M.-H. Mao, N. Kirstaedter, A. Krost, D. Bimberg, A.O. Kosogov, P. Werner, Room-temperature continuous-wave lasing from stacked InAs/GaAs quantum dots grown by metalorganic chemical vapor deposition, Appl. Phys. Lett. 71 (1) (1997) 22–24, https://doi.org/10.1063/1.120556.
[76] F. Heinrichsdorff, Ch. Ribbat, M. Grundmann, D. Bimberg, High-power quantum-dot lasers at 1100 nm, Appl. Phys. Lett. 76 (5) (2000) 556–558, https://doi.org/10.1063/1.125816.
[77] R.L. Sellin, Ch. Ribbat, M. Grundmann, N.N. Ledentsov, D. Bimberg, Close-to-ideal device characteristics of high-power InGaAs/GaAs quantum dot lasers, Appl. Phys. Lett. 78 (9) (2001) 1207–1209, https://doi.org/10.1063/1.1350596.
[78] J. Tatebayashi, M. Nishioka, Y. Arakawa, Over 1.5 μm light emission from InAs quantum dots embedded in InGaAs strain-reducing layer grown by metalorganic chemical vapor deposition, Appl. Phys. Lett. 78 (22) (2001) 3469–3471, https://doi.org/10.1063/1.1375842.
[79] R.L. Sellin, C. Ribbat, D. Bimberg, F. Rinner, H. Konstanzer, M. Kelemen, M.T. Mikulla, High-reliability MOCVD-grown quantum dot laser, Electron. Lett. 38 (16) (2002) 883–884, https://doi.org/10.1049/el:20020602.

[80] R.L. Sellin, I. Kaiander, D. Ouyang, T. Kettler, U.W. Pohl, D. Bimberg, N.D. Zakharov, P. Werner, Alternative-precursor metalorganic chemical vapor deposition of self-organized InGaAs/GaAs quantum dots and quantum-dot lasers, Appl. Phys. Lett. 82 (6) (2003) 841–843, https://doi.org/10.1063/1.1544641.
[81] J. Tatebayashi, N. Hatori, M. Ishida, H. Ebe, M. Sugawara, Y. Arakawa, H. Sudo, A. Kuramata, 1.28 μm Lasing from stacked InAs/GaAs quantum dots with low-temperature-grown AlGaAs cladding layer by metalorganic chemical vapor deposition, Appl. Phys. Lett. 86 (5) (2005) 053107, https://doi.org/10.1063/1.1857075.
[82] D. Bimberg, Quantum dot based nanophotonics and nanoelectronics, Electron. Lett. 44 (3) (2008) 168, https://doi.org/10.1049/el:20080074.
[83] H. Hirayama, K. Matsunaga, M. Asada, Y. Suematsu, Lasing action of $Ga_{0.67}In_{0.33}As$/GaInAsP/InP tensile-strained quantum-box lasers, Electron. Lett. 30 (1994) 142–143, https://doi.org/10.1049/el:19940082.
[84] H. Shoji, K. Mukai, N. Ohtsuka, M. Sugawara, T. Uchida, H. Ishikawa, Lasing at three-dimensionally quantum-confined sublevel of self-organized In/sub 0.5/Ga/sub 0.5/As quantum dots by current injection, IEEE Photon. Technol. Lett. 7 (12) (1995) 1385–1387, https://doi.org/10.1109/68.477257.
[85] K. Kamath, P. Bhattacharya, T. Sosnowski, T. Norris, P.J., Room temperature operation of $In_{0.4}Ga_{0.6}As$/GaAs self-organized quantum dot lasers, Electron. Lett. 32 (1997) 1374–1375, https://doi.org/10.1049/el:19960921.
[86] D.L. Huffaker, G. Park, Z. Zou, O.B. Shchekin, D.G. Deppe, 1.3 μm Room-temperature GaAs-based quantum-dot laser, Appl. Phys. Lett. 73 (18) (1998) 2564–2566, https://doi.org/10.1063/1.122534.
[87] K. Mukai, Y. Nakata, H. Shoji, M. Sugawara, K. Ohtsubo, N. Yokoyama, H. Ishikawa, Lasing with low threshold current and high output power from columnar-shaped InAs/GaAs quantum dots, Electron. Lett. 34 (16) (1998) 1588–1590, https://doi.org/10.1049/el:19981075.
[88] S. Fafard, J.P. McCaffrey, Y. Feng, A.C. Nì, H. Marchand, L. Isnard, P. Desjardins, S. Guillon, R.A. Masut, Towards quantum dot laser diodes emitting at 1.5 microns, in: G.A. Lampropoulos, R.A. Lessard (Eds.), 1998 International Conference on Applications of Photonic Technology III: Closing the Gap between Theory, Development, and Applications, vol. 3491, International Society for Optics and Photonics, SPIE, 1998, pp. 271–276, https://doi.org/10.1117/12.328737.
[89] P.G. Eliseev, H. Li, A. Stintz, G.T. Liu, T.C. Newell, K.J. Malloy, L.F. Lester, Transition dipole moment of InAs/InGaAs quantum dots from experiments on ultralow-threshold laser diodes, Appl. Phys. Lett. 77 (2) (2000) 262–264, https://doi.org/10.1063/1.126944.
[90] A. Patanè, A. Polimeni, L. Eaves, M. Henini, P.C. Main, P.M. Smowton, E.J. Johnston, P. J. Hulyer, E. Herrmann, G.M. Lewis, G. Hill, Experimental studies of the multimode spectral emission in quantum dot lasers, J. Appl. Phys. 87 (4) (2000) 1943–1946, https://doi.org/10.1063/1.372117.
[91] F. Klopf, R. Krebs, J.P. Reithmaier, A. Forchel, High-temperature operating 1.3-μm quantum-dot lasers for telecommunication applications, IEEE Photon. Technol. Lett. 13 (8) (2001) 764–766, https://doi.org/10.1109/68.935796.
[92] D. Bimberg (Ed.), Semiconductor Nanostructures, Nanoscience and Technology, Springer, 2008.
[93] A.E. Kaloyeros, S. Oktyabrsky, Self-assembled quantum dots: atomic scale engineering, in: third ed., Dekker Encyclopedia of Nanoscience and Nanotechnology, CRC Press, 2013, p. 13, https://doi.org/10.1081/E-ENN3-120049704.

[94] V.A. Shchukin, D. Bimberg, Spontaneous ordering of nanostructures on crystal surfaces, Rev. Mod. Phys. 71 (1999) 1125–1171, https://doi.org/10.1103/RevModPhys.71.1125.
[95] P.M. Petroff, S.P. DenBaars, MBE and MOCVD growth and properties of self-assembling quantum dot arrays in III-V semiconductor structures, Superlattice Microstruct. 15 (1) (1994) 15, https://doi.org/10.1006/spmi.1994.1004.
[96] K. Matsuda, T. Saiki, H. Saito, K. Nishi, Room-temperature photoluminescence spectroscopy of self-assembled $In_{0.5}Ga_{0.5}As$ single quantum dots by using highly sensitive near-field scanning optical microscope, Appl. Phys. Lett. 76 (1) (2000) 73–75, https://doi.org/10.1063/1.125660.
[97] Y. Nagamune, H. Watabe, M. Nishioka, Y. Arakawa, Observation of a single photoluminescence peak from a single quantum dot, Appl. Phys. Lett. 67 (22) (1995) 3257–3259, https://doi.org/10.1063/1.114890.
[98] J. Kim, C. Meuer, D. Bimberg, G. Eisenstein, Effect of inhomogeneous broadening on gain and phase recovery of quantum-dot semiconductor optical amplifiers, IEEE J. Quantum Electron. 46 (11) (2010) 1670–1680, https://doi.org/10.1109/JQE.2010.2058793.
[99] D. Gready, G. Eisenstein, Effects of homogeneous and inhomogeneous broadening on the dynamics of tunneling injection quantum dot lasers, IEEE J. Quantum Electron. 47 (7) (2011) 944–949, https://doi.org/10.1109/JQE.2011.2134835.
[100] M. Grundmann, D. Bimberg, Gain and threshold of quantum dot lasers: theory and comparison to experiments, Jpn J. Appl. Phys. 36 (1997) 4181–4187, https://doi.org/10.1143/JJAP.36.4181.
[101] A.R. Kovsh, N.A. Maleev, A.E. Zhukov, S.S. Mikhrin, A.P. Vasil'ev, E.A. Semenova, Yu.M. Shernyakov, M.V. Maximov, D.A. Livshits, V.M. Ustinov, N.N. Ledentsov, D. Bimberg, Zh.I. Alferov, InAs/InGaAs/GaAs quantum dot lasers of 1.3 μm range with enhanced optical gain, J. Cryst. Growth 251 (1) (2003) 729–736, https://doi.org/10.1016/S0022-0248(02)02506-X.
[102] A. Salhi, G. Raino, L. Fortunato, V. Tasco, G. Visimberga, L. Martiradonna, M.T. Todaro, M. De Giorgi, R. Cingolani, A. Trampert, M. De Vittorio, A. Passaseo, Enhanced performances of quantum dot lasers operating at 1.3 μm, IEEE J. Sel. Top. Quantum Electron. 14 (4) (2008) 1188–1196, https://doi.org/10.1109/JSTQE.2008.916182.
[103] M.T. Crowley, N.A. Naderi, H. Su, F. Grillot, L.F. Lester, GaAs-based quantum dot lasers, in: Semiconductors and Semimetals, 86, Elsevier, 2012, pp. 371–417, https://doi.org/10.1016/B978-0-12-391066-0.00010-1. vol.
[104] P.S. Kopév, N.N. Ledentsov, V.M. Ustinov, I.V. Kochmev, N.A. Bert, A.Yu. Egorov, A. E. Zhukov, V.V. Komin, A.O. Kosogov, I.L. Krestnikov, M.V. Maximov, S.S. Ruvimov, A.V. Sakharov, Yu.M. Sherniakov, A.F. Tsatsulńikov, S.V. Zaitsev, Zh.I. Alferov, D. Bimberg, Self organized InAs-GaAs quantum dots injection laser structure, in: Conference on Lasers and Electro-Optics, Optica Publishing Group, 1996.
[105] L. Wang, E. Hughes, C. Zhang, J. Bowers, J. Klamkin, Reliable quantum dot laser grown by MOCVD, in: Advanced Photonics Congress, Optica Publishing Group, 2022.
[106] T.C. Newell, D.J. Bossert, A. Stintz, B. Fuchs, K.J. Malloy, L.F. Lester, Gain and linewidth enhancement factor in InAs quantum-dot laser diodes, IEEE Photon. Technol. Lett. 11 (12) (1999) 1527–1529, https://doi.org/10.1109/68.806834.
[107] S. Fathpour, Z. Mi, P. Bhattacharya, A.R. Kovsh, S.S. Mikhrin, I.L. Krestnikov, A.V. Kozhukhov, N.N. Ledentsov, The role of Auger recombination in the temperature-dependent output characteristics ($T_0 = \infty$) of p-doped 1.3 μm quantum dot lasers, Appl. Phys. Lett. 85 (22) (2004) 5164–5166, https://doi.org/10.1063/1.1829158.

[108] A.E. Zhukov, V.M. Ustinov, A.Yu. Egorov, A.R. Kovsh, A.F. Tsatsulńikov, N.N. Ledentsov, S.V. Zaitsev, N.Yu. Gordeev, P.S. Kopèv, Z.I. Alferov, Negative characteristic temperature of InGaAs quantum dot injection laser, Jpn J. Appl. Phys. 36 (1997) 4216–4218, https://doi.org/10.1143/jjap.36.4216.

[109] T.J. Badcock, R.J. Royce, D.J. Mowbray, M.S. Skolnick, H.Y. Liu, M. Hopkinson, K.M. Groom, Q. Jiang, Low threshold current density and negative characteristic temperature 1.3 μm InAs self-assembled quantum dot lasers, Appl. Phys. Lett. 90 (11) (2007) 111102, https://doi.org/10.1063/1.2713136.

[110] P. Crump, S. Patterson, S. Elim, S. Zhang, M. Bougher, J. Patterson, S. Das, W. Dong, M. Grimshaw, J. Wang, D. Wise, M. DeFranza, J. Bell, J. Farmer, M. DeVito, R. Martinsen, A. Kovsh, F. Toor, C.F. Gmachl, Extending the wavelength range of single-emitter diode lasers for medical and sensing applications: 12xx-nm quantum dots, 2000-nm wells, >5000-nm cascade lasers, in: M.S. Zediker (Ed.), High-Power Diode Laser Technology and Applications V, vol. 6456, International Society for Optics and Photonics, SPIE, 2007, https://doi.org/10.1117/12.706177.

[111] M.J. da Silva, A.A. Quivy, S. Martini, T.E. Lamas, E.C.F. da Silva, J.R. Leite, InAs/GaAs quantum dots optically active at 1.5 μm, Appl. Phys. Lett. 82 (16) (2003) 2646–2648, https://doi.org/10.1063/1.1569053.

[112] N.N. Ledentsov, A.R. Kovsh, A.E. Zhukov, N.A. Maleev, S.S. Mikhrin, A.P. Vasil'ev, E. S. Semenova, M.V. Maximov, Yu.M. Shernyakov, N.V. Kryzhanovskaya, V.M. Ustinov, D. Bimberg, High performance quantum dot lasers on GaAs substrates operating in 1.5 μm range, Electron. Lett. 39 (15) (2003) 1126–1128, https://doi.org/10.1049/el_20030753.

[113] V.M. Ustinov, A.R. Kovsh, A.E. Zhukov, A.Yu. Egorov, N.N. Ledentsov, A.V. Lunev, Yu.M. Shernyakov, M.V. Maksimov, A.F. Tsatsulńikov, B.V. Volovik, P.S. Kopév, Zh.I. Alferov, Low-threshold quantum-dot injection heterolaser emitting at 1.84 μm, Tech. Phys. Lett. 24 (1) (1998) 22–23, https://doi.org/10.1134/1.1261977.

[114] A.E. Zhukov, V.M. Ustinov, A.Yu. Egorov, A.R. Kovsh, S.V. Zaitsev, N.Yu. Gordeev, V.I. Kopchatov, N.N. Ledentsov, A.F. Tsatsulńikov, B.V. Volovik, P.S. Kopév, Zh.I. Alferov, Low-threshold quantum dot injection laser emitting at 1.9 μm, in: Semiconducting and Insulating Materials 1998. Proceedings of the 10th Conference on Semiconducting and Insulating Materials (SIMC-X) (Cat. No. 98CH36159), 1998, pp. 319–322, https://doi.org/10.1109/SIM.1998.785134.

[115] K. Nishi, M. Yamada, T. Anan, A. Gomyo, S. Sugou, Long-wavelength lasing from InAs self-assembled quantum dots on (311) B InP, Appl. Phys. Lett. 73 (4) (1998) 526–528, https://doi.org/10.1063/1.121922.

[116] R.H. Wang, A. Stintz, P.M. Varangis, T.C. Newell, H. Li, K.J. Malloy, L.F. Lester, Room-temperature operation of InAs quantum-dash lasers on InP [001], IEEE Photon. Technol. Lett. 13 (8) (2001) 767–769, https://doi.org/10.1109/68.935797.

[117] M.Z.M. Khan, T.K. Ng, B.S. Ooi, Self-assembled InAs/InP quantum dots and quantum dashes: material structures and devices, Prog. Quantum Electron. 38 (6) (2014) 237–313, https://doi.org/10.1016/j.pquantelec.2014.11.001.

[118] A. Lenz, F. Genz, H. Eisele, L. Ivanova, R. Timm, D. Franke, H. Künzel, U.W. Pohl, M. Dähne, Formation of InAs/InGaAsP quantum-dashes on InP(001), Appl. Phys. Lett. 95 (20) (2009) 203105, https://doi.org/10.1063/1.3265733.

[119] G. Elias, A. Létoublon, R. Piron, I. Alghoraibi, A. Nakkar, N. Chevalier, K. Tavernier, A. L. Corre, N. Bertru, S. Loualiche, Achievement of high density InAs/GaInAsP quantum dots on misoriented InP(001) substrates emitting at 1.55 μm, Jpn J. Appl. Phys. 48 (7) (2009) 070204, https://doi.org/10.1143/JJAP.48.070204.

[120] C.N. Allen, P.J. Poole, P. Barrios, P. Marshall, G. Pakulski, S. Raymond, S. Fafard, External cavity quantum dot tunable laser through 1.55 μm, Physica E 26 (1) (2005) 372–376, https://doi.org/10.1016/j.physe.2004.08.009.

[121] F. Lelarge, B. Rousseau, B. Dagens, F. Poingt, F. Pommereau, A. Accard, Room temperature continuous-wave operation of buried ridge stripe lasers using InAs-InP (100) quantum dots as active core, IEEE Photon. Technol. Lett. 17 (7) (2005) 1369–1371, https://doi.org/10.1109/LPT.2005.848279.

[122] J. Kwoen, N. Morais, W. Zhan, S. Iwamoto, Y. Arakawa, All III-arsenide low threshold InAs quantum dot lasers on InP(001), Electron. Lett. 59 (16) (2023) e12920, https://doi.org/10.1049/ell2.12920.

[123] H. Li, G.T. Liu, P.M. Varangis, T.C. Newell, A. Stintz, B. Fuchs, K.J. Malloy, L.F. Lester, 150-nm tuning range in a grating-coupled external cavity quantum-dot laser, IEEE Photon. Technol. Lett. 12 (7) (2000) 759–761, https://doi.org/10.1109/68.853491.

[124] P. Miska, J. Even, C. Paranthoen, O. Dehaese, H. Folliot, S. Loualiche, M. Senes, X. Marie, Optical properties and carrier dynamics of InAs/InP(113)B quantum dots emitting between 1.3 and 1.55 μm for laser applications, Physica E 17 (2003) 56–59, https://doi.org/10.1016/S1386-9477(02)00749-X.

[125] P. Caroff, C. Paranthoen, C. Platz, O. Dehaese, H. Folliot, N. Bertru, C. Labbé, R. Piron, E. Homeyer, A. Le Corre, S. Loualiche, High-gain and low-threshold InAs quantum-dot lasers on InP, Appl. Phys. Lett. 87 (24) (2005) 243107, https://doi.org/10.1063/1.2146063.

[126] I. Alghoraibi, T. Rohel, N. Bertru, A. Le Corre, A. Létoublon, P. Caroff, O. Dehaese, S. Loualiche, Self-assembled InAs quantum dots grown on InP (311)B substrates: role of buffer layer and amount of InAs deposited, J. Cryst. Growth 293 (2) (2006) 263–268, https://doi.org/10.1016/j.jcrysgro.2006.05.046.

[127] K. Akahane, N. Yamamoto, T. Kawanishi, The dependence of the characteristic temperature of highly stacked InAs quantum dot laser diodes fabricated using a strain-compensation technique on stacking layer number, in: ISLC 2012 International Semiconductor Laser Conference, 2012, pp. 82–83, https://doi.org/10.1109/ISLC.2012.6348369.

[128] S. Yanase, K. Akahane, A. Matsumoto, T. Umezawa, N. Yamamoto, Y. Tominaga, A. Kanno, T. Maeda, H. Sotobayashi, Temperature-independent lasing wavelength of highly stacked InAs quantum dot laser fabricated on InP(311)B substrate with Bi irradiation S, Opt. Lett. 48 (2023) 3287–3290.

[129] R. Yabuki, A. Matsumoto, R. Katsuhara, S. Heinsalu, K. Akahane, Y. Matsushima, H. Ishikawa, K. Utaka, Temperature-insensitive pulse and 120°C CW operation of 1550 nm-band p-doped InAs/InGaAlAs quantum dot lasers on InP(311)B substrate, in: International Conference on Optical Communications (OFC), Optica Publishing Group, 2023.

[130] S.E. Miller, Integrated optics: an introduction, Bell Syst. Tech. J. 48 (7) (1969) 2059–2069, https://doi.org/10.1002/j.1538-7305.1969.tb01165.x.

[131] R.A. Soref, J.P. Lorenzo, Single-crystal silicon: a new material for 1.3 and 1.6 μm integrated-optical components, Electron. Lett. 21 (21) (1985) 953–954, https://doi.org/10.1049/el_19850673.

[132] R.A. Soref, J.P. Larenzo, All-silicon active and passive guided-wave components for $\lambda =$ 1.3 and 1.6 μm, IEEE J. Quantum Electron. 22 (6) (1986) 873–879, https://doi.org/10.1109/JQE.1986.1073057.

[133] C.H. Henry, G.E. Blonder, R.F. Kazarinov, Glass waveguides on silicon for hybrid optical packaging, J. Lightwave Technol. 7 (10) (1989) 1530–1539, https://doi.org/10.1109/50.39094.

[134] R.A. Soref, Silicon-based optoelectronics, Proc. IEEE 81 (12) (1993) 1687–1706, https://doi.org/10.1109/5.248958.

[135] Y. Kawamura, K. Wakita, Y. Itaya, Y. Yoshikuni, H. Asahi, Monolithic integration of InGaAs/InP DFB lasers and InGaAs/InAlAs MQW optical modulators, Electron. Lett. 22 (5) (1986) 242–243, https://doi.org/10.1049/el_19860166.

[136] C.A. Alegria, S.S. Bergstein, K.A. Dixson, C.J. Hunt, The WaveStar^{TM} BandWidth Manager: the key building block in the next-generation transport network, Bell Labs Tech. J. 4 (1) (1999) 42–57, https://doi.org/10.1002/bltj.2146.

[137] R. Nagarajan, C.H. Joyner, R.P. Schneider, J.S. Bostak, T. Butrie, A.G. Dentai, V.G. Dominic, P.W. Evans, M. Kato, M. Kauffman, D.J.H. Lambert, S.K. Mathis, A. Mathur, R.H. Miles, M.L. Mitchell, M.J. Missey, S. Murthy, A.C. Nilsson, F.H. Peters, S.C. Pennypacker, J.L. Pleumeekers, R.A. Salvatore, R.K. Schlenker, R.B. Taylor, H.-S. Tsai, M.F. Van Leeuwen, J. Webjorn, M. Ziari, D. Perkins, J. Singh, S.G. Grubb, M.S. Reffle, D.G. Mehuys, F.A. Kish, D.F. Welch, Large-scale photonic integrated circuits, IEEE J. Sel. Top. Quantum Electron. 11 (1) (2005) 50–65, https://doi.org/10.1109/JSTQE.2004.841721.

[138] J. Summers, T. Vallaitis, P. Evans, M. Ziari, P. Studenkov, M. Fisher, J. Sena, A. James, S. Corzine, D. Pavinski, J. Ou-Yang, M. Missey, D. Gold, W. Williams, M. Lai, D. Welch, F. Kish, Monolithic InP-based coherent transmitter photonic integrated circuit with 2.25 Tbit/s capacity, Electron. Lett. 50 (16) (2014) 1150–1152, https://doi.org/10.1049/el.2014.2011.

[139] C.P. Dietrich, A. Fiore, M.G. Thompson, M. Kamp, S. Höfling, GaAs integrated quantum photonics: towards compact and multi-functional quantum photonic integrated circuits, Laser Photonics Rev. 10 (6) (2016) 870–894, https://doi.org/10.1002/lpor.201500321.

[140] T. Sharma, J. Wang, B.K. Kaushik, Z. Cheng, R. Kumar, Z. Wei, X. Li, Review of recent progress on silicon nitride-based photonic integrated circuits, IEEE Access 8 (2020) 195436–195446, https://doi.org/10.1109/ACCESS.2020.3032186.

[141] C. Xiang, W. Jin, D. Huang, M.A. Tran, J. Guo, Y. Wan, W. Xie, G. Kurczveil, A.M. Netherton, D. Liang, H. Rong, J.E. Bowers, High-performance silicon photonics using heterogeneous integration, IEEE J. Sel. Top. Quantum Electron. 28 (3) (2022) 1–15, https://doi.org/10.1109/JSTQE.2021.3126124.

[142] K. Wörhoff, R.G. Heideman, A. Leinse, M. Hoekman, TriPleX: a versatile dielectric photonic platform, Adv. Opt. Technol. 4 (2) (2015) 189–207, https://doi.org/10.1515/aot-2015-0016.

[143] J.C. Norman, D. Jung, Y. Wan, J.E. Bowers, Perspective: the future of quantum dot photonic integrated circuits, APL Photonics 3 (3) (2018) 030901, https://doi.org/10.1063/1.5021345.

[144] D. Liang, J.E. Bowers, Recent progress in lasers on silicon, Nat. Photonics 4 (8) (2010) 511–517, https://doi.org/10.1038/nphoton.2010.167.

[145] C. Sun, M.T. Wade, Y. Lee, J.S. Orcutt, L. Alloatti, M.S. Georgas, A.S. Waterman, J.M. Shainline, R.R. Avizienis, S. Lin, B.R. Moss, R. Kumar, F. Pavanello, A.H. Atabaki, H. M. Cook, A.J. Ou, J.C. Leu, Y.-H. Chen, K. Asanović, R.J. Ram, M.A. Popović, V.M. Stojanović, Single-chip microprocessor that communicates directly using light, Nature 528 (7583) (2015) 534–538, https://doi.org/10.1038/nature16454.

[146] A.H. Atabaki, S. Moazeni, F. Pavanello, H. Gevorgyan, J. Notaros, L. Alloatti, M.T. Wade, C. Sun, S.A. Kruger, H. Meng, K. Al Qubaisi, I. Wang, B. Zhang, A. Khilo, C. V. Baiocco, M.A. Popović, V.M. Stojanović, R.J. Ram, Integrating photonics with silicon nanoelectronics for the next generation of systems on a chip, Nature 556 (7701) (2018) 349–354, https://doi.org/10.1038/s41586-018-0028-z.

[147] Z. Zhou, B. Yin, J. Michel, On-chip light sources for silicon photonics, Light Sci. Appl. 4 (11) (2015) e358, https://doi.org/10.1038/lsa.2015.131.
[148] A.W. Fang, H. Park, O. Cohen, R. Jones, M.J. Paniccia, J.E. Bowers, Electrically pumped hybrid AlGaInAs-silicon evanescent laser, Opt. Express 14 (20) (2006) 9203–9210, https://doi.org/10.1364/OE.14.009203.
[149] B.R. Koch, E.J. Norberg, B. Kim, J. Hutchinson, J.-H. Shin, G. Fish, A. Fang, Integrated silicon photonic laser sources for telecom and datacom, in: Optical Fiber Communication Conference/National Fiber Optic Engineers Conference 2013, Optica Publishing Group, 2013.
[150] G.-H. Duan, C. Jany, A.L. Liepvre, A. Accard, M. Lamponi, D. Make, P. Kaspar, G. Levaufre, N. Girard, F. Lelarge, J.-M. Fedeli, A. Descos, B. Ben Bakir, S. Messaoudene, D. Bordel, S. Menezo, G de Valicourt, S. Keyvaninia, G. Roelkens, D. Van Thourhout, D.J. Thomson, F.Y. Gardes, G.T. Reed, Hybrid III-V on silicon lasers for photonic integrated circuits on silicon, IEEE J. Sel. Top. Quantum Electron. 20 (4) (2014) 158–170, https://doi.org/10.1109/JSTQE.2013.2296752.
[151] C.T. Santis, S.T. Steger, Y. Vilenchik, A. Vasilyev, A. Yariv, High-coherence semiconductor lasers based on integral high-Q resonators in hybrid Si/III-V platforms, Proc. Natl. Acad. Sci. 111 (8) (2014) 2879–2884, https://doi.org/10.1073/pnas.1400184111.
[152] T. Ferrotti, B. Blampey, C. Jany, H. Duprez, A. Chantre, F. Boeuf, C. Seassal, B.B. Bakir, Co-integrated 1.3 μm hybrid III-V/silicon tunable laser and silicon Mach-Zehnder modulator operating at 25 Gb/s, Opt. Express 24 (26) (2016) 30379–30401, https://doi.org/10.1364/OE.24.030379.
[153] D. Liang, X. Huang, G. Kurczveil, M. Fiorentino, R.G. Beausoleil, Integrated finely tunable microring laser on silicon, Nat. Photonics 10 (11) (2016) 719–722, https://doi.org/10.1038/nphoton.2016.163.
[154] Intel, Intel® silicon photonics 100G PSM4 optical transceiver brief, 2017.
[155] G. de Valicourt, C.-M. Chang, M.S. Eggleston, A. Melikyan, C. Zhu, J. Lee, J.E. Simsarian, S. Chandrasekhar, J.H. Sinsky, K.W. Kim, P. Dong, A. Maho, A. Verdier, R. Brenot, Y.K. Chen, Photonic integrated circuit based on hybrid III-V/silicon integration, J. Lightwave Technol. 36 (2) (2018) 265–273, https://doi.org/10.1109/JLT.2017.2776214.
[156] B. Szelag, K. Hassan, L. Adelmini, E. Ghegin, P. Rodriguez, F. Nemouchi, P. Brianceau, E. Vermande, A. Schembri, D. Carrara, P. Cavalié, F. Franchin, M.-C. Roure, L. Sanchez, C. Jany, S. Olivier, Hybrid III-V/silicon technology for laser integration on a 200-mm fully CMOS-compatible silicon photonics platform, IEEE J. Sel. Top. Quantum Electron. 25 (5) (2019) 1–10, https://doi.org/10.1109/JSTQE.2019.2904445.
[157] V. Cao, J.-S. Park, M. Tang, T. Zhou, A. Seeds, S. Chen, H. Liu, Recent progress of quantum dot lasers monolithically integrated on Si platform, Front. Phys. 10 (2022), https://doi.org/10.3389/fphy.2022.839953.
[158] G. Kurczveil, C. Zhang, A. Descos, D. Liang, M. Fiorentino, R. Beausoleil, On-chip hybrid silicon quantum dot comb laser with 14 error-free channels, in: 2018 IEEE International Semiconductor Laser Conference (ISLC), IEEE, 2018, pp. 1–2, https://doi.org/10.1109/ISLC.2018.8516175.
[159] Cisco, Silicon photonics in pluggable optics white paper, 2021.
[160] J.M. Gérard, C. Weisbuch. Semiconductor structure for optoelectronic components with inclusions, US Patent US5075742A, 1991.
[161] J.M. Gérard, O. Cabrol, B. Sermage, InAs quantum boxes: highly efficient radiative traps for light emitting devices on Si, Appl. Phys. Lett. 68 (22) (1996) 3123–3125, https://doi.org/10.1063/1.115798.

[162] Z. Mi, P. Bhattacharya, J. Yang, K.P. Pipe, Room-temperature self-organised $In_{0.5}Ga_{0.5}As$ quantum dot laser on silicon, Electron. Lett. 41 (13) (2005) 742–744, https://doi.org/10.1049/el_20051558.
[163] L. Li, D. Guimard, M. Rajesh, Y. Arakawa, Growth of InAs/Sb:GaAs quantum dots on silicon substrate with high density and efficient light emission in the 1.3 μm band, Appl. Phys. Lett. 92 (26) (2008) 263105, https://doi.org/10.1063/1.2952594.
[164] T. Wang, H. Liu, A. Lee, F. Pozzi, A. Seeds, 1.3-μm InAs/GaAs quantum-dot lasers monolithically grown on Si substrates, Opt. Express 19 (12) (2011) 11381–11386, https://doi.org/10.1364/OE.19.011381.
[165] A.Y. Liu, C. Zhang, J. Norman, A. Snyder, D. Lubyshev, J.M. Fastenau, A.W.K. Liu, A. C. Gossard, J.E. Bowers, High performance continuous wave 1.3 μm quantum dot lasers on silicon, Appl. Phys. Lett. 104 (4) (2014) 041104, https://doi.org/10.1063/1.4863223.
[166] P. Verrinder, L. Wang, B. Shi, S. Zhu, J. Klamkin, InAs/GaAs quantum dot lasers on CMOS-compatible (001) silicon by MOCVD direct heteroepitaxy, in: CLEO 2023, Optica Publishing Group, 2023, https://doi.org/10.1364/CLEO_SI.2023.SM2J.2.
[167] S. Zhu, B. Shi, K.M. Lau, Electrically pumped 1.5 μm InP-based quantum dot microring lasers directly grown on (001) Si, Opt. Lett. 44 (18) (2019) 4566–4569, https://doi.org/10.1364/OL.44.004566.
[168] P. Dhingra, P. Su, B.D. Li, R.D. Hool, A.J. Muhowski, M. Kim, D. Wasserman, J. Dallesasse, M.L. Lee, Low-threshold InP quantum dot and InGaP quantum well visible lasers on silicon (001), Optica 8 (11) (2021) 1495–1500, https://doi.org/10.1364/OPTICA.443979.
[169] Z. Yan, Y. Han, L. Lin, Y. Xue, C. Ma, W.K. Ng, K.S. Wong, K.M. Lau, A monolithic InP/SOI platform for integrated photonics, Light Sci. Appl. 10 (1) (2021) 200, https://doi.org/10.1038/s41377-021-00636-0.
[170] R.J. Chu, D.-H. Ahn, G. Ryu, W.J. Choi, D. Jung, Optical properties of coherent InAs/InGaAs quantum dash-in-a-well for strong 2 μm emission enabled by ripening process, J. Alloys Compd. 859 (2021) 157783, https://doi.org/10.1016/j.jallcom.2020.157783.
[171] Intel, Intel Launches Integrated Photonics Research Center, 2021.
[172] Tower Semiconductor, Tower semiconductor and Quintessent announce partnership to create foundry silicon photonics platform with integrated quantum dot laser, 2021.
[173] H. Huang, J. Duan, D. Jung, A.Y. Liu, Z. Zhang, J. Norman, J.E. Bowers, F. Grillot, Analysis of the optical feedback dynamics in InAs/GaAs quantum dot lasers directly grown on silicon, J. Opt. Soc. Am. B 35 (11) (2018) 2780–2787, https://doi.org/10.1364/JOSAB.35.002780.
[174] S.L.I. Olsson, J. Cho, S. Chandrasekhar, X. Chen, P.J. Winzer, S. Makovejs, Probabilistically shaped PDM 4096-QAM transmission over up to 200 km of fiber using standard intradyne detection, Opt. Express 26 (4) (2018) 4522–4530, https://doi.org/10.1364/OE.26.004522.
[175] H.H. Elwan, R. Khayatzadeh, J. Poette, B. Cabon, Impact of relative intensity noise on 60-GHz radio-over-fiber wireless transmission systems, J. Lightwave Technol. 34 (20) (2016) 4751–4757, https://doi.org/10.1109/JLT.2016.2544106.
[176] A.D. Ludlow, M.M. Boyd, J. Ye, E. Peik, P.O. Schmidt, Optical atomic clocks, Rev. Mod. Phys. 87 (2) (2015) 637, https://doi.org/10.1103/RevModPhys.87.637.
[177] D.T. Spencer, T. Drake, T.C. Briles, J. Stone, L.C. Sinclair, C. Fredrick, Q. Li, D. Westly, B.R. Ilic, A. Bluestone, N. Volet, T. Komljenovic, L. Chang, S.H. Lee, D.Y. Oh, M.-G. Suh, K.Y. Yang, M.H.P. Pfeiffer, T.J. Kippenberg, E. Norberg, L. Theogarajan, K. Vahala, N.R. Newbury, K. Srinivasan, J.E. Bowers, S.A. Diddams, S.B. Papp, An optical-frequency synthesizer using integrated photonics, Nature 557 (7703) (2018) 81, https://doi.org/10.1038/s41586-018-0065-7.

[178] M.-G. Suh, Q.-F. Yang, K.Y. Yang, X. Yi, K.J. Vahala, Microresonator soliton dual-comb spectroscopy, Science 354 (6312) (2016) 600–603, https://doi.org/10.1126/science.aah6516.
[179] J. Geng, C. Spiegelberg, S. Jiang, Narrow linewidth fiber laser for 100-km optical frequency domain reflectometry, IEEE Photon. Technol. Lett. 17 (9) (2005) 1827–1829, https://doi.org/10.1109/LPT.2005.853258.
[180] M.A. Tran, D. Huang, J.E. Bowers, Tutorial on narrow linewidth tunable semiconductor lasers using Si/III-V heterogeneous integration, APL Photonics 4 (11) (2019) 111101, https://doi.org/10.1063/1.5124254.
[181] A. Yariv, Quantum Electronics, Wiley, 1989.
[182] C. Xiang, P.A. Morton, J.E. Bowers, Ultra-narrow linewidth laser based on a semiconductor gain chip and extended Si_3N_4 Bragg grating, Opt. Lett. 44 (15) (2019) 3825–3828, https://doi.org/10.1364/OL.44.003825.
[183] D. Huang, M.A. Tran, J. Guo, J. Peters, T. Komljenovic, A. Malik, P.A. Morton, J.E. Bowers, High-power sub-kHz linewidth lasers fully integrated on silicon, Optica 6 (6) (2019) 745–752, https://doi.org/10.1364/OPTICA.6.000745.
[184] S. Gomez, H. Huang, J. Duan, S. Combrié, A. Shen, G. Baili, A de Rossi, F. Grillot, High coherence collapse of a hybrid III-V/Si semiconductor laser with a large quality factor, J. Phys. Photonics 2 (2) (2020) 025005, https://doi.org/10.1088/2515-7647/ab6a74.
[185] C.T. Santis, Y. Vilenchik, N. Satyan, G. Rakuljic, A. Yariv, Quantum control of phase fluctuations in semiconductor lasers, Proc. Natl. Acad. Sci. 115 (34) (2018) E7896–E7904, https://doi.org/10.1073/pnas.1806716115.
[186] H. Su, L.F. Lester, Dynamic properties of quantum dot distributed feedback lasers: high speed, linewidth and chirp, J. Phys. D Appl. Phys. 38 (13) (2005) 2112, https://doi.org/10.1088/0022-3727/38/13/006.
[187] Z.G. Lu, P.J. Poole, J.R. Liu, P.J. Barrios, Z.J. Jiao, G. Pakulski, D. Poitras, D. Goodchild, B. Rioux, A.J. Springthorpe, High-performance 1.52 μm InAs/InP quantum dot distributed feedback laser, Electron. Lett. 47 (14) (2011) 818–819, https://doi.org/10.1049/el.2011.0946.
[188] A. Becker, V. Sichkovskyi, M. Bjelica, A. Rippien, F. Schnabel, M. Kaiser, O. Eyal, B. Witzigmann, G. Eisenstein, J.P. Reithmaier, Widely tunable narrow-linewidth 1.5 μm light source based on a monolithically integrated quantum dot laser array, Appl. Phys. Lett. 110 (18) (2017) 181103, https://doi.org/10.1063/1.4982716.
[189] G. Eisenstein, D. Bimberg, Green Photonics and Electronics, Springer, 2017, https://doi.org/10.1007/978-3-319-67002-7.
[190] Y. Wan, C. Xiang, J. Guo, R. Koscica, M.J. Kennedy, J. Selvidge, Z. Zhang, L. Chang, W. Xie, D. Huang, A.C. Gossard, J.E. Bowers, High speed evanescent quantum-dot lasers on Si, Laser Photonics Rev. 15 (2021), https://doi.org/10.1002/lpor.202100057.
[191] J. Duan, H. Huang, D. Jung, Z. Zhang, J. Norman, J.E. Bowers, F. Grillot, Semiconductor quantum dot lasers epitaxially grown on silicon with low linewidth enhancement factor, Appl. Phys. Lett. 112 (25) (2018) 251111, https://doi.org/10.1063/1.5025879.
[192] K. Nishi, K. Takemasa, M. Sugawara, Y. Arakawa, Development of quantum dot lasers for data-com and silicon photonics applications, IEEE J. Sel. Top. Quantum Electron. 23 (6) (2017) 1–7, https://doi.org/10.1109/JSTQE.2017.2699787.
[193] T. Katsuyama, Development of semiconductor laser for optical communication, SEI Tech. Rev. 69 (2009) 13–20.
[194] B. Dong, J. Duan, H. Huang, J.C. Norman, K. Nishi, K. Takemasa, M. Sugawara, J.E. Bowers, F. Grillot, Dynamic performance and reflection sensitivity of quantum dot distributed feedback lasers with large optical mismatch, Photonics Res. 9 (8) (2021) 1550–1558, https://doi.org/10.1364/PRJ.421285.

[195] S. Wang, Z.R. Lv, Q.L. Yang, S.L. Wang, H.Y. Chai, L. Meng, D. Lu, C. Ji, X.G. Yang, T. Yang, High-power, narrow-linewidth, and low-noise quantum dot distributed feedback lasers, Laser Photonics Rev. (2023) 2200979, https://doi.org/10.1002/lpor.202200979.

[196] L. Wu, H. Wang, Q. Yang, Q.-X. Ji, B. Shen, C. Bao, M. Gao, K. Vahala, Greater than one billion Q factor for on-chip microresonators, Opt. Lett. 45 (18) (2020) 5129–5131, https://doi.org/10.1364/OL.394940.

[197] W. Jin, Q.-F. Yang, L. Chang, B. Shen, H. Wang, M.A. Leal, L. Wu, M. Gao, A. Feshali, M. Paniccia, K.J. Vahala, J.E. Bowers, Hertz-linewidth semiconductor lasers using CMOS-ready ultra-high-Q microresonators, Nat. Photonics 15 (5) (2021) 346–353, https://doi.org/10.1038/s41566-021-00761-7.

[198] W.W. Chow, Y. Wan, J.E. Bowers, F. Grillot, Analysis of the spontaneous emission limited linewidth of an integrated III-V/SiN laser, Laser Photonics Rev. (2022) 2100620, https://doi.org/10.1002/lpor.202100620.

[199] E. Alkhazraji, W.W. Chow, F. Grillot, J.E. Bowers, W. Yating, Linewidth narrowing in self-injection-locked on-chip lasers, Light Sci. Appl. 12 (161) (2023) 1–10, https://doi.org/10.1038/s41377-023-01172-9.

[200] J. Duan, Y. Zhou, B. Dong, H. Huang, J.C. Norman, D. Jung, Z. Zhang, C. Wang, J.E. Bowers, F. Grillot, Effect of p-doping on the intensity noise of epitaxial quantum dot lasers on silicon, Opt. Lett. 45 (17) (2020) 4887–4890, https://doi.org/10.1364/OL.395499.

[201] C.H. Cox, E.I. Ackerman, G.E. Betts, J.L. Prince, Limits on the performance of RF-over-fiber links and their impact on device design, IEEE Trans. Microwave Theory Tech. 54 (2) (2006) 906–920, https://doi.org/10.1109/TMTT.2005.863818.

[202] G. Moody, L. Chang, T.J. Steiner, J.E. Bowers, Chip-scale nonlinear photonics for quantum light generation, AVS Quantum Sci. 2 (4) (2020) 041702, https://doi.org/10.1116/5.0020684.

[203] J.-L. Vey, P. Gallion, Semiclassical model of semiconductor laser noise and amplitude noise squeezing. I. Description and application to Fabry-Pérot laser, IEEE J. Quantum Electron. 33 (11) (1997) 2097–2104, https://doi.org/10.1109/3.641325.

[204] F. Lelarge, B. Dagens, J. Renaudier, R. Brenot, A. Accard, F. van Dijk, D. Make, O. Le Gouezigou, J.-G. Provost, F. Poingt, J. Landreau, O. Drisse, E. Derouin, B. Rousseau, F. Pommereau, G.-H. Duan, Recent advances on InAs/InP quantum dash based semiconductor lasers and optical amplifiers operating at 1.55 μm, IEEE J. Sel. Top. Quantum Electron. 13 (1) (2007) 111–124, https://doi.org/10.1109/JSTQE.2006.887154.

[205] A. Capua, L. Rozenfeld, V. Mikhelashvili, G. Eisenstein, M. Kuntz, M. Laemmlin, D. Bimberg, Direct correlation between a highly damped modulation response and ultra low relative intensity noise in an InAs/GaAs quantum dot laser, Opt. Express 15 (9) (2007) 5388–5393, https://doi.org/10.1364/OE.15.005388.

[206] G. Lin, H.-L. Tang, H.-C. Cheng, H.-L. Chen, Analysis of relative intensity noise spectra for uniformly and chirpily stacked InAs-InGaAs-GaAs quantum dot lasers, J. Lightwave Technol. 30 (3) (2012) 331–336, https://doi.org/10.1109/JLT.2011.2179974.

[207] J.-Z. Huang, Z.-T. Ji, J.-J. Chen, W.-Q. Wei, J.-L. Qin, Z.-H. Wang, Z.-Y. Li, T. Wang, X. Xiao, J.-J. Zhang, Ultra-broadband flat-top quantum dot comb lasers, Photonics Res. 10 (5) (2022) 1308–1316, https://doi.org/10.1364/PRJ.446349.

[208] Z. Yang, Z. Ding, L. Liu, H. Zhong, S. Cao, X. Zhang, S. Lin, X. Huang, H. Deng, Y. Yu, S. Yu, High-performance distributed feedback quantum dot lasers with laterally coupled dielectric gratings, Photonics Res. 10 (5) (2022) 1271–1279, https://doi.org/10.1364/PRJ.454200.

[209] A.Y. Liu, T. Komljenovic, M.L. Davenport, A.C. Gossard, J.E. Bowers, Reflection sensitivity of 1.3 μm quantum dot lasers epitaxially grown on silicon, Opt. Express 25 (9) (2017) 9535–9543, https://doi.org/10.1364/OE.25.009535.
[210] M. Liao, S. Chen, Z. Liu, Y. Wang, L. Ponnampalam, Z. Zhou, J. Wu, M. Tang, S. Shutts, Z. Liu, P.M. Smowton, S. Yu, A. Seeds, H. Liu, Low-noise 1.3 μm InAs/GaAs quantum dot laser monolithically grown on silicon, Photonics Res. 6 (11) (2018) 1062–1066, https://doi.org/10.1364/PRJ.6.001062.
[211] Y.-G. Zhou, C. Zhou, C.-F. Cao, J.-B. Du, Q. Gong, C. Wang, Relative intensity noise of InAs quantum dot lasers epitaxially grown on Ge, Opt. Express 25 (23) (2017) 28817–28824, https://doi.org/10.1364/OE.25.028817.
[212] Z. Lv, S. Wang, H. Wang, H.-M. Wang, H. Chai, X. Yang, L. Meng, C. Ji, T. Yang, Significantly improved performances of 1.3 μm InAs/GaAs QD laser by spatially separated dual-doping, Appl. Phys. Lett. 121 (021105) (2022), https://doi.org/10.1063/5.0096367.
[213] K. Lüdge, H.G. Schuster, Nonlinear Laser Dynamics: from Quantum Dots to Cryptography, vol. 5, John Wiley & Sons, 2012.
[214] R.R. Alexander, D.T.D. Childs, H. Agarwal, K.M. Groom, H.-Y. Liu, M. Hopkinson, R. A. Hogg, M. Ishida, T. Yamamoto, M. Sugawara, Y. Arakawa, T.J. Badcock, R.J. Royce, D.J. Mowbray, Systematic study of the effects of modulation p-doping on 1.3-μm quantum-dot lasers, IEEE J. Quantum Electron. 43 (12) (2007) 1129–1139, https://doi.org/10.1109/JQE.2007.907213.
[215] S. Hein, V. Von Hinten, S. Höfling, A. Forchel, The impact of p-doping on the static and dynamic properties of 1.5 μm quantum dash lasers on InP, Appl. Phys. Lett. 92 (1) (2008) 011120, https://doi.org/10.1063/1.2830020.
[216] A. Abdollahinia, S. Banyoudeh, A. Rippien, F. Schnabel, O. Eyal, I. Cestier, I. Kalifa, E. Mentovich, G. Eisenstein, J.P. Reithmaier, Temperature stability of static and dynamic properties of 1.55 μm quantum dot lasers, Opt. Express 26 (5) (2018) 6056–6066, https://doi.org/10.1364/OE.26.006056.
[217] Z. Zhang, D. Jung, J.C. Norman, P. Patel, W.W. Chow, J.E. Bowers, Effects of modulation p doping in InAs quantum dot lasers on silicon, Appl. Phys. Lett. 113 (6) (2018) 061105, https://doi.org/10.1063/1.5040792.
[218] J. Huang, L.W. Casperson, Gain and saturation in semiconductor lasers, Opt. Quant. Electron. 25 (6) (1993) 369–390, https://doi.org/10.1007/BF00420579.
[219] F. Grillot, B. Dagens, J.-G. Provost, H. Su, L.F. Lester, Gain compression and above-threshold linewidth enhancement factor in 1.3-μm InAs-GaAs quantum-dot lasers, IEEE J. Quantum Electron. 44 (10) (2008) 946–951, https://doi.org/10.1109/JQE.2008.2003106.
[220] A. Martinez, Y. Li, L.F. Lester, A.L. Gray, Microwave frequency characterization of undoped and p-doped quantum dot lasers, Appl. Phys. Lett. 90 (25) (2007) 251101, https://doi.org/10.1063/1.2749432.
[221] G. Roelkens, L. Liu, D. Liang, R. Jones, A. Fang, B. Koch, J. Bowers, III-V/silicon photonics for on-chip and intra-chip optical interconnects, Laser Photonics Rev. 4 (6) (2010) 751–779, https://doi.org/10.1002/lpor.200900033.
[222] K. Tanabe, K. Watanabe, Y. Arakawa, III-V/Si hybrid photonic devices by direct fusion bonding, Sci. Rep. 2 (2012) 349, https://doi.org/10.1038/srep00349.
[223] K. Schires, N. Girard, G. Baili, G.-H. Duan, S. Gomez, F. Grillot, Dynamics of hybrid III-V silicon semiconductor lasers for integrated photonics, IEEE J. Sel. Top. Quantum Electron. 22 (6) (2016) 43–49, https://doi.org/10.1109/JSTQE.2016.2565462.
[224] L. Pavesi, D.J. Lockwood, Silicon Photonics II: Components and Integration, Springer, 2011, https://doi.org/10.1007/978-3-642-10506-7.

[225] D. Vermeulen, Y. De Koninck, Y. Li, E. Lambert, W. Bogaerts, R. Baets, G. Roelkens, Reflectionless grating couplers for Silicon-on-Insulator photonic integrated circuits, Opt. Express 20 (20) (2012) 22278–22283, https://doi.org/10.1364/OE.20.022278.
[226] Z. Zhang, K. Zou, H. Wang, P. Liao, N. Satyan, G. Rakuljic, A.E. Willner, A. Yariv, High-speed coherent optical communication with isolator-free heterogeneous Si/III-V Lasers, J. Lightwave Technol. 38 (2020) 6584–6590, https://doi.org/10.1109/JLT.2020.3015738.
[227] L. Bi, J. Hu, P. Jiang, D.H. Kim, G.F. Dionne, L.C. Kimerling, C.A. Ross, On-chip optical isolation in monolithically integrated non-reciprocal optical resonators, Nat. Photonics 5 (12) (2011) 758, https://doi.org/10.1038/nphoton.2011.270.
[228] Y. Zhang, Q. Du, C. Wang, T. Fakhrul, L. Bi, Monolithic integration of broadband optical isolators for polarization-diverse silicon photonics, Optica 6 (2019) 473–478, https://doi.org/10.1364/OPTICA.6.000473.
[229] D. Huang, P. Pintus, J.E. Bowers, Towards heterogeneous integration of optical isolators and circulators with lasers on silicon, Opt. Mater. Express 8 (9) (2018) 2471–2483, https://doi.org/10.1364/OME.8.002471.
[230] J. Kwoen, B. Jang, J. Lee, T. Kageyama, K. Watanabe, Y. Arakawa, All MBE grown InAs/GaAs quantum dot lasers on on-axis Si (001), Opt. Express 26 (9) (2018) 11568–11576, https://doi.org/10.1364/OE.26.011568.
[231] D. Lenstra, B. Verbeek, A. Den Boef, Coherence collapse in single-mode semiconductor lasers due to optical feedback, IEEE J. Quantum Electron. 21 (6) (1985) 674–679, https://doi.org/10.1109/JQE.1985.1072725.
[232] F. Grillot, B. Thedrez, O. Gauthier-Lafaye, M.F. Martineau, V. Voiriot, J.L. Lafragette, J. L. Gentner, L. Silvestre, Coherence-collapse threshold of 1.3-μm semiconductor DFB lasers, IEEE Photon. Technol. Lett. 15 (1) (2003) 9–11, https://doi.org/10.1109/LPT.2002.805771.
[233] J. Ohtsubo, Semiconductor Lasers: Stability, Instability and Chaos, vol. 111, Springer, 2012, https://doi.org/10.1007/978-3-642-30147-6.
[234] A. Uchida, Optical Communication with Chaotic Lasers: Applications of Nonlinear Dynamics and Synchronization, John Wiley & Sons, 2012, https://doi.org/10.1002/9783527640331.
[235] Q. Zou, S. Azouigui, Analysis of coherence-collapse regime of semiconductor lasers under external optical feedback by perturbation method, in: Semiconductor Laser Diode Technology and Applications, 2012, https://doi.org/10.5772/37074.
[236] H. Temkin, N. Olsson, J. Abeles, R. Logan, M. Panish, Reflection noise in index-guided InGaAsP lasers, IEEE J. Quantum Electron. 22 (2) (1986) 286–293, https://doi.org/10.1109/JQE.1986.1072947.
[237] F. Grillot, B. Thedrez, G.-H. Duan, Feedback sensitivity and coherence collapse threshold of semiconductor DFB lasers with complex structures, IEEE J. Quantum Electron. 40 (3) (2004) 231–240, https://doi.org/10.1109/JQE.2003.823031.
[238] F. Grillot, J.C. Norman, J. Duan, Z. Zhang, B. Dong, H. Huang, W.W. Chow, J.E. Bowers, Physics and applications of quantum dot lasers for silicon photonics, Nanophotonics 9 (2020) 1271–1286, https://doi.org/10.1515/nanoph-2019-0570.
[239] R. Koscica, Y. Wan, W. He, M.J. Kennedy, J.E. Bowers, Heterogeneous integration of a III-V quantum dot laser on high thermal conductivity silicon carbide, Opt. Lett. 48 (2023) 2539–2542.
[240] F.I. Zubov, M.V. Maximov, E.I. Moiseev, A.V. Savelyev, Y.M. Shernyakov, D.A. Livshits, N.V. Kryzhanovskaya, A.E. Zhukov, Observation of zero linewidth enhancement factor at excited state band in quantum dot laser, Electron. Lett. 51 (21) (2015) 1686–1688, https://doi.org/10.1049/el.2015.2512.

[241] D. Inoue, D. Jung, J. Norman, Y. Wan, N. Nishiyama, S. Arai, A.C. Gossard, J.E. Bowers, Directly modulated 1.3 μm quantum dot lasers epitaxially grown on silicon, Opt. Express 26 (6) (2018) 7022–7033, https://doi.org/10.1364/OE.26.007022.

[242] M. Matsuda, N. Yasuoka, K. Nishi, K. Takemasa, T. Yamamoto, M. Sugawara, Y. Arakawa, Low-noise characteristics on 1.3-μm-wavelength quantum-dot DFB lasers under external optical feedback, in: 2018 IEEE International Semiconductor Laser Conference (ISLC), 2018, pp. 1–2, https://doi.org/10.1109/ISLC.2018.8516191.

[243] K. Mizutani, K. Yashiki, M. Kurihara, Y. Suzuki, Y. Hagihara, N. Hatori, T. Shimizu, Y. Urino, T. Nakamura, K. Kurata, Y. Arakawa, Isolator free optical I/O core transmitter by using quantum dot laser, in: 2015 IEEE 12th International Conference on Group IV Photonics (GFP), IEEE, 2015, pp. 177–178, https://doi.org/10.1109/Group4.2015.7305921.

[244] B. Dong, J.-D. Chen, F.-Y. Lin, J.C. Norman, J.E. Bowers, F. Grillot, Dynamic and nonlinear properties of epitaxial quantum-dot lasers on silicon operating under long- and short-cavity feedback conditions for photonic integrated circuits, Phys. Rev. A 103 (2021), https://doi.org/10.1103/PhysRevA.103.033509.

[245] H. Huang, J. Duan, B. Dong, J. Norman, D. Jung, J.E. Bowers, F. Grillot, Epitaxial quantum dot lasers on silicon with high thermal stability and strong resistance to optical feedback, APL Photonics 5 (1) (2020) 016103, https://doi.org/10.1063/1.5120029.

[246] S. Ding, B. Dong, H. Huang, J. Bowers, F. Grillot, Reflection sensitivity of InAs/GaAs epitaxial quantum dot lasers under direct modulation, Electron. Lett. 58 (9) (2022) 363–365, https://doi.org/10.1049/ell2.12440.

[247] Y. He, Z. Zhang, Z. Lv, T. Yang, D. Lu, L. Zhao, 10-Gbps 20-km feedback-resistant transmission using directly modulated quantum-dot lasers, IEEE Photon. Technol. Lett. 32 (21) (2020) 1353–1356, https://doi.org/10.1109/LPT.2020.3025209.

[248] S. Liu, D. Jung, J.C. Norman, M.J. Kennedy, A.C. Gossard, J.E. Bowers, 490 fs Pulse generation from passively mode-locked single section quantum dot laser directly grown on on-axis GaP/Si, Electron. Lett. 54 (7) (2018) 432–433, https://doi.org/10.1049/el.2017.4639.

[249] B. Dong, H. Huang, J. Duan, G. Kurczveil, D. Liang, R.G. Beausoleil, F. Grillot, Frequency comb dynamics of a 1.3 μm hybrid-silicon quantum dot semiconductor laser with optical injection, Opt. Lett. 44 (23) (2019) 5755–5758, https://doi.org/10.1364/OL.44.005755.

[250] P. Bardella, L.L. Columbo, M. Gioannini, Self-generation of optical frequency comb in single section quantum dot Fabry-Pérot lasers: a theoretical study, Opt. Express 25 (21) (2017) 26234–26252, https://doi.org/10.1364/OE.25.026234.

[251] B. Stern, X. Zhu, C.P. Chen, L.D. Tzuang, J. Cardenas, K. Bergman, M. Lipson, On-chip mode-division multiplexing switch, Optica 2 (6) (2015) 530–535, https://doi.org/10.1364/OPTICA.2.000530.

[252] Q. Cheng, M. Bahadori, M. Glick, S. Rumley, K. Bergman, Recent advances in optical technologies for data centers: a review, Optica 5 (11) (2018) 1354–1370, https://doi.org/10.1364/OPTICA.5.001354.

[253] W.W. Chow, S. Liu, Z. Zhang, J.E. Bowers, M. Sargent, Multimode description of self-mode locking in a single-section quantum-dot laser, Opt. Express 28 (4) (2020) 5317–5330, https://doi.org/10.1364/OE.382821.

[254] H. Huang, K. Schires, P.J. Poole, F. Grillot, Non-degenerate four-wave mixing in an optically injection-locked InAs/InP quantum dot Fabry-Pérot laser, Appl. Phys. Lett. 106 (14) (2015) 143501, https://doi.org/10.1063/1.4916738.

[255] M. Sugawara, H. Ebe, N. Hatori, M. Ishida, Y. Arakawa, T. Akiyama, K. Otsubo, Y. Nakata, Theory of optical signal amplification and processing by quantum-dot semiconductor optical amplifiers, Phys. Rev. B 69 (2004) 235332, https://doi.org/10.1103/PhysRevB.69.235332.
[256] D. Nielsen, S.L. Chuang, Four-wave mixing and wavelength conversion in quantum dots, Phys. Rev. B 81 (3) (2010) 035305, https://doi.org/10.1103/PhysRevB.81.035305.
[257] H. Ishikawa, Chapter 7 - Applications of quantum dot to optical devices, in: M. Sugawara (Ed.), Self-Assembled InGaAs/GaAs Quantum Dots, Semiconductors and Semimetals, 60, Elsevier, 1999, pp. 287–323, https://doi.org/10.1016/S0080-8784(08)62533-8. vol.
[258] P. Borri, W. Langbein, J.M. Hvam, F. Heinrichsdorff, M.-H. Mao, D. Bimberg, Spectral hole-burning and carrier-heating dynamics in InGaAs quantum-dot amplifiers, IEEE J. Sel. Top. Quantum Electron. 6 (3) (2000) 544–551, https://doi.org/10.1109/2944.865110.
[259] P. Borri, W. Langbein, J.M. Hvam, F. Heinrichsdorff, M.-H. Mao, D. Bimberg, Ultrafast gain dynamics in InAs-InGaAs quantum-dot amplifiers, IEEE Photon. Technol. Lett. 12 (6) (2000) 594–596, https://doi.org/10.1109/68.849054.
[260] T. Akiyama, H. Kuwatsuka, T. Simoyama, Y. Nakata, K. Mukai, M. Sugawara, O. Wada, H. Ishikawa, Nonlinear gain dynamics in quantum-dot optical amplifiers and its application to optical communication devices, IEEE J. Quantum Electron. 37 (8) (2001) 1059–1065, https://doi.org/10.1109/3.937395.
[261] J. Kim, M. Laemmlin, C. Meuer, D. Bimberg, G. Eisenstein, Theoretical and experimental study of high-speed small-signal cross-gain modulation of quantum-dot semiconductor optical amplifiers, IEEE J. Quantum Electron. 45 (3) (2009) 240–248, https://doi.org/10.1109/JQE.2008.2010881.
[262] S. Ding, B. Dong, H. Huang, J. Bowers, F. Grillot, Spectral dispersion of the linewidth enhancement factor and four wave mixing conversion efficiency of an InAs/GaAs multimode quantum dot laser, Appl. Phys. Lett. 120 (8) (2022) 081105, https://doi.org/10.1063/5.0077221.
[263] M. Saldutti, A. Tibaldi, F. Cappelluti, M. Gioannini, Impact of carrier transport on the performance of QD lasers on silicon: a drift-diffusion approach, Photonics Res. 8 (8) (2020) 1388–1397, https://doi.org/10.1364/PRJ.394076.
[264] J.-C. Diels, W. Rudolph, Ultrashort Laser Pulse Phenomena, Elsevier, 2006, https://doi.org/10.1016/B978-0-12-215493-5.X5000-9.
[265] Y. Ding, W. Rehbein, M. Moehrle, M. Zander, M. Schell, K. Kolpatzeck, J.C. Balzer, Group velocity dispersion in high-performance BH InAs/InP QD and InGaAsP/InP QW two-section passively mode-locked lasers, Opt. Express 30 (14) (2022) 24353–24361, https://doi.org/10.1364/OE.456823.
[266] F. Grillot, W.W. Chow, B. Dong, S. Ding, H. Huang, J. Bowers, Multimode physics in the mode locking of semiconductor quantum dot lasers, Appl. Sci. 12 (7) (2022) 3504, https://doi.org/10.3390/app12073504.
[267] M. Kuntz, G. Fiol, M. Laemmlin, C. Meuer, D. Bimberg, High-speed mode-locked quantum-dot lasers and optical amplifiers, Proc. IEEE 95 (9) (2007) 1767–1778, https://doi.org/10.1109/JPROC.2007.900949.
[268] E.A. Viktorov, T. Erneux, P. Mandel, T. Piwonski, G. Madden, J. Pulka, G. Huyet, J. Houlihan, Recovery time scales in a reversed-biased quantum dot absorber, Appl. Phys. Lett. 94 (26) (2009) 263502, https://doi.org/10.1063/1.3159838.
[269] E.U. Rafailov, M.A. Cataluna, W. Sibbett, Mode-locked quantum-dot lasers, Nat. Photonics 1 (7) (2007) 395–401, https://doi.org/10.1038/nphoton.2007.120.

[270] X. Huang, A. Stintz, H. Li, L.F. Lester, J. Cheng, K.J. Malloy, Passive mode-locking in 1.3 μm two-section InAs quantum dot lasers, Appl. Phys. Lett. 78 (19) (2001) 2825–2827, https://doi.org/10.1063/1.1371244.

[271] M.G. Thompson, C. Marinelli, K.T. Tan, K.A. Williams, R.V. Penty, I.H. White, I.N. Kaiander, R.L. Sellin, D. Bimberg, D.-J. Kang, M.G. Blamire, F. Visinka, S. Jochum, S. Hansmann, 10 GHz hybrid modelocking of monolithic InGaAs quantum dot lasers, Electron. Lett. 39 (2003) 1121–1122, https://doi.org/10.1049/el:20030734.

[272] J. Renaudier, R. Brenot, B. Dagens, F. Lelarge, B. Rousseau, F. Poingt, O. Legouezigou, F. Pommereau, A. Accard, P. Gallion, G.-H. Duan, 45 GHz self-pulsation with narrow linewidth in quantum dot Fabry-Pérot semiconductor lasers at 1.5 μm, Electron. Lett. 41 (18) (2005) 1007–1008, https://doi.org/10.1049/el:20052173.

[273] M.A. Cataluna, W. Sibbett, D.A. Livshits, J. Weimert, A.R. Kovsh, E.U. Rafailov, Stable mode locking via ground- or excited-state transitions in a two-section quantum-dot laser, Appl. Phys. Lett. 89 (8) (2006) 081124, https://doi.org/10.1063/1.2338767.

[274] H. Schmeckebier, G. Fiol, C. Meuer, D. Arsenijević, D. Bimberg, Complete pulse characterization of quantum-dot mode-locked lasers suitable for optical communication up to 160 Gbit/s, Opt. Express 18 (4) (2010) 3415–3425, https://doi.org/10.1364/OE.18.003415.

[275] A. Sobiesierski, P.M. Smowton, 6.09 - Quantum-dot lasers: physics and applications, in: P. Bhattacharya, R. Fornari, H. Kamimura (Eds.), Comprehensive Semiconductor Science and Technology, Elsevier, Amsterdam, 2011, pp. 353–384, https://doi.org/10.1016/B978-0-44-453153-7.00034-1.

[276] S. Liu, X. Wu, D. Jung, J.C. Norman, M.J. Kennedy, H.K. Tsang, A.C. Gossard, J.E. Bowers, High-channel-count 20 GHz passively mode-locked quantum dot laser directly grown on Si with 4.1 Tbit/s transmission capacity, Optica 6 (2) (2019) 128–134, https://doi.org/10.1364/OPTICA.6.000128.

[277] J.C. Norman, Z. Zhang, D. Jung, C. Shang, M.J. Kennedy, M. Dumont, R.W. Herrick, A. C. Gossard, J.E. Bowers, The importance of p-doping for quantum dot laser on silicon performance, IEEE J. Quantum Electron. 55 (6) (2019) 1–11, https://doi.org/10.1109/JQE.2019.2941579.

[278] P. Bardella, L. Drzewietzki, M. Krakowski, I. Krestnikov, S. Breuer, Mode locking in a tapered two-section quantum dot laser: design and experiment, Opt. Lett. 43 (12) (2018) 2827–2830, https://doi.org/10.1364/OL.43.002827.

[279] F. Grillot, D. Arsenijevic, H. Huang, D. Bimberg, Ultrafast and nonlinear dynamics of InAs/GaAs semiconductor quantum dot lasers, in: D.L. Huffaker, H. Eisele (Eds.), Quantum Dots and Nanostructures: Growth, Characterization, and Modeling XV, vol. 10543, International Society for Optics and Photonics, SPIE, 2018, https://doi.org/10.1117/12.2299678.

[280] Y.-C. Xin, Y. Li, V. Kovanis, A.L. Gray, L. Zhang, L.F. Lester, Reconfigurable quantum dot monolithic multi-section passive mode-locked lasers, Opt. Express 15 (12) (2007) 7623–7633, https://doi.org/10.1364/OE.15.007623.

[281] M.G. Thompson, A.R. Rae, M. Xia, R.V. Penty, I.H. White, InGaAs quantum-dot mode-locked laser diodes, IEEE J. Sel. Top. Quantum Electron. 15 (3) (2009) 661–672, https://doi.org/10.1109/JSTQE.2008.2012265.

[282] S. Cheung, Y. Yuan, Y. Peng, G. Kurczveil, S. Srinivasan, Y. Hu, A. Descos, D. Liang, R.G. Beausoleil, Demonstration of a 17 × 25 Gb/s heterogeneous III-V/Si DWDM transmitter based on (De-) interleaved quantum dot optical frequency combs, J. Lightwave Technol. 40 (19) (2022) 6435–6443, https://doi.org/10.1109/JLT.2022.3196914.

[283] Z.G. Lu, J.R. Liu, S. Raymond, P.J. Poole, P.J. Barrios, D. Poitras, 312-fs Pulse generation from a passive C-band InAs/InP quantum dot mode-locked laser, Opt. Express 16 (14) (2008) 10835–10840, https://doi.org/10.1364/OE.16.010835.

[284] A. Akrout, A. Shen, R. Brenot, F. Van Dijk, O. Legouezigou, F. Pommereau, F. Lelarge, A. Ramdane, G.-H. Duan, Separate error-free transmission of eight channels at 10 Gb/s using comb generation in a quantum-dash-based mode-locked laser, IEEE Photon. Technol. Lett. 21 (23) (2009) 1746–1748, https://doi.org/10.1109/LPT.2009.2032243.

[285] R. Rosales, K. Merghem, A. Martinez, A. Akrout, J.-P. Tourrenc, A. Accard, F. Lelarge, A. Ramdane, InAs/InP quantum-dot passively mode-locked lasers for 1.55-μm applications, IEEE J. Sel. Top. Quantum Electron. 17 (5) (2011) 1292–1301, https://doi.org/10.1109/JSTQE.2011.2116772.

[286] M. Zander, W. Rehbein, M. Moehrle, S. Breuer, D. Franke, M. Schell, K. Kolpatzeck, J. C. Balzer, High performance BH InAs/InP QD and InGaAsP/InP QW mode-locked lasers as comb and pulse sources, in: Optical Fiber Communication Conference, Optica Publishing Group, 2020.

[287] Z. Lu, J. Liu, P.J. Poole, Y. Mao, J. Weber, G. Liu, P. Barrios, InAs/InP quantum dash semiconductor coherent comb lasers and their applications in optical networks, J. Lightwave Technol. 39 (12) (2021) 3751–3760, https://doi.org/10.1109/JLT.2020.3043284.

[288] E.U. Rafailov, M.A. Cataluna, W. Sibbett, N.D. Il'inskaya, Yu.M. Zadiranov, A.E. Zhukov, V.M. Ustinov, D.A. Livshits, A.R. Kovsh, N.N. Ledentsov, High-power picosecond and femtosecond pulse generation from a two-section mode-locked quantum-dot laser, Appl. Phys. Lett. 87 (8) (2005) 081107, https://doi.org/10.1063/1.2032608.

[289] M. Dumont, S. Liu, M.J. Kennedy, J. Bowers, High-efficiency quantum dot lasers as comb sources for DWDM applications, Appl. Sci. 12 (4) (2022) 1836, https://doi.org/10.3390/app12041836.

[290] S. Pan, H. Zhang, Z. Liu, M. Liao, M. Tang, D. Wu, X. Hu, J. Yan, L. Wang, M. Guo, Z. Wang, T. Wang, P.M. Smowton, A. Seeds, H. Liu, X. Xiao, S. Chen, Multi-wavelength 128 Gbit $s^{-1}\lambda^{-1}$ PAM4 optical transmission enabled by a 100 GHz quantum dot mode-locked optical frequency comb, J. Phys. D Appl. Phys. 55 (14) (2022) 144001, https://doi.org/10.1088/1361-6463/ac4365.

[291] B. Dong, M. Dumont, O. Terra, H. Wang, A. Netherton, J.E. Bowers, Broadband quantum-dot frequency-modulated comb laser, Light Sci. Appl. 12 (1) (2023) 182, https://doi.org/10.1038/s41377-023-01225-z.

[292] D. Liang, S. Srinivasan, G. Kurczveil, B. Tossoun, S. Cheung, Y. Yuan, A. Descos, Y. Hu, Z. Huang, P. Sun, T. Van Vaerenbergh, C. Zhang, X. Zeng, S. Liu, J.E. Bowers, M. Fiorentino, R.G. Beausoleil, An energy-efficient and bandwidth-scalable DWDM heterogeneous silicon photonics integration platform, IEEE J. Sel. Top. Quantum Electron. 28 (6) (2022) 1–19, https://doi.org/10.1109/JSTQE.2022.3181939.

[293] C.-Y. Lin, F. Grillot, N.A. Naderi, Y. Li, L.F. Lester, RF linewidth reduction in a quantum dot passively mode-locked laser subject to external optical feedback, Appl. Phys. Lett. 96 (5) (2010) 051118, https://doi.org/10.1063/1.3299714.

[294] B. Dong, X.C. de Labriolle, S. Liu, M. Dumont, H. Huang, J. Duan, J.C. Norman, J.E. Bowers, F. Grillot, 1.3-μm passively mode-locked quantum dot lasers epitaxially grown on silicon: gain properties and optical feedback stabilization, J. Phys. Photonics 2 (4) (2020) 045006, https://doi.org/10.1088/2515-7647/aba5a6.

[295] P.J. Poole, Z. Lu, J. Liu, P. Barrios, Y. Mao, G. Liu, A performance comparison between quantum dash and quantum well Fabry-Pérot lasers, IEEE J. Quantum Electron. 57 (6) (2021) 1–7, https://doi.org/10.1109/JQE.2021.3107850.

[296] D. Arsenijević, M. Kleinert, D. Bimberg, Phase noise and jitter reduction by optical feedback on passively mode-locked quantum-dot lasers, Appl. Phys. Lett. 103 (23) (2013) 231101.
[297] T. Verolet, G. Aubin, Y. Lin, C. Browning, K. Merghem, F. Lelarge, C. Calo, A. Delmade, K. Mekhazni, E. Giacoumidis, A. Shen, L. Barry, A. Ramdane, Mode locked laser phase noise reduction under optical feedback for coherent DWDM communication, J. Lightwave Technol. 38 (20) (2020) 5708–5715, https://doi.org/10.1109/JLT.2020.3002653.
[298] Z.-H. Wang, W.-Q. Wei, Q. Feng, T. Wang, J.-J. Zhang, InAs/GaAs quantum dot single-section mode-locked lasers on Si (001) with optical self-injection feedback, Opt. Express 29 (2) (2021) 674–683, https://doi.org/10.1364/OE.411551.
[299] R.H. Dicke, Coherence in spontaneous radiation processes, Phys. Rev. 93 (1954) 99–110, https://doi.org/10.1103/PhysRev.93.99.
[300] M. Xia, R.V. Penty, I.H. White, P.P. Vasil'ev, Femtosecond superradiant emission in AlGaInAs quantum-well semiconductor laser structures, Opt. Express 20 (8) (2012) 8755–8760, https://doi.org/10.1364/OE.20.008755.
[301] M. Scheibner, T. Schmidt, L. Worschech, A. Forchel, G. Bacher, T. Passow, D. Hommel, Superradiance of quantum dots, Nat. Phys. 3 (2) (2007) 106–110, https://doi.org/10.1038/nphys494.
[302] M. Xia, R.V. Penty, I.H. White, P.P. Vasil'ev, Superradiant emission from a tapered quantum-dot semiconductor diode emitter, in: Conference on Lasers and Electro-Optics 2010, Optica Publishing Group, 2010, https://doi.org/10.1364/CLEO.2010.CMY2.
[303] N. Opačak, B. Schwarz, Theory of frequency-modulated combs in lasers with spatial hole burning, dispersion, and Kerr nonlinearity, Phys. Rev. Lett. 123 (24) (2019) 243902, https://doi.org/10.1103/PhysRevLett.123.243902.
[304] J. Hillbrand, D. Auth, M. Piccardo, N. Opačak, E. Gornik, G. Strasser, F. Capasso, S. Breuer, B. Schwarz, In-phase and anti-phase synchronization in a laser frequency comb, Phys. Rev. Lett. 124 (2) (2020) 023901.
[305] C. Silvestri, Theory and Modelization of Quantum Cascade Laser Dynamics: Comb Formation, Field Structures and Feedback-Based Imaging (Ph.D. thesis), 2022.
[306] J.N. Kemal, P. Marin-Palomo, K. Merghem, G. Aubin, F. Lelarge, A. Ramdane, S. Randel, W. Freude, C. Koos, 32QAM WDM transmission at 12 Tbit/s using a quantum-dash mode-locked laser diode (QD-MLLD) with external-cavity feedback, Opt. Express 28 (16) (2020) 23594–23608, https://doi.org/10.1364/OE.392007.
[307] X. Li, J.X.B. Sia, W. Wang, Z. Qiao, X. Guo, G.I. Ng, Y. Zhang, Z. Niu, C. Tong, H. Wang, C. Liu, Phase noise reduction of a 2 μm passively mode-locked laser through hybrid III-V/silicon integration, Optica 8 (6) (2021) 855–860, https://doi.org/10.1364/OPTICA.416007.
[308] E.K. Lau, L.J. Wong, M.C. Wu, Enhanced modulation characteristics of optical injection-locked lasers: a tutorial, IEEE J. Sel. Top. Quantum Electron. 15 (3) (2009) 618–633, https://doi.org/10.1109/JSTQE.2009.2014779.
[309] C. Lin, F. Mengel, Reduction of frequency chirping and dynamic linewidth in high-speed directly modulated semiconductor lasers by injection locking, Electron. Lett. 20 (25) (1984) 1073–1075, https://doi.org/10.1049/el:19840734.
[310] N. Schunk, K. Petermann, Noise analysis of injection-locked semiconductor injection lasers, IEEE J. Quantum Electron. 22 (5) (1986) 642–650, https://doi.org/10.1109/JQE.1986.1073018.
[311] A. Hayat, A. Bacou, A. Rissons, J.-C. Mollier, V. Iakovlev, A. Sirbu, E. Kapon, Long wavelength VCSEL-by-VCSEL optical injection locking, IEEE Trans. Microwave Theory Tech. 57 (7) (2009) 1850–1858, https://doi.org/10.1109/TMTT.2009.2022809.

[312] T. Habruseva, N. Rebrova, S.P. Hegarty, G. Huyet, Mode-locked semiconductor lasers with optical injection, in: Quantum Dot Devices, Springer, 2012, pp. 65–91, https://doi.org/10.1007/978-1-4614-3570-9_4.
[313] A. Martinez, K. Merghem, S. Bouchoule, G. Moreau, A. Ramdane, J.-G. Provost, F. Alexandre, F. Grillot, O. Dehaese, R. Piron, S. Loualiche, Dynamic properties of InAs/InP (311)B quantum dot Fabry-Pérot lasers emitting at 1.52 μm, Appl. Phys. Lett. 93 (2) (2008) 021101, https://doi.org/10.1063/1.2957479.
[314] D. Gready, G. Eisenstein, V. Ivanov, C. Gilfert, F. Schnabel, A. Rippien, J.P. Reithmaier, C. Bornholdt, High speed 1.55 μm InAs/InGaAlAs/InP quantum dot lasers, IEEE Photon. Technol. Lett. 26 (1) (2013) 11–13, https://doi.org/10.1109/LPT.2013.2287502.
[315] D. Arsenijević, D. Bimberg, Quantum-dot lasers for 35 Gbit/s pulse-amplitude modulation and 160 Gbit/s differential quadrature phase-shift keying, in: Semiconductor Lasers and Laser Dynamics VII, vol. 9892, International Society for Optics and Photonics, SPIE, 2016, https://doi.org/10.1117/12.2230758.
[316] S. Bhowmick, Md. Zunaid Baten, T. Frost, B.S. Ooi, P. Bhattacharya, High performance InAs/$In_{0.53}Ga_{0.23}Al_{0.24}As$/InP quantum dot 1.55 μm tunnel injection laser, IEEE J. Quantum Electron. 50 (1) (2013) 7–14, https://doi.org/10.1109/JQE.2013.2290943.
[317] B. Shi, S. Pinna, W. Luo, H. Zhao, S. Zhu, S.T.S. Brunelli, K.M. Lau, J. Klamkin, Comparison of static and dynamic characteristics of 1550 nm quantum dash and quantum well lasers, Opt. Express 28 (18) (2020) 26823–26835, https://doi.org/10.1364/OE.399188.
[318] S. Hein, V. Von Hinten, W. Kaiser, S. Höfling, A. Forchel, Dynamic properties of 1.5 μm quantum dash lasers on (100) InP, Electron. Lett. 43 (20) (2007) 1, https://doi.org/10.1049/el:20072292.
[319] O. Mollet, A. Martinez, K. Merghem, S. Joshi, J.-G. Provost, F. Lelarge, A. Ramdane, Dynamic characteristics of undoped and p-doped Fabry-Pérot InAs/InP quantum dash based ridge waveguide lasers for access/metro networks, Appl. Phys. Lett. 105 (14) (2014) 141113, https://doi.org/10.1063/1.4898005.
[320] Z. Mi, P. Bhattacharya, DC and dynamic characteristics of p-doped and tunnel injection 1.65-μm InAs quantum-dash lasers grown on InP (001), IEEE J. Quantum Electron. 42 (12) (2006) 1224–1232, https://doi.org/10.1109/JQE.2006.883497.
[321] W. Kaiser, K. Mathwig, S. Deubert, J.P. Reithmaier, A. Forchel, O. Parillaud, M. Krakowski, D. Hadass, V. Mikhelashvili, G. Eisenstein, Static and dynamic properties of laterally coupled DFB lasers based on InAs/InP QDash structures, Electron. Lett. 41 (14) (2005) 1, https://doi.org/10.1049/el:20051160.
[322] Q. Zou, K. Merghem, S. Azouigui, A. Martinez, A. Accard, N. Chimot, F. Lelarge, A. Ramdane, Feedback-resistant p-type doped InAs/InP quantum-dash distributed feedback lasers for isolator-free 10 Gb/s transmission at 1.55 μm, Appl. Phys. Lett. 97 (23) (2010) 231115, https://doi.org/10.1063/1.3525374.
[323] N. Chimot, S. Joshi, G. Aubin, K. Merghem, S. Barbet, A. Accard, A. Ramdane, F. Lelarge, 1550 nm InAs/InP quantum dash based directly modulated lasers for next generation passive optical network, in: 2012 International Conference on Indium Phosphide and Related Materials, IEEE, 2012, pp. 177–180, https://doi.org/10.1109/ICIPRM.2012.6403351.
[324] S. Joshi, N. Chimot, L.A. Neto, A. Accard, J.-G. Provost, F. Franchin, A. Ramdane, F. Lelarge, Quantum dash based directly modulated lasers for long-reach access networks, Electron. Lett. 50 (7) (2014) 534–536, https://doi.org/10.1049/el.2013.4121.
[325] K.T. Tan, C. Marinelli, M.G. Thompson, A. Wonfor, M. Silver, R.L. Sellin, R.V. Penty, I. H. White, M. Kuntz, M. Lammlin, N.N. Ledentsov, D. Bimberg, A.E. Zhukov, V.M. Ustinov, A.R. Kovsh, High bit rate and elevated temperature data transmission using

InGaAs quantum-dot lasers, IEEE Photon. Technol. Lett. 16 (5) (2004) 1415–1417, https://doi.org/10.1109/LPT.2004.826009.

[326] X.-Y. MaXueer, Y.-M. He, Z.-R. Lv, Z.-K. Zhang, H.-Y. Chai, D. Lu, X.-G. Yang, T. Yang, 1.3 μm p-modulation doped InGaAs/GaAs quantum dot lasers with high speed direct modulation rate and strong optical feedback resistance, Crystals 10 (11) (2020) 980, https://doi.org/10.3390/cryst10110980.

[327] M. Ishida, Y. Tanaka, K. Takada, T. Yamamoto, H.-Z. Song, Y. Nakata, M. Yamaguchi, K. Nishi, M. Sugawara, Y. Arakawa, Effect of carrier transport on modulation bandwidth of 1.3-μm InAs/GaAs self-assembled quantum-dot lasers, in: 22nd IEEE International Semiconductor Laser Conference, IEEE, 2010, pp. 174–175, https://doi.org/10.1109/ISLC.2010.5642656.

[328] T. Kageyama, K. Watanabe, Q.H. Vo, K. Takemasa, M. Sugawara, S. Iwamoto, Y. Arakawa, InAs/GaAs quantum dot lasers with GaP strain-compensation layers grown by molecular beam epitaxy, Phys. Status Solidi A 213 (4) (2016) 958–964, https://doi.org/10.1002/pssa.201532555.

[329] M. Ishida, M. Matsuda, Y. Tanaka, K. Takada, M. Ekawa, T. Yamamoto, T. Kageyama, M. Yamaguchi, K. Nishi, M. Sugawara, Y. Arakawa, Temperature-stable 25-Gbps direct-modulation in 1.3-μm InAs/GaAs quantum dot lasers, in: CLEO: Science and Innovations, Optical Society of America, 2012, https://doi.org/10.1364/CLEO_SI.2012.CM1I.2.

[330] T. Kageyama, Q.H. Vo, K. Watanabe, K. Takemasa, M. Sugawara, S. Iwamoto, Y. Arakawa, Large modulation bandwidth (13.1 GHz) of 1.3 μm-range quantum dot lasers with high dot density and thin barrier layer, in: 2016 Compound Semiconductor Week (CSW) [Includes 28th International Conference on Indium Phosphide & Related Materials (IPRM) & 43rd International Symposium on Compound Semiconductors (ISCS)], IEEE, 2016, pp. 1–2, https://doi.org/10.1109/ICIPRM.2016.7528535.

[331] K. Takada, Y. Tanaka, T. Matsumoto, M. Ekawa, H.Z. Song, Y. Nakata, M. Yamaguchi, K. Nishi, T. Yamamoto, M. Sugawara, Y. Arakawa, Wide-temperature-range 10.3 Gbit/s operations of 1.3-μm high-density quantum-dot DFB lasers, Electron. Lett. 47 (3) (2011) 1, https://doi.org/10.1049/el.2010.3312.

[332] C. Hantschmann, P.P. Vasil'ev, A. Wonfor, S. Chen, M. Liao, A.J. Seeds, H. Liu, R.V. Penty, I.H. White, Understanding the bandwidth limitations in monolithic 1.3 μm InAs/GaAs quantum dot lasers on silicon, J. Lightwave Technol. 37 (3) (2019) 949–955, https://doi.org/10.1109/JLT.2018.2884025.

[333] Y. Wan, J.C. Norman, Y. Tong, M.J. Kennedy, W. He, J. Selvidge, C. Shang, M. Dumont, A. Malik, H.K. Tsang, A.C. Gossard, J.E. Bowers, 1.3 μm Quantum dot-distributed feedback lasers directly grown on (001) Si, Laser Photonics Rev. 14 (7) (2020) 2000037, https://doi.org/10.1002/lpor.202000037.

[334] Y. Ding, W.J. Fan, D.W. Xu, C.Z. Tong, S.F. Yoon, D.H. Zhang, L.J. Zhao, W. Wang, Y. Liu, N.H. Zhu, Fabrication and modulation characteristics of 1.3 μm p-doped InAs quantum dot vertical cavity surface emitting lasers, J. Phys. D Appl. Phys. 42 (8) (2009) 085117, https://doi.org/10.1088/0022-3727/42/8/085117.

[335] M. Laemmlin, G. Fiol, M. Kuntz, F. Hopfer, A. Mutig, N.N. Ledentsov, A.R. Kovsh, C. Schubert, A. Jacob, A. Umbach, D. Bimberg, Quantum dot based photonic devices at 1.3 μm: direct modulation, mode-locking, SOAs and VCSELs, Phys. Status Solidi C 3 (3) 391–394, 10.1002/pssc.200564142.

[336] N.N. Ledentsov, F. Hopfer, D. Bimberg, High-speed quantum-dot vertical-cavity surface-emitting lasers, Proc. IEEE 95 (9) (2007) 1741–1756, https://doi.org/10.1109/JPROC.2007.900898.

[337] D. Bimberg, U.W. Pohl, Quantum dots: promises and accomplishments, Mater. Today 14 (9) (2011) 388–397, https://doi.org/10.1016/S1369-7021(11)70183-3.
[338] G. Larisch, S. Tian, D. Bimberg, Optimization of VCSEL photon lifetime for minimum energy consumption at varying bit rates, Opt. Express 28 (13) (2020) 18931, https://doi.org/10.1364/OE.391781.
[339] R.D. Schur, F. Sogawa, M. Nishioka, S. Ishida, Y. Arakawa, Vertical microcavity lasers with InGaAs/GaAs quantum dots formed by spinodal phase separation, Jpn J. Appl. Phys. 36 (3B) (1997) L357, https://doi.org/10.1143/JJAP.36.L357.
[340] H. Saito, K. Nishi, I. Ogura, S. Sugou, Y. Sugimoto, Room-temperature lasing operation of a quantum-dot vertical-cavity surface-emitting laser, Appl. Phys. Lett. 69 (21) (1996) 3140–3142, https://doi.org/10.1063/1.116808.
[341] J.A. Lott, N.N. Ledentsov, V.M. Ustinov, A.Yu. Egorov, A.E. Zhukov, P.S. Kopév, Zh.I. Alferov, D. Bimberg, Vertical cavity lasers based on vertically coupled quantum dots, Electron. Lett. 33 (13) (1997) 1150–1151, https://doi.org/10.1049/el_19970785.
[342] N. Ledentsov, M. Agustin, V.A. Shchukin, J.R. Kropp, N.N. Ledentsov, Ł. Chorchos, J.P. Turkiewicz, Z. Khan, C.L. Cheng, J.W. Shi, N. Cherkashin, Quantum dot 850 nm VCSELs with extreme high temperature stability operating at bit rates up to 25 Gbit/s at 150°C, Solid-State Electron. 155 (2019) 150–158, https://doi.org/10.1016/j.sse.2019.03.018.
[343] H. Li, P. Wolf, P. Moser, G. Larisch, J.A. Lott, D. Bimberg, Temperature-stable 980-nm VCSELs for 35-Gb/s operation at 85°C with 139-fJ/bit dissipated heat, IEEE Photon. Technol. Lett. 26 (23) (2014) 2349–2352, https://doi.org/10.1109/LPT.2014.2354736.
[344] J.A. Lott, N.N. Ledentsov, V.M. Ustinov, N.A. Maleev, A.E. Zhukov, A.R. Kovsh, M.V. Maximov, B.V. Volovik, Zh.I. Alferov, D. Bimberg, InAs-InGaAs quantum dot VCSELs on GaAs substrates emitting at 1.3 μm, Electron. Lett. 36 (16) (2000) 1384–1385, https://doi.org/10.1049/el_20000988.
[345] D. Xu, C. Tong, S.F. Yoon, W. Fan, D.H. Zhang, M. Wasiak, Ł. Piskorski, K. Gutowski, R.P. Sarzała, W. Nakwaski, Room-temperature continuous-wave operation of the In (Ga) As/GaAs quantum-dot VCSELs for the 1.3 μm optical-fibre communication, Semicond. Sci. Technol. 24 (5) (2009) 055003, https://doi.org/10.1088/0268-1242/24/5/055003.
[346] C. Paranthoen, C. Levallois, G. Brévalle, M. Perrin, A. Le Corre, N. Chevalier, P. Turban, C. Cornet, H. Folliot, M. Alouini, Low threshold 1550-nm emitting QD optically pumped VCSEL, IEEE Photon. Technol. Lett. 33 (2) (2021) 69–72, https://doi.org/10.1109/LPT.2020.3044457.
[347] C.-Z. Ning, Semiconductor nanolasers, Phys. Status Solidi B 247 (4) (2010) 774–788, https://doi.org/10.1002/pssb.200945436.
[348] K. Srinivasan, M. Borselli, O. Painter, A. Stintz, S. Krishna, Cavity Q, mode volume, and lasing threshold in small diameter AlGaAs microdisks with embedded quantum dots, Opt. Express 14 (3) (2006) 1094–1105, https://doi.org/10.1364/OE.14.001094.
[349] A. Khalatpour, J.L. Reno, N.P. Kherani, Q. Hu, Unidirectional photonic wire laser, Nat. Photonics 11 (9) (2017) 555–559, https://doi.org/10.1038/nphoton.2017.129.
[350] H.-G. Park, S.-H. Kim, S.-H. Kwon, Y.-G. Ju, J.-K. Yang, J.-H. Baek, S.-B. Kim, Y.-H. Lee, Electrically driven single-cell photonic crystal laser, Science 305 (5689) (2004) 1444–1447, https://doi.org/10.1126/science.1100968.
[351] D. Wiersma, The smallest random laser, Nature 406 (6792) (2000) 133–135, https://doi.org/10.1038/35018184.
[352] Y. Wan, J. Norman, Q. Li, M.J. Kennedy, D. Liang, C. Zhang, D. Huang, Z. Zhang, A.Y. Liu, A. Torres, D. Jung, A.C. Gossard, E.L. Hu, K.M. Lau, J.E. Bowers, 1.3 μm Sub-milliamp threshold quantum dot micro-lasers on Si, Optica 4 (8) (2017) 940–944, https://doi.org/10.1364/OPTICA.4.000940.

[353] A. Osada, Y. Ota, R. Katsumi, M. Kakuda, S. Iwamoto, Y. Arakawa, Strongly coupled single-quantum-dot-cavity system integrated on a CMOS-processed silicon photonic chip, Phys. Rev. Appl. 11 (2) (2019) 024071, https://doi.org/10.1103/PhysRevApplied.11.024071.

[354] P. Munnelly, T. Heindel, A. Thoma, M. Kamp, S. Höfling, C. Schneider, S. Reitzenstein, Electrically tunable single-photon source triggered by a monolithically integrated quantum dot microlaser, ACS Photonics 4 (4) (2017) 790–794, https://doi.org/10.1021/acsphotonics.7b00119.

[355] D. Bimberg, E. Stock, A. Lochmann, A. Schliwa, W. Unrau, M. Münnix, S. Rodt, A.I. Toropov, A. Bakarov, A.K. Kalagin, V.A. Haisler, Quantum dots for single and entangled photon emitters, in: K.G. Eyink, F. Szmulowicz, D.L. Huffaker (Eds.), Quantum Dots and Nanostructures: Synthesis, Characterization, and Modeling VII, 7610, SPIE, 2010, https://doi.org/10.1117/12.846782. vol.

[356] E. Stock, T. Warming, I. Ostapenko, S. Rodt, A. Schliwa, J.A. Töfflinger, A. Lochmann, A.I. Toropov, S.A. Moshchenko, D.V. Dmitriev, V.A. Haisler, D. Bimberg, Single-photon emission from InGaAs quantum dots grown on (111) GaAs, Appl. Phys. Lett. 96 (9) (2010) 093112, https://doi.org/10.1063/1.3337097.

[357] Y. Arakawa, Advances in quantum dot lasers - 40 years of history, in: 2022 28th International Semiconductor Laser Conference (ISLC), 2022, pp. 1–2, https://doi.org/10.23919/ISLC52947.2022.9943404.

[358] T. Zhou, M. Tang, G. Xiang, B. Xiang, S. Hark, M. Martin, T. Baron, S. Pan, J.-S. Park, Z. Liu, S. Chen, Z. Zhang, H. Liu, Continuous-wave quantum dot photonic crystal lasers grown on on-axis Si (001), Nat. Commun. 11 (1) (2020) 1–7, https://doi.org/10.1038/s41467-020-14736-9.

[359] H.-Y. Lu, S.-C. Tian, C.-Z. Tong, L.-J. Wang, J.-M. Rong, C.-Y. Liu, H. Wang, S.-L. Shu, L.-J. Wang, Extracting more light for vertical emission: high power continuous wave operation of 1.3-μm quantum-dot photonic-crystal surface-emitting laser based on a flat band, Light Sci. Appl. 8 (1) (2019) 1–6, https://doi.org/10.1038/s41377-019-0214-2.

[360] C. Zhang, D. Liang, G. Kurczveil, A. Descos, R.G. Beausoleil, Hybrid quantum-dot microring laser on silicon, Optica 6 (9) (2019) 1145–1151, https://doi.org/10.1364/OPTICA.6.001145.

[361] B. Tossoun, X. Sheng, J.P. Strachan, D. Liang, R.G. Beausoleil, Memristor photonics, in: Photonics in Switching and Computing 2021, Optica Publishing Group, 2021, https://doi.org/10.1364/PSC.2021.Tu5B.3.

[362] C. Weisbuch, H. Benisty, R. Houdre, Overview of fundamentals and applications of electrons, excitons and photons in confined structure, J. Lumin. 85 (2000) 271–293.

[363] B.A. Burnett, B.S. Williams, Design strategy for terahertz quantum dot cascade lasers, Opt. Express 24 (22) (2016) 25471, https://doi.org/10.1364/OE.24.025471.

[364] N. Zhuo, F.Q. Liu, J.C. Zhang, L.J. Wang, J.Q. Liu, S.Q. Zhai, Z.G. Wang, Quantum dot cascade lasers, Nanoscale Res. Lett. 9 (144) (2014) 1, https://doi.org/10.1186/1556-276X-9-144.

[365] W. Luo, L. Lin, J. Huang, Q. Lin, K.M. Lau, Electrically pumped InP/GaAsP quantum dot lasers grown on (001) Si emitting at 750 nm, Opt. Express 30 (22) (2022) 40750–40755, https://doi.org/10.1364/OE.474320.

[366] W. You, R. Arefin, F. Uzgur, S. Lee, S.J. Addamane, B. Liang, A.S., Enhancement in electro-optic performance of InAlGaAs/GaAs quantum dot lasers by ex situ thermal annealing, Opt. Lett. 48 (2023) 1938–1941.